2009

Surface functionalized mesoporous silica nanoparticles for intracellular drug delivery

Juan Luis Vivero-escoto
Iowa State University

Surface functionalized mesoporous silica nanoparticles for intracellular drug delivery

by

Juan Luis Vivero-Escoto

A dissertation submitted to the graduate faculty

in partial fulfillment of the requirements for the degree of

DOCTOR OF PHILOSOPHY

Major: Organic Chemistry

Program of Study Committee:
Victor Shang-Yi Lin, Major Professor
George Kraus
Nicola L. Pohl
Marek Pruski
Yan Zhao

Iowa State University

Ames, Iowa

2009

"Where nature finishes producing its own species,
man begins, using natural things and with the help
of this nature, to create an infinity of species."
Leonardo da Vinci

"True wisdom comes to each of us when we realize how little
we understand about life, ourselves, and the world around us."
Socrates (BC 469 – 399)

ACKNOWLEDGMENTS

I would like to express my appreciation for the support that I have received during these years from so many wonderful people.

To my major Professor Victor Shang-Yi Lin, for his mentoring, for showing me that the hard work together with creativity and wisdom can overcome any challenge.

To the past and present members of my POS committee, Prof. Dr. George Kraus, Prof. Dr. Nicola Pohl, Prof. Dr. Marek Pruski, Prof. Dr. Hans Stauffer, and Prof. Dr. Yan Zhao for their time and excellent suggestions.

To the staff of the cell, hybridoma, confocal microscopy, DNA, protein and image analysis facilities of Iowa State University for their generous help and patience.

To all the funding agencies for their support of the projects in this dissertation, in special the U.S. National Science Foundation, the U.S. Department of Energy, Ames

To my family for staying close to me during all the difficult times, in especial to my mother Juana Escoto Noriega for supporting me to achieve my dreams.

To my wife Yazaret Chavez Figueroa for all her support and encouragement; first as a very good friend, and now as my loved partner.

To the Slowing-Romero family, Anika, Soledad, Flor de Maria, and Igor, for their friendship during all these years.

ABSTRACT

Mesoporous silica nanoparticles (MSNs) are a highly promising platform for intracellular controlled release of drugs and biomolecules. Despite that the application of MSNs in the field of intracellular drug delivery is still at its infancy very exciting breakthroughs have been achieved in the last years. A general review of the most recent progress in this area of research is presented, including a description of the latest findings on the pathways of entry into live mammalian cells together with the intracellular trafficking, a summary on the contribution of MSNs to the development of site-specific drug delivery systems, a report on the biocompatibility of this material *in vitro* and *in vivo*, and a discussion on the most recent breakthroughs in the synthesis and application of stimuli-responsive mesoporous silica-based delivery vehicles.

A gold nanoparticles (AuNPs)-capped MSNs-based intracellular photoinduced drug delivery system (PR-AuNPs-MSNs) for the controlled release of anticancer drug inside of human fibroblast and liver cells was synthesized and characterized. We found that the mesoporous channels of MSNs could be efficiently capped by the photoresponsive AuNPs without leaking the toxic drug, paclitaxel, inside of human cells. Furthermore, we demonstrated that the cargo-release property of this PR-AuNPs-MSNs system could be easily photo-controlled under mild and biocompatible conditions *in vitro*.

In collaboration with Renato Mortera (a visiting student from Italy), a MSNs based intracellular delivery system for controlled release of cell membrane impermeable cysteine was developed. A large amount of cysteine molecules were covalently attached to the silica surface of MSNs through cleavable disulfide linkers. These cysteine-containing nanoparticles were efficiently endocytosed by human cervical cancer cells HeLa. These materials exhibit

450 times higher cell growth inhibition capability than that of the conventional N-acetylcysteine prodrug.

The ability to functionalize the surface of the MSNs with organic groups was used as a way to incorporate functional molecules that can interact with intracellular structures. A series of oligonucleotides intercalating (propidium) derivative functionalized MSNs (PAP-LP-MSNs and AP-PAP-MSNs) materials were synthesized. We selectively decorated the exterior particle surface of PAP-LP-MSN and the interior pore surface of AP-PAP-MSN with the oligonucleotide intercalating functionality. We observed that these materials are internalized by HeLa cells despite that the propidium group is known by its cell membrane impermeable properties. By confocal microscopy and flow cytometry, we demonstrated that indeed PAP-LP-MSNs were able to bind to cytoplasmic oligonucleotides; such as messenger RNA, resulting in severe cell growth inhibition. In contrast, the cytotoxicity of AP-PAP-MSN, where the same oligonucleotide intercalating molecules were anchored inside the pores, was significantly lowered upon the endocytosis by HeLa cells. The results obtained prove that the biocompatibility and cell membrane trafficking properties of MSNs could be modified by selective functionalization of the two different surfaces (exterior particle and interior pore surfaces) and morphology control of MSNs.

CHAPTER 1. DISSERTATION ORGANIZATION

This thesis is organized in six chapters. Chapter 1 describes an overview of this dissertation. Chapters 2 to 5 are journal articles; Chapter 3 and 4 have already been published, Chapter 2 and 5 have been submitted for publication, and Chapter 6 describes the significance and future work of the research done in this dissertation.

Chapter 2 describes a general introduction about the application of MSNs for intracellular drug delivery. Some of the most important topics in this area are addressed in this literature review. The aim of this chapter is to describe the latest breakthroughs in the field and to put them together in the context of the development of MSNs as a promising platform for drug delivery.

The ability to release drugs in a time- and site-controlled fashion is one of the most desired features for a drug delivery carrier. Chapter 3 is a study on the synthesis and application of a gold nanoparticles capped MSNs-based drug delivery vehicle. The novel feature of this system is that the release of drugs is controlled by an external trigger (irradiation under mild conditions). The application of this carrier was successfully demonstrated in human cells.

Some of the outstanding features that make MSNs a unique material for drug delivery are their high surface area and efficient internalization by mammalian cells. Chapter 4 describes the synthesis of a cysteine functionalized MSNs material. The intracellular release of cell impermeable cysteine was controlled by the reducing environment. The high loading and efficient release of cysteine from MSNs was demonstrated against the conventional N-acetylcysteine prodrug.

Different inorganic nanoparticles are being investigated for their biomedical and biological applications. However, MSN is one of the few nanomaterials that have the structural feature of possessing two different surfaces. Chapter 5 involves the description of the development of a series of intercalator-functionalized MSNs that bind specifically to oligonucleotides. The intercalating group (phenanthridium molecule) was selectively grafted on the exterior particle surface and interior pore surface of MSNs. The effect of the localization of the phenanthridium group on the biocompatibility and cell membrane trafficking properties of these materials are reported.

Finally in Chapter 6 describes a general conclusion for this research and gives future directions for the continuous development of this field.

CHAPTER 2. MESOPOROUS SILICA NANOPARTICLES FOR INTRACELLULAR CONTROLLED DRUG DELIVERY

A manuscript submitted to Small

Juan L. Vivero-Escoto, Igor I. Slowing, Brian G. Trewyn and Victor S.-Y. Lin

Abstract

The application of nanotechnology in the field of drug delivery has attracted a lot of attention in the last decades. Recently, the development of new delivery vehicles based on inorganic nanomaterials has brought new possibilities to this area of research. In the case of mesoporous silica nanoparticles recent breakthroughs have demonstrated its high potential in this field. The ability to functionalize the surface of this silica-based nanocarrier with stimuli-responsive nanoparticles that work as gatekeepers, the binding of bio-functional moieties, and its high surface area are just some of the outstanding features that make this material a serious candidate to become a drug delivery platform. This review focuses on the most recent progress in the application of mesoporous silica nanoparticles for intracellular drug delivery. The latest research on the pathways of entry into mammalian cells together with intracellular trafficking are described. One of the main areas of interest in the last years in this field is the development of site-specific drug delivery vehicles; the contribution of mesoporous silica nanoparticles toward this topic is also summarized. In addition, the current research on the biocompatibility of this material *in vitro* and *in vivo* is discussed. Finally, the latest breakthroughs in intracellular controlled drug release using stimuli-responsive mesoporous silica-based systems are described.

1. Introduction

The design of site-specific stimuli-responsive controlled drug delivery systems (DDS) is of utmost importance for the continued advancement of biomedical, personal health care, and pharmaceutical industry. DDS that could manipulate the biological profiles such as pharmacokinetics, pharmacodynamics, therapeutic index, biodistribution, and tissue uptake of therapeutic agents are of major interest of researchers worldwide. One of the key challenges of such DDS is to have the ability of transporting an effective amount of drug with fewer acute and chronic side effects than those of the current treatment methods, such as chemotherapy.[1-3] Obviously, to successfully achieve these goals several prerequisites need to be incorporated into such delivery carriers. Some of the most important prerequisites for designing these systems are outlined below:

- The vehicle should be biocompatible
- High loading and protection of the desired guest molecule
- Zero premature release before reaching its target
- Efficient cellular uptake
- Effective endosomal escape
- Controllable rate of release to achieve an effective local concentration
- Cell and tissue targeting

In the past decades different strategies have been developed to design drug delivery materials to accomplish the aforementioned prerequisites. For instance, several drug delivery nanocarriers based on organic platforms such as liposomes, polymers, and dendrimers have been used as “smart” systems that can release therapeutic agents under physiological conditions.[2, 4-6] Moreover, recent discoveries based on inorganic nanoparticles and carbon

nanotubes have opened up new and exciting possibilities in this field.[7-9] Nanoparticles such as gold,[10] semiconductor nano-crystals,[11] superparamagnetic nanoparticles,[12] silicon-,[13] and silica-based nanosystems have been extensively studied as promising candidates for drug delivery.[14]

Among these inorganic-based materials, mesoporous silica nanoparticles (MSNs) have attracted much research attention for their potential application in the fields of biotechnology and biomedicine. MSNs are solid materials, which contain hundreds of empty channels (mesopores) arranged in a honeycomb-like porous structure (Figure 1). In contrast to the low biocompatibility of other amorphous silica materials, recent studies have shown that MSNs exhibit superior biocompatibility at concentrations adequate for pharmacological applications.[15, 16] These silica-based nanoparticles also offer several unique and advantageous structural properties, such as high surface area (> 700 m^2/g), pore volume (> 1 cm^3/g), stable mesostructure, tunable pore diameter (2-10 nm), two functional surfaces (exterior particle and interior pore surfaces), and modifiable morphology (controllable particle sizes and shapes). For instance, their high surface area and pore volume allows for high drug loading. The tunable diffusional release of drug molecules from the highly ordered mesoporous structure gives rise to a biogenic local concentration at the targeted area, which reduces the overall dosage and prevents any acute or chronic complications. In addition, MSNs offer the ability of effectively protect the precious pharmaceutical cargos, such as drugs, imaging agents, enzymes, and oligonucleotides from premature release and the undesired degradation in harsh environments, such as stomach and intestine, before reaching the designated target. In contrast to other DDS, the guest molecules can be loaded to MSNs without adsorbing the solvent molecules that are often toxic for healthy cells.[17]

Another advantage of MSNs is the possibility to be further functionalized adding features either onto their external surface or inside the nano-channels.[18, 19] These features may include: functionalization with stimuli-responsive tethers that could be attached to nanoparticles (gold, quantum dots, and iron oxide). These nanoparticles could work as gatekeepers, which once the MSNs-based vehicle is in the designated site they can be removed by either an intracellular or external trigger such as change in pH, reducing environment, enzymatic activity, light, electromagnetic field, or ultrasound. In addition, MSNs surface can be engineered with cell specific moieties such as organic molecules, peptides or antibodies to achieve cell type or tissue specificity. Moreover, optical and magnetic contrast agents can be introduced to develop multi-purpose DDS. Figure 1 illustrates more features that could be added to MSNs to develop a highly promising drug delivery platform. As one can conclude from the above mentioned features, MSN has not only potential for cancer treatment but maybe also for metabolic diseases, autoimmune diseases, and gene therapy.[20]

2. Synthesis of mesoporous silica nanoparticles

The synthesis of structurally ordered (MCM-type) mesoporous silica materials was first reported by scientists of Mobil Company in 1992.[21-23] The methodology was based on the condensation of silica precursors (i.e, sodium silicate, tetramethylammonium silicate, or tetraethyl orthosilicate) in presence of structure-directing agents (quaternary ammonium cationic surfactants) under hydrothermal and basic conditions. The scope of this micelle-templated approach was extended by a number of variations leading to a wide variety of mesoporous silica materials, such as SBA-,[24] MSU-,[25] and FSM-types of mesoporous silica.[26, 27] Some of the novel features of these silica-based materials are unique porous

structure, tunable pore size, high thermal and hydrolytic stability, narrow pore size distribution, high surface area and large pore volume. However, the large size (above micron in diameter) and the irregularity in particle shape of these mesoporous silica particles had prevented the applications of these materials in areas such as separation (chromatography), biotechnology, and medicine (Figure 2).[28, 29] For this reason, novel synthetic strategies have been developed for controlling the structural (size and shape) and chemical properties of these silica-based materials.

2.1 Control of structural properties (size and shape)

The capability of tuning the structural features of MCM-type materials has a direct outcome in regulating the mass-transport properties of guest molecules and improving its biocompatibility as has been demonstrated by our group and others.[30-32] Different methods for tuning the structural properties of MSN have been developed based on the synergy between the Stöber process and the micelle-templated approach. For instance, Unger and co-workers,[33] reported the shape-, and size-control of MCM-type mesoporous silica particles using the above strategy. They modified the Stöber process using a cationic surfactant as structure-directing agent. MSNs with MCM-41 type structure, spherical shape, and submicrometer-size (400-1100 nm) were obtained. The synthetic conditions such as pH and temperature can also affect the final properties of the resulting MSN material. For example, Cai and co-workers tuned the morphology of MSNs simply by selecting different pH-adjusting agents.[34] This procedure yielded hexagonally ordered nanospheres (roughly 100 nm in diameter) and nanorods (700-1000 nm in length, and 300-500 nm in width). In addition, Mou and co-workers,[35, 36] developed a pH-controlled method. The synthesis was carried out through a fast transfer from the original acid solution to basic media modifying

the kinetics of silica condensation. This method afforded well ordered type MCM-41 nanorods and disordered nanospheres.

On the other hand, Lin and co-workers have developed different strategies based on the co-condensation method for controlling the morphology of MSNs. One of the advantages of this process is that at the same time organic functional groups can be incorporated in the MSN.[37] Therefore, in addition to manipulate the shape of MSNs, this procedure also affords multi-functionalized materials. In this method different parameters have to be considered; such as, concentration, molecular size, and hydrophilicity/hydrophobicity of the organoalkoxysilanes (OAS) precursors. By tuning these parameters, we obtained nanoparticles with different shapes ranging from spherical, twisted columns, rod-shape, to tubular particles. All materials synthesized by this methodology showed a high surface area (> 600 m^2/g), narrow pore size distribution (2.0-2.9 nm), and different mesoporous structures as summarized in Table 1. The working principle of this method is based on the hydrophilic/hydrophobic interaction between the OAS precursors and the CTAB surfactant micelle. To further gain structural control of MSNs by this methodology, we studied the effect of tuning the concentrations of OAS introduced in the synthesis of these materials.[30] For instance, in the case of using 3-[2-(2-aminoethylamino)ethylamino]propyltrimethoxysilane (AEP-TMS) and 3-cyanopropyl trimethoxysilane (CP-TMS) mixture, particles with different sizes ranging from 3 μm to less than 500 nm were obtained. The different particle shapes obtained from this procedure varied from spherical to rods. Moreover, we demonstrated that the nanoparticle shape of these materials could be tuned and controlled by the hydrophilicity of OAS (AEP-TMS) groups.

Another strategy developed by our group to fine-tune the morphology of MSNs was the use of room-temperature ionic liquids (RTILs) as structure-directing agents.[38] Interestingly, the MSNs obtained through this method showed various particle shapes such as spheres, ellipsoids, rods, and tubes. We also obtained different mesoporous structures, such as hexagonal, rotational moiré type, and wormhole-like (Table 2). It is noteworthy to mention that in contrast to Tatsumi's material,[39] the rotational moiré pattern of mesoporous obtained in this report was based on an achiral surfactant. In addition to these achievements, we also published a report on the synthesis of large pore MSNs (3-6 nm) by using a pore expanding-agent (mesitylene).[40] The synthesis of this large pore MSNs was carried out to achieve the goal of releasing proteins (i.e. cytochrome *c*) inside mammalian cells.

From the exciting results aforementioned we can conclude that it is possible to synthesize MSNs with the following unique features:

- High surface area and large pore volume
- Chemical and mechanical stability
- Unique mesoporous structure
- Narrow and tunable pore size
- Well-define particle shape
- Monodisperse particles
- Tunable particle size

2.2 Control of surface functionalization

The capability of developing methods for controlling the degree of organic functionalization in MSNs is important in order to fine-tune its chemical properties. In this respect, one of the interesting advantages of MSNs is the fact that this material has two

functional surfaces; external (outside surface of the nanoparticles) and internal (nanochannels). The ability of selectively and efficiently functionalizing both surfaces is crucial for fine tuning the chemical and physical performance of MSN. Generally, two well-established methods for the functionalization of MSNs materials have been applied: co-condensation, and grafting.[41, 42]

The co-condensation method has the advantages of homogeneous surface coverage in one-pot synthesis, better control over the amount of OAS groups incorporated in the MSNs, and the possibility of using a wide variety of organo-functional groups.[41] However, this method is not useful to functionalize the external surface of MSNs and there is a limitation in the amount of OAS groups incorporated to the material without compromising the mesostructure. To overcome these drawbacks some novel approaches have been reported in the literature.[43] For instance, our group used the co-condensation method to functionalize the MSNs with a wide variety of OAS groups (Table 1).[37] OAS with different molecular sizes, hydrophobic/hydrophilic properties, and concentrations were successfully incorporated into the MSNs nanochannels. The co-condensation of two different OAS groups was also carried out,[30] which opened the pathway for the synthesis of more sophisticated MSNs for catalysis and biosensors applications. Besides our group, Mann and co-workers have also used the co-condensation strategy to functionalized MSNs through a controlled quenching procedure.[44]

On the other hand, the grafting procedure yields hydrothermally stable MSNs, and can selectively functionalize the exterior surface of MSNs materials.[42] This method also presents its own drawbacks, such as heterogeneous surface coverage and the fact that OAS groups tend to be grafted in the opening of the mesoporous blocking the interior of the

channels. Different factors can be involved in the efficient performance of the grafting method such as the type of solvent used for the reaction, temperature, type of OAS precursor, and reaction time. Asefa and co-workers have studied the influence of the polarity and dielectric constant of different solvents in the grafting method.[45] Three main properties were affected by the solvent: concentration of grafted groups, degree of site-isolation, and catalytic properties. The researchers found that polar-protic solvents resulted in lower concentrations of grafted groups, higher site-isolated organic groups, and more efficient catalytic properties. On the contrary, dipolar-aprotic and nonpolar solvents resulted in larger concentrations of grafted groups, more densely populated organic groups, and poor to efficient catalytic properties.

The combination of both, the grafting and co-condensation method, can afford the selective functionalization of the exterior and/or interior surface of MSNs. The clever use of this combination has resulted in nanodevices with outstanding properties. For instance, our group published a report on the internal surface functionalization of MSNs with *o*-phtalic hemithiacetal (OPTA) group using the co-condensation method, and later the external surface of this MSNs material was functionalized with poly-(lactic acid) via the grafting method (Figure 3).[46] This nanodevice was used for the selective sensing of amino-containing neurotransmitters. In this case, the poly-(lactic acid) polymer coated in the exterior of MSNs has the role of gatekeeper to selectively allow the diffusion of certain neurotransmitters. The OPTA group reacted with the neurotransmitters when they reached the interior of the MSN. This reaction affords a fluorescent product that is the principle for detecting the neurotransmitters. Recently, we used a similar approach to selectively functionalize MSNs with poly(N-isopropylacrylamide) polymer (PNiPAm) on its exterior surface. This PNiPAm-

coated MSNs exhibited interesting water solubility behavior which is controlled by the critical solution temperature of the polymer.[47]

3. Intracellular uptake of mesoporous silica nanoparticles

The most important barrier to overcome for intracellular drug delivery carriers is the cell membrane. MSNs uptake through mammalian cells can be challenging due to the large variety of intracellular transport mechanisms. Thorough understanding of the pathways for the cellular internalization of MSNs is a central challenge for many of its applications in biotechnology and biomedicine. There are a wide variety of pathways in mammalian cells for internalization of external material, and more are been discovered every year, but in general we can divide these mechanisms in two categories: phagocytosis, and pinocytosis (macropinocytosis and endocytosis) (Figure 4).[48, 49] Depending on the size of the particles to be engulfed the cells can use any of these internalization processes. Specialized cells such as macrophages use phagocytosis to engulf micro-size particles (> 1μm). On the other hand, the cellular uptake of small particles (<200-300 nm) such as MSNs, polymers, quantum dots, or carbon nanotubes is found to involve endocytosis for the majority of cases.[1] The process of endocytosis is mediated by several mechanisms that can transport the MSNs to different locations inside of the cytoplasm. Some of these endocytic routes are: clathrin-, and caveolin-dependent, receptor-mediated, and clathrin-, and caveolin-independent endocytosis (Figure 2). Endocytosis is a very complex process that consists of the selection at the cell surface, invagination and pinching-off, and finally tethering the just formed vesicles to the next stop in the intracellular trafficking journey.[48-50] So far, there is not “rule of thumb” to predict which endocytic pathway bare or functionalized MSNs follow for intracellular uptake. The

understanding and control of its internalization pathways is of utmost importance in its development as drug delivery platform.

Previous reports on the intracellular uptake of silica-coated nanoparticles showed that it was possible to internalize these materials through endocytic pathways.[51, 52] However, in the case of MSNs none reports were found that demonstrated its intracellular uptake until we published our work on the synthesis and application of dendrimer-capped MSNs (PAMAM-MSNs) for intracellular drug/gene delivery in 2004. Using transmission electron microscopy (TEM) we demonstrated the successful uptake of PAMAM-coated MSNs material in Chinese hamster ovarian (CHO) cells.[53] We observed that PAMAM-MSNs were localized nearby to subcellular organelles such as mitochondria and Golgi, as a clear demonstration of its successful uptake by mammalian cells. Later on, using a fluorescein isothiocyanate labeled MSNs (FITC-MSNs) material, flow cytometry, and confocal microscopy we were able to corroborate the internalization of MSNs inside cervical cancer cells (HeLa).[31] Moreover, we found that the uptake of FITC-MSNs is concentration dependent and follows a typical sigmoidal behavior of dose-response endocytosis. We further investigated the possible mechanisms for the endocytic trafficking of MSNs testing the cellular uptake of this material in presence of specific endocytic trafficking inhibitors. We found that the uptake of FITC-MSNs is through a clathrin-dependent endocytosis mechanism (Table 3). Y. Hung, and coworkers also reported the efficient uptake of FITC-MSNs materials by 3T3-L1 fibroblast cells.[32] Moreover in a complementary report, Y.-C. Chen, and coworkers found that the internalization of FITC-MSN is concentration-, time-, and cell-dependent.[54] In this report the authors used human mesenchymal stem cells (hMSCs) and 3T3-L1 fibroblasts to demonstrate that the internalization of FITC-MSNs is mediated by a clathrin-dependent

endocytosis process. Recently, Zink and co-workers studied the energy-dependence of the cellular uptake of MSNs. By incubating the cells with MSNs at different temperatures, they found that the uptake of MSNs is higher at 37 °C than at 4 °C. This finding demonstrated that the uptake of MSNs is driven by an energy-dependent process confirming previous reports.[55]

3.1 Effect of surface functionalization on the endocytic pathway

The cell membrane is a very complex system that consists mainly of lipids, proteins, cholesterol, and receptors. One of its features is the highly negative charge on its surroundings. It is well established that either the charge of the nanocarrier or attaching cell membrane receptors can affect the endocytic trafficking in mammalian cells.[56] Considering these properties we were interested to investigate the charge effect on the uptake of MSNs by HeLa cells.[31] Four different MSNs materials were synthesized, tuning the surface charge based on either amino or guanidine functionalities; besides FITC-labeled MSNs was used as the control material, the carrier with the most negative charge. We found, as was expected, a trend in the internalization of the materials related with the surface charge. The ED_{50} values for these materials increased with the increase in the negative value of their surface charge. Interestingly, we also found that these materials did not follow the same endocytic pathway. Some of them were endocytosed through clathrin-mediated endocytosis (FITC-MSNs), and others through caveolin-mediated endocytosis (Table 3). Recently, Huang, D.-M., Mou, C.-Y., and coworkers reported on the effect of the surface charge on the cellular uptake of MSNs in hMSCs and 3T3-L1 cells.[54] They found a correlation between the positive charge of MSNs and its internalization in 3T3-L1 cells. Interestingly, this correlation was not observed in hMSCs cells as an indication that the surface charge effect could also be cell type

dependent. Two inhibitors, phenylarsine oxide (PAO) and cytochalasin D (Cyt D) were used to investigate the endocytic pathways of these materials. The authors found that the endocytosis was carried through a clathrin- and an actin-dependent process.

As part of our research on the effect of surface functionalization of MSNs on its internalization by HeLa cells, we also explored the possibility of modifying the MSNs surface with a receptor group (folic acid). We found a highly efficient endocytosis of this folic acid functionalized-MSNs (FA-MSNs) by HeLa cells.[31] Through a receptor competition experiment, we were able to prove that the endocytic mechanism of FA-MSNs is mediated by folic acid receptors. Further developments related with target specific systems based on MSNs will be described below.

3.2 Effect of MSNs size and shape on the endocytic pathway

Since the first applications of nanotechnology to intracellular gene/drug delivery, the researchers were aware of the possible effects that size and shape of nanocarriers could have on the intracellular uptake of nanomaterials. Several studies were done to address this issue using drug/gene release vehicles (polyplexes, liposomes, polystyrene) to find out the size effect for the uptake of these nanomaterials in a wide variety of cell lines.[56-59] Some of the main outcomes reported on these works are: the size limits for internalization of nanoparticles through endocytosis are clearly cell dependent, nanoparticles below 200 nm will follow mainly endocytic pathways, particles above this size can be either engulf through endocytosis or non-internalized at all, and large particles have to be internalized by phagocytic pathways. Recently, with the continued development of inorganic nanoparticles as nanocarriers, a high interest has risen about the thorough understanding of the effect of structural properties of inorganic nanomaterials (size/shape) toward their endocytic

uptake.[60-63] Outstanding results have been reported in relation to this subject; for instance, W. Chan and coworkers found that in the case of spherical-shaped gold nanoparticles (AuNPs) the maximum uptake of nanospheres occurred at the diameter size of 50 nm, which is in agreement with previous reports. They also found that the internalization of nanorods AuNPs is less efficient than nanospheres.[60, 61] They account for these results based on the so called "wrapping time" parameter, which describes how a membrane encloses a particle based on its surface area.[64] The internalization of nanospheres was more efficient because it takes shorter time to wrap a sphere than an entire rod due to the increase in the surface area.

Our group has also studied the effect of these structural properties (shape and size) on the uptake of MSNs by mammalian cells. In this work two nanoparticles were investigated, nanorods (600 nm in length and 100 nm in width) and nanospheres (80-100 nm in diameter).[65] The cellular uptake and kinetics were evaluated in CHO and human fibroblast cells. We found that the uptake of MSNs was both shape and cell-line dependent. CHO cells showed a more efficient uptake capacity than fibroblast cells for both materials. Moreover the rate of uptake was different in the case of fibroblast cells, for instance spherical-shaped MSNs reached 100% uptake in 180 min, while rod-shaped MSNs needed 360 min to achieve the same uptake percentage, which is in complete agreement with the "wrapping time" theory mentioned above. Other groups have studied similar properties in different variety of cells; for example, Vallhov and coworkers studied the effect of MSNs' size on human monocyte-derived dendritic cells (MDDC). Two materials with spherical shape, and different size (270 nm and 2.5 μm) were tested. The authors demonstrated that the size and concentration have an effect on the viability, uptake, and immune regulatory markers.[66] They found that smaller MSNs in lower concentrations influence the MDDC viability to a minor degree.

Interestingly, their results showed that both materials are found in different locations inside the MDDC. Recently, C.-Y. Mou, and coworkers also reported on the size effect of spherical MSNs toward its internalization on HeLa cells. The authors synthesized MSNs with similar surface chemistry, charge, and different sizes (30, 50, 110, 170, and 280 nm). In agreement with previous reports, the authors found that a diameter of 50 nm is the optimal size for the most efficient endocytosis of MSNs.[67]

4. Intracellular trafficking

Once the MSN vehicle has overcome the cell membrane barrier, it has to reach the cytoplasm to release its cargo. The understanding of these intracellular pathways that MSNs undergoes after its endocytosis could help to improve the design of more efficient drug delivery systems. The internalization of the MSNs through endocytosis results in the formation of vesicles that capture MSNs present in the extracellular environment. These vesicles then undergo a complex series of fusion events directing the internalized MSNs to the cytosolic compartment. According to our current knowledge, the series of events after the MSNs have been endocytosed can be divided as follow; the material is transported to primary endosomes and then to sorting endosomes. From sorting endosomes, a fraction of MSNs is sorted back to the cell exterior through recycling endosomes, while the remaining fraction is transported to secondary endosomes, which fuse with lysosomes. The MSNs then escape the endo-lyso-somes and enter the cytosolic compartment. Once the MSN is in the cytoplasm, the material would release its drug/gene cargoes. And finally, the cell would eliminate MSN from the cytoplasm through an exocytosis process (Figure 5).[50] Our group has investigated the intracellular trafficking pathways of FITC-MSNs, mainly its endosome escape and the effect that surface functionalization could have toward this property. We followed the

internalization of these materials by confocal microscopy using an endosome marker. We found that more negatively charged MSNs materials are able to escape from endosomes, while positively charged remained trapped within endosomes at the conditions used in our experiment. These results were explained based on the surface charge reversal of MSNs that results from transfer of protons ions from bulk solution to its surface under acidic conditions, better known as "proton sponge effect".[31] Y.-C. Chen and coworkers also reported on the MSNs trafficking inside the cells. They were able to investigate the endo-lysosomal escape of MSNs using LysoTrack-label. Moreover, they found that some of the material was localized in the mitochondria, according to the nonyl acridine orange probe.[32]

5. Cell targeting

The combination of drug delivery and site targeting to specific cell/tissue populations is a key issue in biomedical science; especially in cancer therapy, where the antitumor drugs that lack the target specificity result in adverse side effects and have limited effectiveness due to unspecific action on healthy cells.[1] Therefore, research efforts are being placed on generating cell-targeting drug delivery systems to specifically release the desired drugs to unhealthy cells without side damages. Different strategies could be used for cell targeting such as chemically attached antibodies, proteins, peptides or specific ligands to MSNs carrier. These systems rely on the ability of the targeting agents to selectively bind receptors on the cell surface to trigger receptor-mediated endocytosis pathway. Our group reported for the first time on the synthesis of a receptor functionalized MSN vehicle. We were able to decorate the surface of MSNs with folate groups, which are specific for human cancer cells that contain high abundance of α-folate receptors. We further demonstrated that the endocytosis of this material is via a receptor-mediated endocytosis and that this process is

inhibited by folic acid.[31] Other groups have demonstrated that this strategy is indeed successful for the selective targeting and drug release in cancer cells. For instance, M. Lindén and coworkers reported on the performance of a MSN-based core-shell-shell system containing PEI at the surface of MSN; moreover, the authors attached to the amine groups of PEI, folic acid and FITC molecules (FA-PEI-MSN).[68] The particularities of this material allowed the authors to study the selective internalization of FA-PEI-MSN on HeLa cells. The authors proved that the uptake of this material was an order of magnitude higher in HeLa cells versus embryonic kidney epithelial 293 cells (low folate receptors expression). In addition, Tamanoi and coworkers successfully demonstrated the target-specific drug release of an anticancer drug camptothecin/paclitaxel on cancer cells (PANC-1) using this folate functionalization strategy.[69] As we mentioned above other targeting strategies could be used. For instance, C.-Y. Mou reported on functionalization of MSNs with monoclonal antibody (anti-HER2/neu mAb) for selective targeting of breast cancer cells.[70] Other groups have also shown the successful application of mannosylated MSNs nanocarriers as target-specific systems for gene delivery and photodynamic therapy.[71, 72] Despite all these promising examples *in vitro*, the application of target-specific MSN vehicles *in vivo* has not yet been reported.

6. Biocompatibility

To completely take advantage of the potential of MSNs in nanomedicine, full attention is required to safety and toxicological issues. Information regarding to biocompatibility *in vitro*, and absorption, biodistribution, retention, degradation, clearance and safety of MSNs *in vivo* is of vital importance for this matter. The biocompatibility of MSNs *in vitro* with different cells lines has been proved by us and other groups. But

surprisingly, despite the great potential that MSNs show for biomedical applications, our knowledge of the toxicological effects *in vivo* exposure is still very limited. This maybe because many features can be included as potentially toxic triggers such as surface area and size distribution, chemical composition, surface structure, solubility, shape and aggregation. The biocompatibility of MSNs *in vitro* is concentration-dependent and has been thoroughly studied in different cell lines. For instance, our group reported on the cytotoxicity of MSNs toward HeLa and CHO cells finding that at concentration below 100 μg/mL the material is biocompatible.[17, 31] The increase of MSNs concentration to above 200 μg/mL resulted in cell damage. The exact mechanism responsible for the cytotoxicity of this type of amorphous silica materials is not well understood. Some authors have reported that this material at high doses induces cell membrane damage;[73] however, others involve the enhanced of reactive oxygen species (ROS) formation by the material to induce toxic oxidative stress.[74] In addition, Asefa and co-workers have reported on the inhibition of cellular respiration by MSNs.[75]

As we mentioned above, the structural properties of MSNs can affect their biocompatibility, this was cleverly demonstrated by our group in a recent report. In this study we reported on the hemolytic properties of MSNs toward mammalian red blood cells (RBCs).[76] The cytotoxicity of amorphous silica toward RBCs has been previously reported, the mechanism proposed to account for this cytotoxicity is based on the interaction between the surface silanol groups and the tetra-alkyl ammonium groups that are found on the membrane of RBCs. We synthesized a regular MSN material and compared its properties with commercially available amorphous silica material. The solid state NMR experiment showed that MSNs contain twice the ratio of (Q2 + Q3)/Q4 sites unreacted than amorphous

silica, as a clear indication that the amount of silanols in MSNs is much higher than in amorphous silica. Surprisingly, the ζ-potential of MSNs (-35 mV) is lower than the one found for amorphous silica (-49 mV), which suggests that most of the silanol groups in MSNs are contained inside the nanochannels. When we tested the hemolytic properties of these two materials at different concentrations (20 – 100 μg/mL) we found that MSNs are non-toxic toward RBCs; on the contrary, amorphous silica induced a high degree of hemolysis confirming previous reports. To account for this performance we hypothesized that the strong electrostatic interaction between the continuous surface of silanol groups in the amorphous silica material with the RBCs membrane is the reason for its hemolytic properties. On the contrary, MSNs contain most of the silanol groups inside the nanochannels; moreover, their external surface is discontinuous because of mesoporosity, which results in a low hemolytic behavior. To further confirm that the silanol groups are responsible for the hemolytic properties of amorphous silica and MSNs, both were grafted with positive and negatively charged groups. After evaluating the hemolytic properties of these modified materials, none of them showed considerable cytotoxicity toward RBCs as a confirmation that indeed the silanol groups on the external surface of amorphous silica are the reason of its hemolytic properties. This report illustrated that contrary to the cytotoxicity of amorphous silica toward RBCs, MSNs showed a high biocompatibility upon the concentrations evaluated in this study. This finding offers promising potential for the application of MSNs in the fields of biomedicine and biotechnology. This study was recently confirmed by Haynes and co-workers using a mesoporous silica coated iron oxide nanoparticle.[77]

Applications of MSNs *in vivo* have been recently reported that might give us a general idea of their toxicological performance in animals. For instance, D.-M. Huang,[78, 79] T. Hyeon,[80] W. Lin,[81] and co-workers have demonstrated the use of MSNs as bio-imaging vehicles *in vivo*. Under the conditions used for their experiments, none of the authors observed toxicity effects *in vivo* during short-term. In addition, T. Hyeon and co-workers, followed the biodistribution of the material after 24h of intravenous injection, they found that MSNs nanoparticles accumulated mainly in liver, kidney, and spleen.

Recently, Langer and his group published a systematic investigation on the biocomaptibility of MSNs *in vitro* and *in vivo*.[82] As we mentioned before, the *in vitro* studies have previously shown that the biocompatibility of MSNs is concentration- and cell type-dependent, and this finding was just corroborated in this report. In the case of *in vivo* experiments the authors selected three different routes of administration; subcutaneous, intraperitoneal, and intravenous. The subcutaneous administration did not show a significant toxicity after long-term investigation on rats (3 months), even though high doses of MSNs were introduced (30 mg/mL). In the case of peritoneal administration, the authors found that the material is letal to SV129 mice during the first 24h after injection, but reducing the dose of material to 1mg/mL or less resulted in complete reduction of the toxicity. The same lethal effect as in the peritoneal injection was observed on the intravenous administration. The authors hypothesized that this toxicity maybe due to pulmonary embolism and/or thrombosis, but the death mechanism is still under investigation. It is important to mention that due to the chemical versatility of MSNs toward further functionalization, the toxicity at high concentrations of this material in vivo could be mitigated using polymers, liposomes, proteins, and/or other functional groups.[82-84]

Another important concern for the application of MSNs as drug delivery nanocarrier is what the final fate of the vehicle will be after it has accomplished its diagnostic/therapeutic purpose. The ideal situation would be that the material is biologically degraded in harmless byproducts, and finally cleared from the animal body through a safe route. Recently two studies related to this issue have been published. The authors reported on the degradability and clearance of silicon and silica materials *in vivo*.[84, 85] Because of their chemical similarity with MSNs we think that the findings reported in these papers could give us a close insight toward the final fate of MSNs *in vivo*. For instance, M. Sailor and co-workers studied the biodistribution of porous silicon nanoparticles. The authors found that the accumulation of material is mainly in the mononuclear phagocytic system organs, such as kidney, liver, and spleen.[85] A noticeable silicon clearance was observed from the mice body within a period of 1 week and the material was completely cleared in 4 weeks. The porous silicon nanoparticles did not show any considerable toxicity to the mice organs and their growth was similar as the control. The mechanism of clearance for these silicon nanoparticles after being degraded, presumably by lysosomes and released by cells, is attributed to its decomposition in soluble silicic acid followed by excretion through the renal system.

In a similar research, K. Wang and co-workers reported on the biodistribution an elimination of silica nanoparticles.[84] The authors found that these nanoparticles are accumulated mainly in the liver, kidney, and urinary bladder after few hours of being administrated through an intravenous injection. They also reported that the blood circulation time can be modified by coating the nanoparticles with different functional groups. Finally, the authors demonstrated that the silica nanoparticles are safely excreted through a renal route.

We anticipate that the data reported so far about the toxicological properties of MSNs *in vitro* and *in vivo* could be further improved, because the chemical versatility of MSNs to afford materials with better blood circulation times, adsorption-specificity, biodegradability, and clearance from animal/human body. We envision that these further MSNs modifications will show promising data for its future application as "theragnostic" nanovehicle in clinical trials.

7. Drug delivery systems

At the beginning of this century, the application of mesoporous silica as drug delivery vehicle was proposed.[17, 86] Our group has been the pioneer in the use of MSNs as platform for intracellular drug delivery. We have developed DDS based on MSNs capped with solid nanoparticles such as cadmium sulfide (CdS-),[17] gold (Au-),[87, 88] and iron oxide (IO-NPs),[89] and soft nanoparticles such as dendrimers,[53] proteins,[90] and polymers.[46] This gatekeeper strategy has allowed us to have site- and time-control of the release of the biogenic agent based on stimuli responsive linkers (Figure 6). We have used different biocompatible stimuli responsive triggers such as chemical reactions and light. Moreover, we have demonstrated that the use of nanoparticles as caps results in "zero premature release" of cargo before reaching the targeted site. All these advantages have resulted in promising applications of MSNs as drug delivery vehicles *in vitro* as we will describe below. We envision that soon these strategies will be applied to *in vivo* systems.

Our first approach to demonstrate the application of MSNs as DDS was based on the release of neurotransmitters using CdS-NPs as caps.[17] The CdS-NPs-MSNs system was synthesized using MSNs as the guest reservoir and a chemically labile disulfide bond linker. This linker was chemically attached to the CdS-NPs to afford the stimuli-responsive

gatekeeper approach. MSNs were loaded with biogenic cargoes (adenosine triphosphate (ATP), and vancomycin) and their release was triggered by reducing agents (dithiothreitol (DTT), and mercaptoethanol (ME). We successfully demonstrated the stimuli-responsive release of vancomycin/ATP in solution using DTT and ME as reducing agents. We later applied this system in astrocyte cell culture, where the stimuli-triggered release of ATP was monitored in an indirect way by the change in concentration of intracellular Ca^{2+}. Although, the release of ATP/vancomycin in this study was not intracellular; it demonstrated the utility of this material to carry a biogenic molecule without any premature release. In addition, the release was carried out in a stimuli-responsive fashion, and the vehicle showed a suitable biocompatibility *in vitro*. Following this first report, we also published on the use of MSNs as both gene and drug delivery system. This nanocarrier was synthesized based on MSNs and PAMAM dendrimers as caps.[53] Taking advantage of the positive charge of the PAMAM dendrimers we demonstrated the intracellular release of the plasmid DNA that encodes for an enhanced green fluorescence protein (EGFP) (Figure 7). We also tested the performance of the PAMAM-MSNs vehicle against enzymatic cleavage. We found that the PAMAM-MSNs material could protect DNA from enzymatic degradation. Interestingly, the gen transfection efficacy was better than current commercially available transfection agents. This demonstrated the ability of MSNs to carry, protect, transfer and release DNA vectors inside the cells. To prove the multi-task properties of this system, Texas red was loaded and localized intracellularly by confocal microscopy. In this report we demonstrated for the first time that MSNs can be applied as both drug and gene delivery vehicle.

One of the desirable features for any DDS is to have the ability to move the vehicle at will toward a specific-site. Following this idea we developed a MSN vehicle capped with

magnetic nanoparticles. In this material we kept the extraordinary advantages of MSNs as DDS, such as stimuli-responsive capability via a labile disulfide bond that is triggered using the intracellular reducing environment; "zero premature release"; biocompatibility; and efficient uptake by cells.[89] In addition to the above mentioned features we also added the ability of moving the nanocarriers to any desired site by means of an external magnetic field as we demonstrated in solution and *in vitro* in this study. This is the first report published on the synthesis and application of a drug delivery vehicle based on MSNs capped with magnetic nanoparticles.

As was mentioned above, different stimuli-responsive DDS can be developed based on MSNs. The stimuli to trigger these systems can be divided in two main categories; internal and external. The internal stimuli, such as change in pH, reducing environment, and enzymatic activity, depend upon the homeostasis of the cell. The external stimuli, such as light, ultrasound, and electromagnetic field these stimuli can be controlled and thus have the advantage of being time- and location-specific.[19] We recently reported on the synthesis and application in vitro of MSNs capped with photo responsive AuNPs (PR-AuNPs).[88] The working principle of this system is based on the electrostatic interaction between MSNs and PR-AuNPs (Figure 8). Upon irradiation with UV light, the umpolung of surface charge leads to repulsion of AuNPs releasing the cargo. We demonstrated this concept through photo-induced release of encapsulated fluorescein dyes. After that, we inoculated human cells (liver and fibroblast) with paclitaxel-loaded PR-AuNPs-MSNs and measured the viability of the cells. The cell proliferation was inhibited with the drug-loaded PR-AuNPs-MSN material after irradiation under mild conditions. We demonstrated for the first time that MSNs capped

with AuNPs can be efficiently loaded with drugs and can release inside human cells their cargo in a controlled fashion using an external trigger under biological conditions.

The ability to selectively functionalize the external surface of MSNs opens a wide range of possibilities in the field of drug delivery. We can foresee the development of a co-delivery system where different guest molecules could be loaded to and released in a controlled sequence. Indeed, we recently published a study that accomplished this target. We developed a glucose-responsive MSN vehicle that contains both insulin and cyclic adenosine monophosphate (cAMP). We were able to precisely control the sequence of release of both biogenic cargos.[90] The working principle of this system is based on the interaction of phenylboronic acid-modified MSNs (BA-MSNs) and gluconic acid-modified insulin (G-Ins) that works as cap. This interaction can be disrupted by the addition of different saccharides (glucose, fructose, galactose, mannose) that could displace G-Ins from MSNs opening the pore. Inside the nanochannels we loaded cAMP, which could be released in a controlled fashion after the displacement of G-Ins by saccharides. We successfully proved the release of both G-Ins and cAMP using different saccharides and pH conditions. Interestingly, the system showed to be selective toward glucose in typical diabetic levels. The system is biocompatible at the concentrations needed to have a therapeutic effect. We investigated the intracellular release of cAMP with rat pancreatic islet tumor (RIN-5F) cells using a Millipore cAMP HTS immunoassay to quantify the amount of cAMP. After comparing with cAMP in solution, we demonstrated that cAMP loaded G-Ins-MSNs efficiently released cAMP inside RIN-5F. This was further proved by confocal microscopy.

On the other hand, the versatility of MSNs can be demonstrated by just covalently linked a biogenic molecule onto its surface and intracellularly releasing it. This strategy

could increase the amount of cargo loaded keeping the "zero premature release" property. We demonstrated this concept by developing a cysteine-loaded MSN system. Cysteine is an amino acid required for the biological synthesis of glutathione (GSH), which is of vital importance for controlling the homeostasis of live cells.[91] We chemically anchored cysteine molecules on the surface of MSNs through a labile disulfide linker and measured their release. The release was triggered by different reducing agents in solution. The cysteine molecules have been chemically incorporated in MSNs with high efficiency through this approach. Moreover, we demonstrated the efficient endocytosis and cargo release of this material in HeLa cells by flow cytometry and confocal microscopy. We successfully demonstrated by a viability assay that this system is roughly 400 times more effective than conventional cysteine pro-drug (i.e. N-acetyl cysteine).

Uncapped MSNs have also shown their efficacy in the release of different cargos. For instance, we reported on the successful release of a membrane impermeable protein (cytochrome *c*).[40] To achieve this goal, we synthesized a large pore MSNs (5.4 nm). We demonstrated that the enzymatic activity of the cytochrome *c* after being loaded and released in solution was preserved. Besides, we corroborated by confocal microscopy that MSNs can efficiently transfer cytochrome *c* through the cell membrane and release it in the cytoplasm. Other biogenic molecules have been released using uncapped MSNs, such as camptothecin,[92] propidium iodide,[93] paclitaxel,[55] doxorubicin,[94] and different fluorophores.[95] To improve the release of these drug delivery vehicles Zink, Stoddart, and co-workers have developed the use of nanoimpellers.[93] The working principle for this system is based on the photoisomerization of azobenzene derivatives. The back and forth wagging of the azobenzene group acts as a molecular impeller that regulates the release of

cargoes from the channels of MSNs. The authors have demonstrated the successful application of this strategy in vitro using rhodamine B, propidium iodide, and camptothecin as cargoes.

8. Conclusions

In this review, we have described the most recent breakthroughs in the application of mesoporous silica nanoparticles for intracellular drug delivery. This research has taken us through a very exciting journey; starting from the investigation of the endocytic pathways for the uptake of MSNs, their intracellular trafficking, the ability of developing site-specific systems, their biocompatibility *in vivo* and *in vitro*, and finally their application as intracellular drug delivery vehicle. The studies reported in this review established the ability of the material to be efficiently internalized by cells and released from endosomes. Some of the endocytic and trafficking mechanisms have been described, but still some questions have to be answered in the near future. For instance, the final fate of MSNs is still unknown. In the case of the MSN-based target-specific nanovehicles encouraging results have been obtained *in vitro*, but these systems have not been applied *in vivo* and therefore its complete success is still questionable.

The investigation of the toxicological properties of nanomaterials is an area that has attracted a lot of attention in the last few years, mainly because this is the principal obstacle for applying nanomaterials *in vivo*. This research area for MSNs is still in its infancy; however, recent studies of biocompatibility *in vivo* have shown promising results. We believe that these toxicological issues can be overcome by using versatile functionalization schemes.

The use of MSNs as stimuli-responsive intracellular controlled drug delivery carrier using nanoparticles as gatekeepers has demonstrated a complete success *in vitro*. We

envision that new strategies could be developed based on external triggers such as near infrared, magnetic field and ultrasound. In addition, the ability of these nanocarriers to release the guest molecules in a site- and time-specific fashion has to be tested *in vivo*.

Finally, we envision that base on the knowledge that has been generated in the past few years, future breakthroughs addressing the synthesis of new nanocarriers and the clinical implementation of this nanotechnology will be developed.

Acknowledgement

The authors thank U.S. NSF (CHE-0239570), U.S. DOE, Office of Basic Energy Sciences (DE-AC02-07CH11358), and Plant Science Institute at Iowa State University for financial support.

REFERENCES

[1] A. Prokop, J. M. Davidson, J. Pharm. Sci. 2008, 97, 3518.

[2] R. Haag, F. Kratz, Angew. Chem., Int. Ed. 2006, 45, 1198.

[3] W. H. De Jong, P. J. A. Borm, Int. J. Nanomed. 2008, 3, 133.

[4] E. Soussan, S. Cassel, M. Blanzat, I. Rico-Lattes, Angew. Chem., Int. Ed. 2009, 48, 274.

[5] U. Boas, P. M. H. Heegaard, Chem. Soc. Rev. 2004, 33, 43.

[6] V. P. Torchilin, Nat. Rev. Drug Discovery 2005, 4, 145.

[7] N. Sanvicens, M. P. Marco, Trends Biotechnol. 2008, 26, 425.

[8] Z. Liu, X. Sun, N. Nakayama-Ratchford, H. Dai, ACS Nano 2007, 1, 50.

[9] T. A. Hilder, J. M. Hill, Small 2009, 5, 300.

[10] P. Ghosh, G. Han, M. De, C. K. Kim, V. M. Rotello, Adv. Drug Delivery Rev. 2008, 60, 1307.

[11] A. M. Smith, H. Duan, A. M. Mohs, S. Nie, Adv. Drug Delivery Rev. 2008, 60, 1226.

[12] C. Sun, S. H. Lee Jerry, M. Zhang, Adv Drug Deliv Rev 2008, 60, 1252.

[13] E. J. Anglin, L. Cheng, W. R. Freeman, M. J. Sailor, Adv. Drug Delivery Rev. 2008, 60, 1266.

[14] Y. Piao, A. Burns, J. Kim, U. Wiesner, T. Hyeon, Adv. Funct. Mater. 2008, 18, 3745.

[15] A. B. Descalzo, R. Martinez-Manez, F. Sancenon, K. Hoffmann, K. Rurack, Angew. Chem., Int. Ed. 2006, 45, 5924.

[16] B. G. Trewyn, I. I. Slowing, S. Giri, H.-T. Chen, V. S. Y. Lin, Acc. Chem. Res. 2007, 40, 846.

[17] C.-Y. Lai, B. G. Trewyn, D. M. Jeftinija, K. Jeftinija, S. Xu, S. Jeftinija, V. S. Y. Lin, J. Am. Chem. Soc. 2003, 125, 4451.

[18] S. Angelos, E. Johansson, J. F. Stoddart, J. I. Zink, Adv. Funct. Mater. 2007, 17, 2261.

[19] I. I. Slowing, J. L. Vivero-Escoto, C.-W. Wu, V. S. Y. Lin, Adv. Drug Delivery Rev. 2008, 60, 1278.

[20] M. A. Mintzer, E. E. Simanek, Chem. Rev. 2009, 109, 259.

[21] J. S. Beck, J. C. Vartuli, W. J. Roth, M. E. Leonowicz, C. T. Kresge, K. D. Schmitt, C. T. W. Chu, D. H. Olson, E. W. Sheppard, et al., J. Am. Chem. Soc. 1992, 114, 10834.

[22] A. Monnier, F. Schuth, Q. Huo, D. Kumar, D. Margolese, R. S. Maxwell, G. D. Stucky, M. Krishnamurty, P. Petroff, et al., Science 1993, 261, 1299.

[23] C. T. Kresge, M. E. Leonowicz, W. J. Roth, J. C. Vartuli, J. S. Beck, Nature 1992, 359, 710.

[24] D. Zhao, J. Feng, Q. Huo, N. Melosh, G. H. Frederickson, B. F. Chmelka, G. D. Stucky, Science 1998, 279, 548.

[25] S. A. Bagshaw, E. Prouzet, T. J. Pinnavaia, Science 1995, 269, 1242.

[26] S. Inagaki, Y. Fukushima, K. Kuroda, Chem. Commun. 1993, 680.

[27] S. Inagaki, A. Koiwai, N. Suzuki, Y. Fukushima, K. Kuroda, Bull. Chem. Soc. Jpn. 1996, 69, 1449.

[28] K. K. Unger, D. Kumar, M. Grun, G. Buchel, S. Ludtke, T. Adam, K. Schumacher, S. Renker, J. Chromatogr., A 2000, 892, 47.

[29] J. Rejman, V. Oberle, I. S. Zuhorn, D. Hoekstra, Biochem. J. 2004, 377, 159.

[30] S. Huh, J. W. Wiench, B. G. Trewyn, S. Song, M. Pruski, V. S. Y. Lin, Chem. Commun. 2003, 2364.

[31] I. Slowing, B. G. Trewyn, V. S. Y. Lin, J. Am. Chem. Soc. 2006, 128, 14792.

[32] D.-M. Huang, Y. Hung, B.-S. Ko, S.-C. Hsu, W.-H. Chen, C.-L. Chien, C.-P. Tsai, C.-T. Kuo, J.-C. Kang, C.-S. Yang, C.-Y. Mou, Y.-C. Chen, FASEB J. 2005, 19, 2014.

[33] M. Gruen, I. Lauer, K. K. Unger, Adv. Mater. 1997, 9, 254.

[34] Q. Cai, Z.-S. Luo, W.-Q. Pang, Y.-W. Fan, X.-H. Chen, F.-Z. Cui, Chem. Mater. 2001, 13, 258.

[35] H.-P. Lin, C.-Y. Mou, Acc. Chem. Res. 2002, 35, 927.

[36] M.-C. Chao, H.-P. Lin, C.-Y. Mou, Chem. Lett. 2004, 33, 672.

[37] S. Huh, J. W. Wiench, J.-C. Yoo, M. Pruski, V. S. Y. Lin, Chem. Mater. 2003, 15, 4247.

[38] B. G. Trewyn, C. M. Whitman, V. S. Y. Lin, Nano Lett. 2004, 4, 2139.

[39] S. Che, Z. Liu, T. Ohsuna, K. Sakamoto, O. Terasaki, T. Tatsumi, Nature 2004, 429, 281.

[40] I. I. Slowing, B. G. Trewyn, V. S. Y. Lin, J. Am. Chem. Soc. 2007, 129, 8845.

[41] A. Stein, B. J. Melde, R. C. Schroden, Adv. Mater. 2000, 12, 1403.

[42] J. Liu, Y. Shin, Z. Nie, J. H. Chang, L.-Q. Wang, G. E. Fryxell, W. D. Samuels, G. J. Exarhos, J. Phys. Chem. A 2000, 104, 8328.

[43] A. Vinu, K. Z. Hossain, K. Ariga, J. Nanosci. Nanotechnol. 2005, 5, 347.

[44] S. Sadasivan, D. Khushalani, S. Mann, J. Mater. Chem. 2003, 13, 1023.

[45] K. K. Sharma, A. Anan, R. P. Buckley, W. Ouellette, T. Asefa, J. Am. Chem. Soc. 2008, 130, 218.

[46] D. R. Radu, C.-Y. Lai, J. W. Wiench, M. Pruski, V. S. Y. Lin, J. Am. Chem. Soc. 2004, 126, 1640.

[47] P.-W. Chung, R. Kumar, M. Pruski, V. S. Y. Lin, Adv. Funct. Mater. 2008, 18, 1390.

[48] S. D. Conner, S. L. Schmid, Nature 2003, 422, 37.

[49] S. Mayor, R. E. Pagano, Nat. Rev. Mol. Cell Biol. 2007, 8, 603.

[50] F. R. Maxfield, T. E. McGraw, Nat. Rev. Mol. Cell Biol. 2004, 5, 121.

[51] R. A. Gemeinhart, D. Luo, W. M. Saltzman, Biotechnol. Prog. 2005, 21, 532.

[52] X. Xing, X. He, J. Peng, K. Wang, W. Tan, J. Nanosci. Nanotechnol. 2005, 5, 1688.

[53] D. R. Radu, C.-Y. Lai, K. Jeftinija, E. W. Rowe, S. Jeftinija, V. S. Y. Lin, J. Am. Chem. Soc. 2004, 126, 13216.

[54] T.-H. Chung, S.-H. Wu, M. Yao, C.-W. Lu, Y.-S. Lin, Y. Hung, C.-Y. Mou, Y.-C. Chen, D.-M. Huang, Biomaterials 2007, 28, 2959.

[55] J. Lu, M. Liong, S. Sherman, T. Xia, M. Kovochich, A. E. Nel, J. I. Zink, F. Tamanoi, NanoBiotechnology 2007, 3, 89.

[56] A. E. Nel, L. Madler, D. Velegol, T. Xia, E. M. V. Hoek, P. Somasundaran, F. Klaessig, V. Castranova, M. Thompson, Nat. Mater. 2009, 8, 543.

[57] W. Zauner, N. A. Farrow, A. M. R. Haines, J. Controlled Release 2001, 71, 39.

[58] N. Yamamoto, F. Fukai, H. Ohshima, H. Terada, K. Makino, Colloids Surf., B 2002, 25, 157.

[59] D. Goula, J. S. Remy, P. Erbacher, M. Wasowicz, G. Levi, B. Abdallah, B. A. Demeneix, Gene Ther. 1998, 5, 712.

[60] B. D. Chithrani, A. A. Ghazani, W. C. W. Chan, Nano Lett. 2006, 6, 662.

[61] B. D. Chithrani, W. C. W. Chan, Nano Lett. 2007, 7, 1542.

[62] W. Jiang, B. Y. S. Kim, J. T. Rutka, W. C. W. Chan, Nat. Nanotechnol. 2008, 3, 145.

[63] H. Jin, D. A. Heller, R. Sharma, M. S. Strano, ACS Nano 2009, 3, 149.

[64] H. Gao, W. Shi, L. B. Freund, Proc. Natl. Acad. Sci. 2005, 102, 9469.

[65] B. G. Trewyn, J. A. Nieweg, Y. Zhao, V. S. Y. Lin, Chem. Eng. J. 2008, 137, 23.

[66] H. Vallhov, S. Gabrielsson, M. Stromme, A. Scheynius, A. E. Garcia-Bennett, Nano Lett. 2007, 7, 3576.

[67] F. Lu, S.-H. Wu, Y. Hung, C.-Y. Mou, Small 2009, 5, 1408.

[68] J. M. Rosenholm, A. Meinander, E. Peuhu, R. Niemi, J. E. Eriksson, C. Sahlgren, M. Linden, ACS Nano 2009, 3, 197.

[69] M. Liong, J. Lu, M. Kovochich, T. Xia, S. G. Ruehm, A. E. Nel, F. Tamanoi, J. I. Zink, ACS Nano 2008, 2, 889.

[70] C.-P. Tsai, C.-Y. Chen, Y. Hung, F.-H. Chang, C.-Y. Mou, J. Mater. Chem. 2009, 19, 5737.

[71] I. Y. Park, I. Y. Kim, M. K. Yoo, Y. J. Choi, M.-H. Cho, C. S. Cho, Int. J. Pharm. 2008, 359, 280.

[72] D. Brevet, M. Gary-Bobo, L. Raehm, S. Richeter, O. Hocine, K. Amro, B. Loock, P. Couleaud, C. Frochot, A. Morere, P. Maillard, M. Garcia, J.-O. Durand, Chem. Commun. 2009, 1475.

[73] J.-S. Chang, B. Chang Ke Liang, D.-F. Hwang, Z.-L. Kong, Environ Sci Technol 2007, 41, 2064.

[74] W. Lin, Y.-w. Huang, X.-D. Zhou, Y. Ma, Toxicol. Appl. Pharmacol. 2006, 217, 252.

[75] Z. Tao, M. P. Morrow, T. Asefa, K. K. Sharma, C. Duncan, A. Anan, H. S. Penefsky, J. Goodisman, A.-K. Souid, Nano Lett. 2008, 8, 1517.

[76] I. I. Slowing, C.-W. Wu, J. L. Vivero-Escoto, V. S. Y. Lin, Small 2009, 5, 57.

[77] Y.-S. Lin, C. L. Haynes, Chem. Mater. 2009, 21, 3979.

[78] H.-M. Liu, S.-H. Wu, C.-W. Lu, M. Yao, J.-K. Hsiao, Y. Hung, Y.-S. Lin, C.-Y. Mou, C.-S. Yang, D.-M. Huang, Y.-C. Chen, Small 2008, 4, 619.

[79] J.-K. Hsiao, C.-P. Tsai, T.-H. Chung, Y. Hung, M. Yao, H.-M. Liu, C.-Y. Mou, C.-S. Yang, Y.-C. Chen, D.-M. Huang, Small 2008, 4, 1445.

[80] J. Kim, H. S. Kim, N. Lee, T. Kim, H. Kim, T. Yu, I. C. Song, W. K. Moon, T. Hyeon, Angew. Chem., Int. Ed. 2008, 47, 8438.

[81] K. M. L. Taylor, J. S. Kim, W. J. Rieter, H. An, W. Lin, W. Lin, J. Am. Chem. Soc. 2008, 130, 2154.

[82] S. P. Hudson, R. F. Padera, R. Langer, D. S. Kohane, Biomaterials 2008, 29, 4045.

[83] M. M. van Schooneveld, E. Vucic, R. Koole, Y. Zhou, J. Stocks, D. P. Cormode, C. Y. Tang, R. E. Gordon, K. Nicolay, A. Meijerink, Z. A. Fayad, W. J. M. Mulder, Nano Lett. 2008, 8, 2517.

[84] X. He, H. Nie, K. Wang, W. Tan, X. Wu, P. Zhang, Anal. Chem. 2008, 80, 9597.

[85] J.-H. Park, L. Gu, G. von Maltzahn, E. Ruoslahti, S. N. Bhatia, M. J. Sailor, Nat. Mater. 2009, 8, 331.

[86] M. Vallet-Regi, A. Ramila, R. P. del Real, J. Perez-Pariente, Chem. Mater. 2001, 13, 308.

[87] F. Torney, B. G. Trewyn, V. S. Y. Lin, K. Wang, Nat. Nanotechnol. 2007, 2, 295.

[88] J. L. Vivero-Escoto, I. I. Slowing, C.-W. Wu, V. S. Y. Lin, J. Am. Chem. Soc. 2009, 131, 3462.

[89] S. Giri, B. G. Trewyn, M. P. Stellmaker, V. S. Y. Lin, Angew. Chem., Int. Ed. 2005, 44, 5038.

[90] Y. Zhao, B. G. Trewyn, I. I. Slowing, V. S. Y. Lin, J. Am. Chem. Soc. 2009, 131, 8398.

[91] R. Mortera, J. Vivero-Escoto, I. I. Slowing, E. Garrone, B. Onida, V. S. Y. Lin, Chem. Commun. 2009, 3219.

[92] J. Lu, M. Liong, J. I. Zink, F. Tammanoi, Small 2007, 3, 1341.

[93] J. Lu, E. Choi, F. Tamanoi, J. I. Zink, Small 2008, 4, 421.

[94] T. Lebold, C. Jung, J. Michaelis, C. Braeuchle, Nano Lett. 2009, 9, 2877.

[95] J. M. Rosenholm, E. Peuhu, J. E. Eriksson, C. Sahlgren, M. Linden, Nano Lett. 2009, 9, 3308.

Table 1. Structural properties of organo-functionalized mesoporous silica nanoparticles.

Sample[a]	S[b] (m^2/g)	V[b] (cm^3/g)	MD[b] (nm)	OAS[b] (mmol/g)	Shape	PS[b]
AP-	721.7	0.45	2.37	1.7	Tubular	1-3 μm
AAP-	664.6	0.48	2.59	0.7	Twisted Columns	1-3 μm
AEP-	805.8	0.57	2.60	1.0	Spherical	0.5-2 μm
UDP-	1022.4	0.78	2.86	0.9	Spherical	0.5-2 μm
ICP-	840.1	0.66	2.58	1.5	Spherical	0.1-0.5 μm
CP-	1012.5	0.68	2.35	1.4	Rod	0.5-1 μm
AL-	1080.5	0.65	1.97	1.7	Rod	0.05-0.5 μm
MCM-41	767.1	0.55	2.55		Spherical	0.3-0.6 μm

[a] MSNs were functionalized with: 3-aminopropyltrimethoxysilane (AP-); N-(2-aminoethyl)-3-amino-propyltrimethoxysilane (AAP-); 3-[3-(2-aminoethylamino)ethylamino]-propyltrimethoxysilane (AEP-); ureido-propyltrimethoxysilane (UDP-); 3-isocyanto-propyltrimethoxysilane (ICP-); 3-cyano-propytriethoxysilane; allyl-trimethoxysilane (AL-)

[b] BET surface area (S); Mesopore volume (V); Mesopore diameter (MD); Amount of organic group (OAS); and Particle size (PS)

Table 2. Structural properties of mesoporous silica nanoparticles synthesized with room-temperature ionic liquids.

RTILs	S^b (m^2/g)	V^b (cm^3/g)	MD^b (nm)	Shape/Mesopore Structure
C_{14}MIM-MSN	729	0.664	2.71	Spherical/Hexagonal
C_{16}MIM-MSN	924	0.950	3.03	Ellipsoids/Hexagonal
C_{18}MIM-MSN	893	0.995	3.27	Rod/Pseudo-moiré
C_{14}OCMIM-MSN	639	0.695	2.61	Tubular/Wormhole

[a] MSNs were synthesized with: 1-tetradecyl-3-methylimidazolium bromide (C_{14}MIMBr); 1-hexadecyl-3-methylimidazolium bromide (C_{16}MIMBr); 1-octadecyl-3-methylimidazolium bromide (C_{18}MIMBr); and 1-tetradecyl-oxymethyl-3-3methylimidazolium chloride (C_{14}OCMIMCl).

[b] BET surface area (S); Mesopore volume (V); Mesopore diameter (MD); Amount of organic group (OAS); and Particle size (PS)

Table 3. Endocytic pathways for the internalization of mesoporous silica nanoparticles.

MSN material	Clathrin	Caveolae	Macropinocytosis
Non-functionalized	Yes	No	Yes
Receptor Functionalized	Yes	No	No
Amine-, guanidinio-functionalized	No	No	No

FIGURE CAPTIONS

Figure 1. Mesoporous silica nanoparticles as platform for drug delivery. (**A**) Nanoparticles attached to MSNs as functional gatekeepers. (**B**) Hydrophobic/hydrophilic guest molecules entrapped in the interior of the nanochannels. (**C**) Stimuli-responsive linkers chemically attached to MSN and nanoparticles. (**D**) Grafting with a protecting polymer such as PEG, which shields the MSN surface from interaction with opsonizing proteins. (**E**) Bioimaging agents such as magnetic nanoparticles, quantum dots, or fluorophores. (**F**) Targeting ligands such as antibodies. (**G**) Complexation with plasmid DNA. (**H**) Additional ligands such as the attachment of cell-penetrating peptides. (**I**) Incorporation of a diagnostic label. (**J**) Stimuli-responsive polymers. (**K**) Attachment of functional groups that could modify the metabolism of cells.

Figure 2. Scanning electron microscopy images of amorphous silica (left), and mesoporous silica nanoparticles (right).

Figure 3. Poly(lactic acid)-coated MSNs with fluorescence probe inside the channels. This system was synthesized based on our ability to selectively functionalize both surfaces (external/internal) of MSNs.

Figure 4. Pathways of mesoporous silica nanoparticles for entry to cells. Large particles are internalized by phagocytosis, whereas fluid uptake occurs by macropinocytosis. In the case of MSNs material, most of its internalization is via endocytic pathways. These pathways differ with regard to the nature of the surface functionalization and structural properties of MSNs.

Figure 5. Intracellular trafficking of mesoporous silica nanoparticles. (**A**) MSN is wrapped through specific (ligand-receptor) and nonspecific (hydrophobic, Coulombic) binding

interactions.(**B**) Once the MSN is internalized, depending on the endocytic pathway, it can be delivered to intermediate compartments (for example, caveosome). (**C**) Later these compartments are transported to early endosomes and then to sorting endosomes. From sorting endosomes, a fraction of the MSN is sorted back to the cell exterior through recycling endosomes (not showed in the scheme). (**D**) The remaining fraction is transported to secondary endosomes, (**E**) which fuse then with lysosomes. (**F**) The MSN then escape the endo-lysosomes and enter the cytosolic compartment.

Figure 6. Mesoporous silica nanoparticles have been engineered with nanoparticles that work as gatekeepers. These nanoparticles are attached to MSNs through stimuli-responsive linkers. This combination has afforded drug delivery vehicles that release its cargo in a space- and time-controlled fashion without any "premature release".

Figure 7. Mesoporous silica nanoparticles have been used for both gene and drug delivery. In this approach we used PAMAM dendrimers attached by a stimuli-responsive linker to the MSN as caps. The positive charge of the dendrimer complex to plasmid DNA and a guest molecule could be introduced in the nanochannels of the MSN. The release of plasmid DNA was successfully demonstrated by the expression of a green fluorescent protein (EGFP).

Figure 8. The application of external stimuli for the timing- and space-control release of guest molecules has been achieved using mesoporous silica nanoparticles. For example, we used a photo-responsive linker, which under biocompatible irradiation conditions can release its cargo *in vitro*.

Figure 1

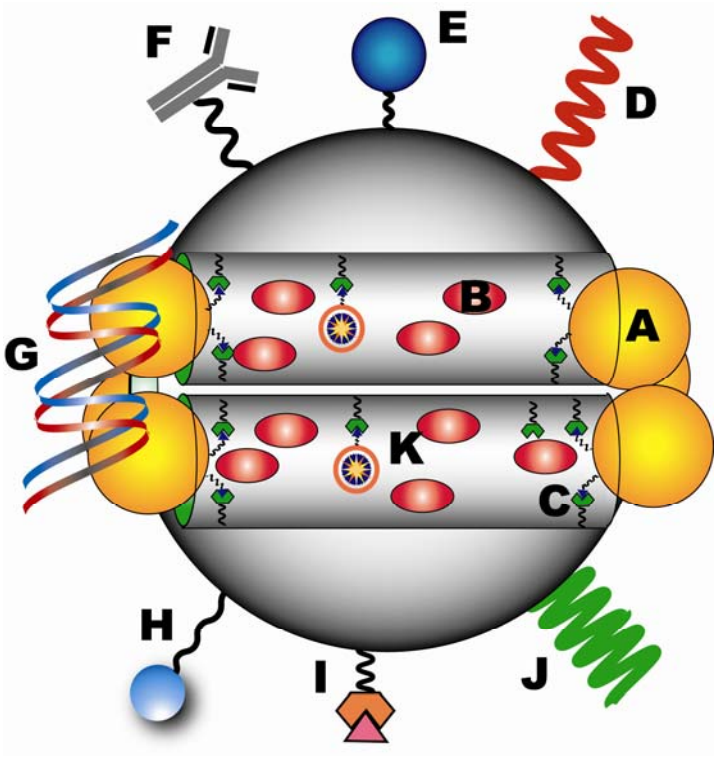

Figure 2

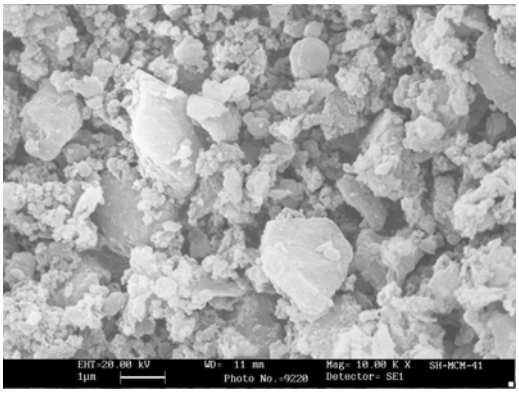
EHT=20.00 kV
WD= 11 mm
Mag= 10.00 K X
SH-MCM-41
1µm
Photo No.=9220
Detector= SE1

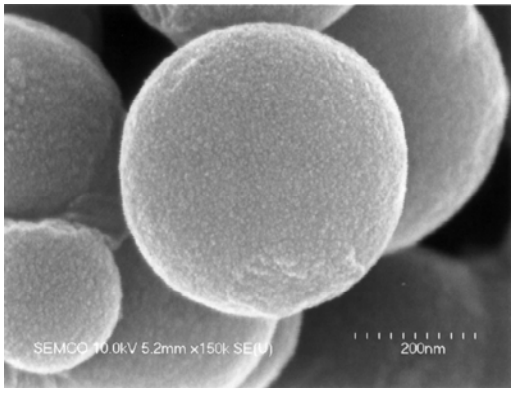
SEMCO 10.0kV 5.2mm x150k SE(U)
200nm

Figure 3

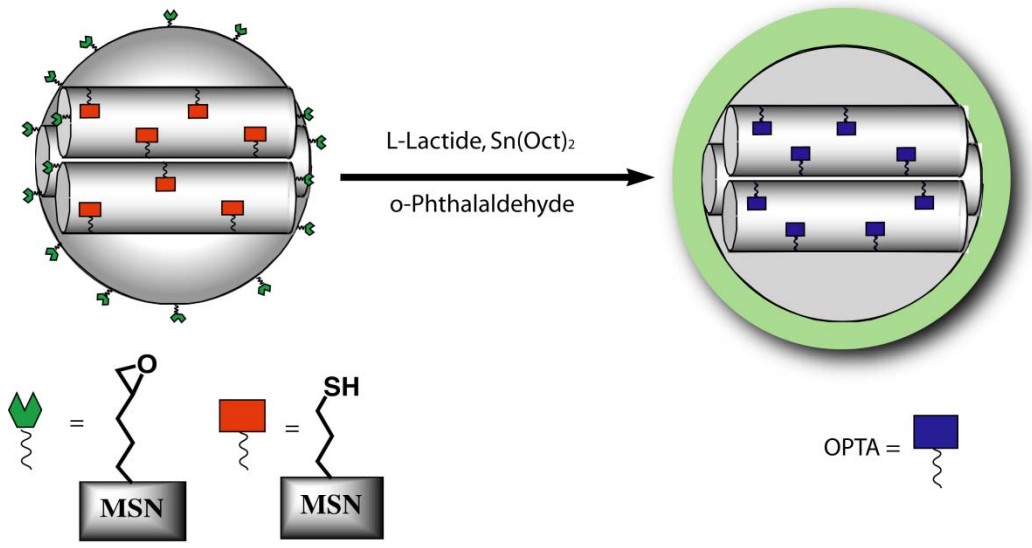

Figure 4

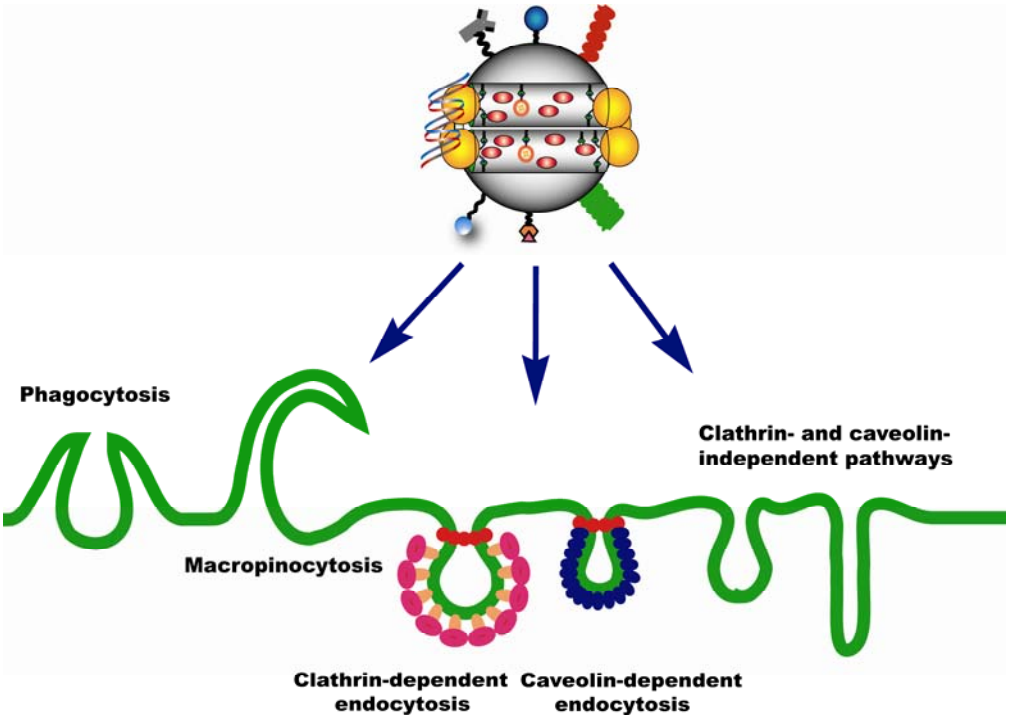
Phagocytosis
Clathrin- and caveolin-independent pathways
Macropinocytosis
Clathrin-dependent endocytosis
Caveolin-dependent endocytosis

Figure 5

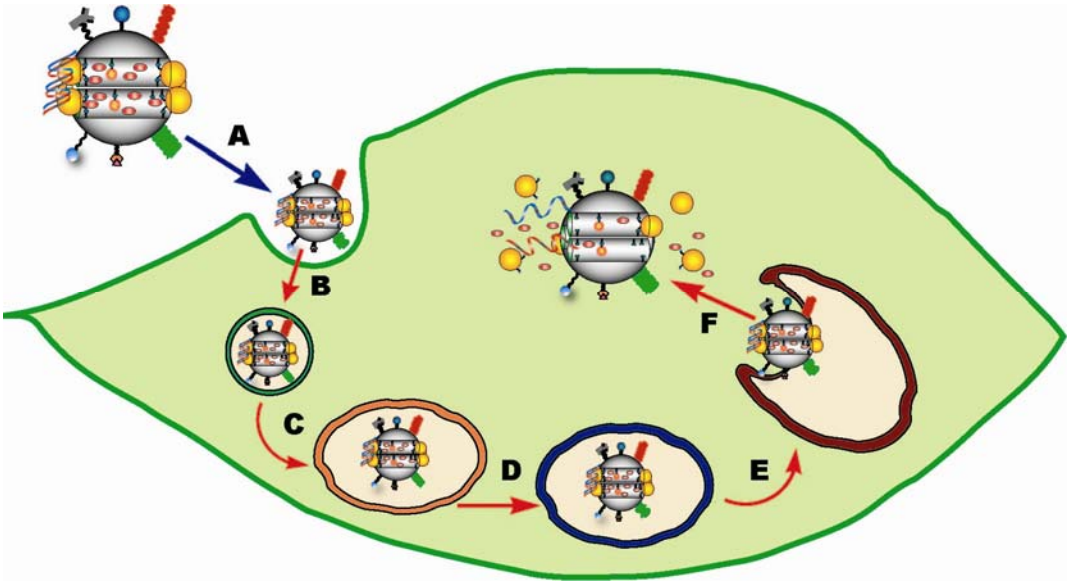

Figure 6

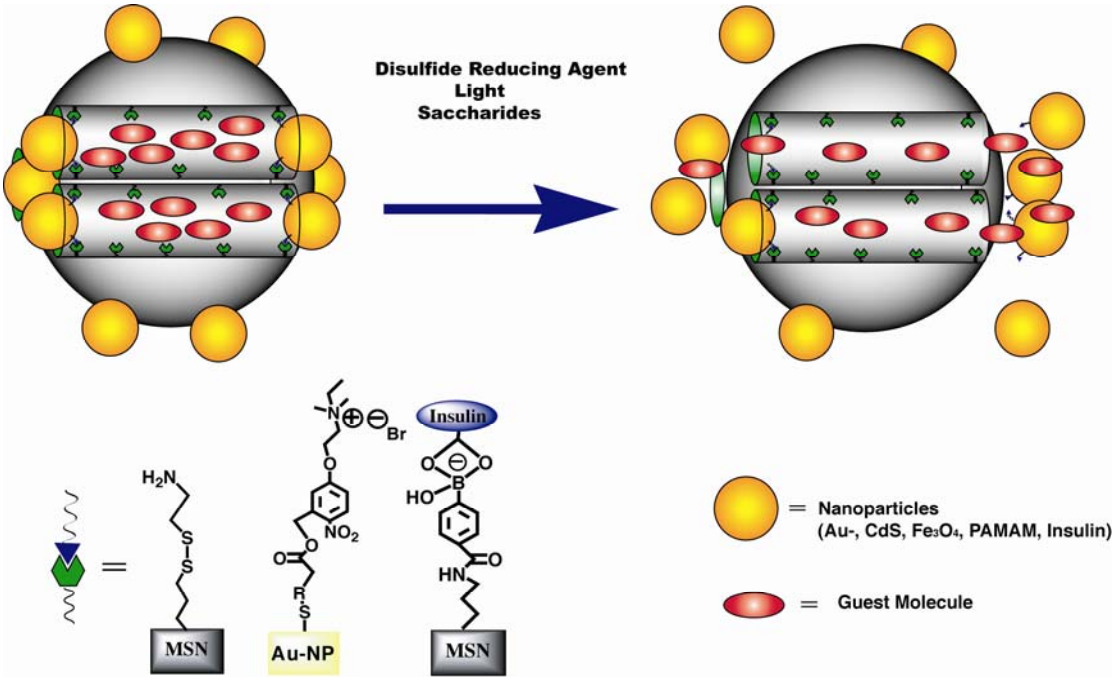
Disulfide Reducing Agent
Light
Saccharides
Insulin
MSN
Au-NP
MSN
= Nanoparticles
(Au-, CdS, Fe3O4, PAMAM, Insulin)
= Guest Molecule

Figure 7

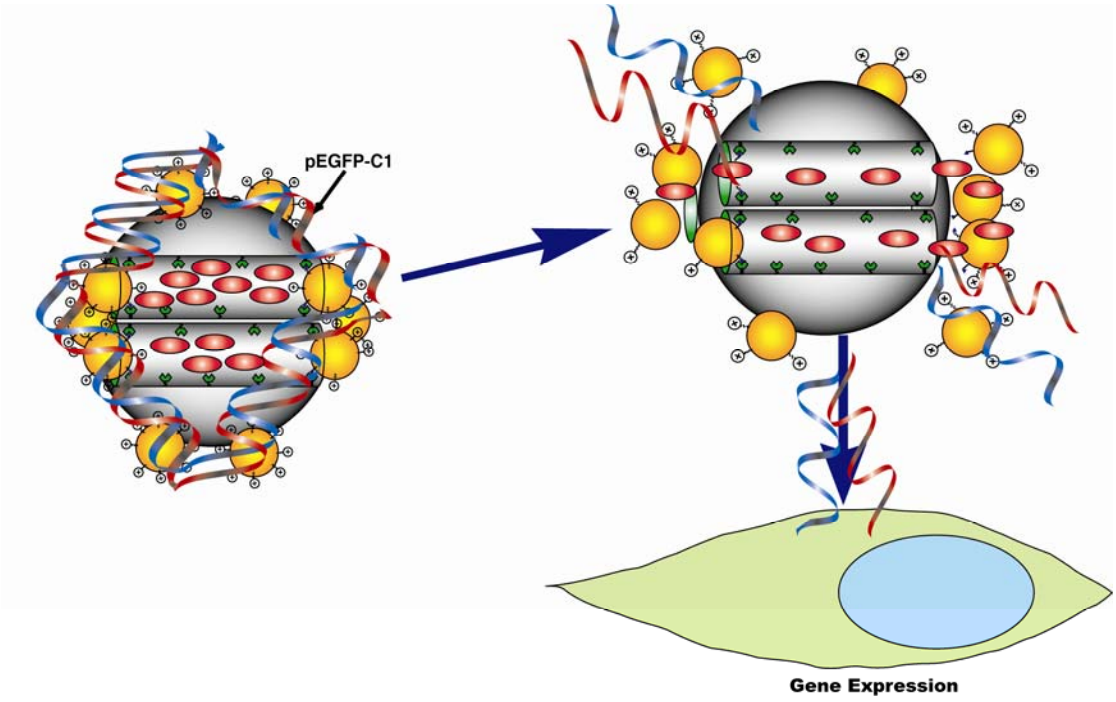

Figure 8

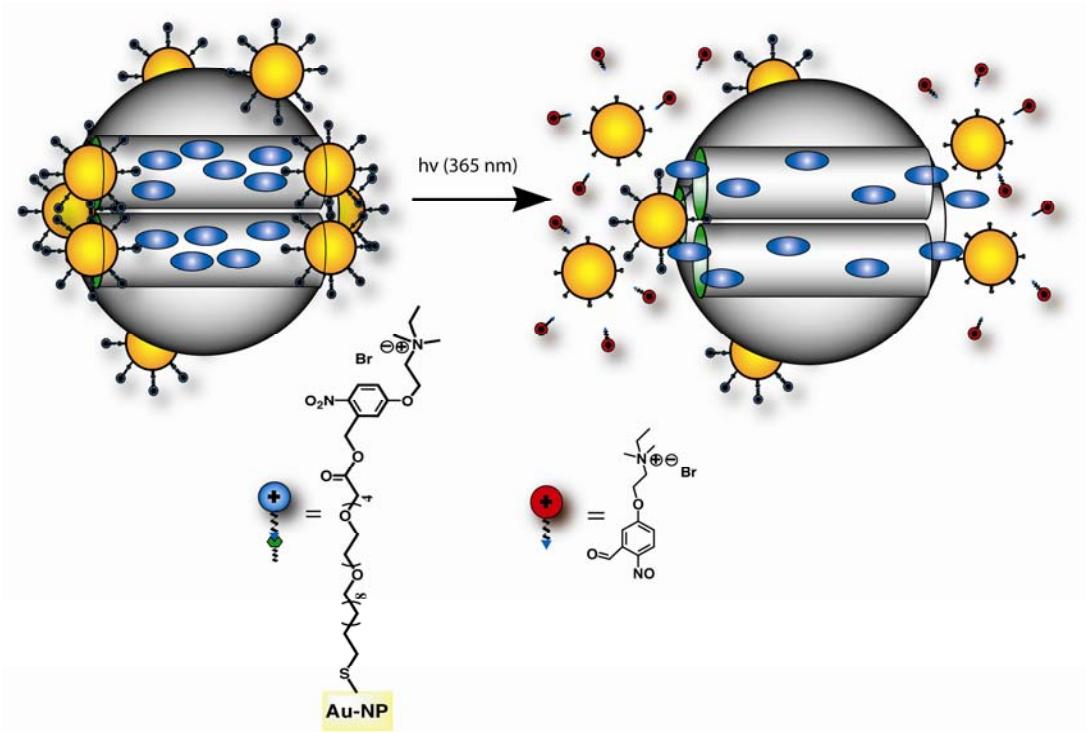

CHAPTER 3. PHOTO-INDUCED INTRACELLULAR CONTROLLED RELEASE DRUG DELIVERY IN HUMAN CELLS BY GOLD-CAPPED MESOPOROUS SILICA NANOSPHERE

A paper published on the **Journal of the American Chemical Society**
2009, 131, 3462-3463
Juan L. Vivero-Escoto, Igor I. Slowing, Chia-Wen Wu, and Victor S.-Y. Lin

Abstract

A gold nanoparticle (AuNP)-capped mesoporous silica nanosphere (MSN)-based intracellular drug delivery system (PR-AuNPs-MSN) for the photo-induced controlled release of an anticancer drug inside of human fibroblast and liver cells was synthesized, characterized, and evaluated. We found that the mesopores of MSN could be efficiently capped by the photo-responsive AuNPs without leaking the toxic drug, paclitaxel, in solution and *in vitro*. This "zero premature release" characteristic is of importance for delivery of toxic drugs that could produce side effects on healthy cells such as the ones used in chemotherapy. Furthermore, we demonstrated that the cargo-release property of this PR-AuNPs-MSN system could be easily controlled by an external stimulus using a low-power photo-irradiation source under biocompatible and physiological condition. We envision that our results would play a significant role in designing new generations of "remote control" nano-carrier materials for intracellular delivery of a variety of hydrophobic toxic drugs.

Introduction

Recent developments in designing surface functionalized mesoporous silica nanoparticles (MSNs) have revealed the promising potential of utilizing these structurally ordered materials for drug/gene delivery.[1-4] For many practical drug delivery applications,

such as chemotherapy, "zero-premature release" and "stimuli-responsive controlled release" of the precious and often toxic pharmaceutical cargo are two important prerequisites that would impact the therapeutic efficacy and cytotoxicity of drug delivery. Unfortunately, constructing drug delivery carriers with control over the location and timing of drug release under physiological conditions remains a challenge.

Recently, several MSN-based controlled-release systems with the "zero-premature release" property have been synthesized by using different kinds of pore-blocking caps, such as nanoparticles (NPs),[5-7] organic molecules,[8, 9] and supramolecular assemblies.[10, 11] Different stimuli-responsive strategies, such as chemical,[5] pH,[9, 12, 13] electrostatic interaction,[14] enzymatic,[15] redox,[16] and photo irradiation,[17-21] have been applied as "triggers" for uncapping the pores and releasing the guest molecules from MSNs. Despite these burgeoning developments, many of the MSN-based controlled release systems possess only one of the two features, but not both, and are unable to function under physiological conditions. For efficient controlled release of toxic drugs *in vitro* and/or *in vivo*, it would be advantageous to design a capped MSN material that would respond to a non-invasive and externally controllable trigger, such as photo-irradiation, under the physiological condition. Herein, we report on the synthesis of a gold nanoparticle-capped MSN material for the photo-induced intracellular controlled release of an anticancer drug, paclitaxel, inside of human fibroblast and liver cells as depicted in Scheme 1.

Results and Discussion

We first functionalized the surface of gold nanoparticle with a photo-responsive linker (thioundecyl-tetraethyleneglycolester-o-nitrobenzylethyldimethyl ammonium bromide, TUNA) by following a procedure reported by Rotello and co-workers[22] with modifications

as detailed in the Supporting Information (SI). The organically derivatized gold nanoparticles (PR-AuNPs) are positively charged (ζ-potential= +4.2 ± 1.4 mV) in PBS (pH 7.4) with an average particle diameter of 5 nm as determined by the transmission electron microscopy (Figure S1 of SI).

We then synthesized a MSN material according to our previously reported method.[11] The honey-comb like, MCM-41 type of mesoporous structure was confirmed by TEM (Figure 1a) and powder X-Ray diffractometry (Figure S2 of SI). As shown in Figure 1a, the MSN particle is spherical in shape with an average diameter of 100 nm. The N_2 sorption analysis of MSN further revealed a type IV BET isotherm with a total surface area of 1083 m^2/g. Also, a narrow BJH pore size distribution was observed with an average pore diameter of 3.0 nm (Figure S3 of SI).

The capping mechanism of this PR-AuNPs-MSN system is based on the electrostatic interaction between the positively charged PR-AuNPs and the negatively charged MSN material (ζ-potential= -23.8 ± 1.8 mV) in water. As illustrated in Scheme 1, upon photo-irradiation, the photo-labile linker covalently attached to the surface of PR-AuNPs would be cleaved, resulting in the formation of a cationic compound (1) as well as the negatively charged, thioundecyltetraethyleneglycolcarboxylate (TUEC)-functionalized AuNPs (NC-AuNPs).[22] The charge repulsion between the NC-AuNPs and MSN would then uncap the mesopores and allowed the release of guest molecules.

TEM microscopy was used to confirm the interaction between MSN and PR-AuNPs. Figure 1 shows the TEM micrographs of MSN before and after capping with PR-AuNPs. In the case of the uncapped MSN (Figure 1a), the hexagonally packed mesoporous channels could be clearly visualized. In contrast, the TEM micrograph of PR-AuNPs-capped MSN

(Figure 1b) shows dark spots on the outside edges of the mesopores, representing the aggregation of PR-AuNPs on the exterior surface of MSN. The presence of AuNPs was also confirmed by energy dispersive X-ray (EDX) analysis and powder XRD (Figure S4 of SI).

To investigate the photo-induced controlled release property of the PR-AuNPs-MSN system in aqueous solution, fluorescein was used as a model guest molecule. The fluorescein-loaded PR-AuNPs-MSN sample was prepared and the loading of fluorescein was determined to be 1.51 μmol/g of MSN as described in SI. To examine the capping efficiency, the fluorescein-loaded PR-AuNPs-MSN sample was first stirred for 21 h before irradiation. Less than 0.003 μmol/g of fluorescein was leached into the aqueous solution. This amount of leaching is similar to that of the control MSN sample without capping (Figure 2a). The result indicated that the capping strategy was successful with good efficiency. The photo-induced controlled release of fluorescein was investigated at 365 nm under low-power (0.49 mW/cm^2) UV irradiation for 10 min. The release reached 100% after stirring in water for 35 h as depicted in Figure 2a. The amount of fluorescein released from MSN was 0.11 μmol/g. A control experiment without UV irradiation was also carried out. No release of fluorescein was observed even after 80 h (Figure 2a). Furthermore, we examined the controlled release property at a wavelength (530 nm) that is known to induce local heating of AuNPs.[23] As detailed in Figure S7 of SI, less than 10% release of fluorescein was observed under much higher irradiation intensity (3 mW/cm^2) than that of the aforementioned condition at 365 nm (0.49 mW/cm^2). The result indicated that the release of fluorescein from PR-AuNPs-MSN was not due to the photothermal effect of AuNP.

To validate the feasibility of using the PR-AuNPs-MSN system for intracellular drug delivery in live human cells, a hydrophobic anticancer drug (paclitaxel) was chosen as the

guest molecule for the controlled release study in human liver and fibroblast cells. We found that the paclitaxel-loaded PR-AuNPs-MSN material was endocytosed rapidly by these two cell types as determined by flow cytometry as detailed in SI. After UV irradiation for 10 min, significant decreases in the cell viability, 44.2 and 43.5%, were observed for liver and fibroblast cells containing paclitaxel-loaded PR-AuNPs-MSN, respectively (Figure 2b, c, and 3). This result indicated that PR-AuNPs-MSN could indeed transport and release paclitaxel inside these live human cells under the control of photo-irradiation. Interestingly, without paclitaxel, the PR-AuNPs-MSN material alone, before and after the UV irradiation, was not toxic to cells as indicated in Figure 3. Also, by encapsulating the paclitaxel inside of MSN with the PR-AuNPs cap, the cytotoxicity of paclitaxel to liver and fibroblast cells was significantly lowered (Figure 3).

Conclusions

In conclusion, we have demonstrated that paclitaxel molecules could be encapsulated inside of PR-AuNPs-MSN without the undesired drug leaching inside of live human fibroblast and liver cells. This "zero premature release" characteristic is of importance for delivery of toxic drugs in chemotherapy. Furthermore, we proved that the cargo-release property of our PR-AuNPs-MSN system could be easily controlled by low-power photo-irradiation under biocompatible and physiological condition. We envision that our results would lead to a new generation of carrier materials for intracellular delivery of a variety of hydrophobic toxic drugs.

Acknowledgement

This work was supported by the U.S. National Science Foundation (CHE-0809521).

References

[1] I. I. Slowing, B. G. Trewyn, S. Giri, V. S. Y. Lin, Adv. Funct. Mater. 2007, 17, 1225.

[2] B. G. Trewyn, I. I. Slowing, S. Giri, H.-T. Chen, V. S. Y. Lin, Acc. Chem. Res. 2007, 40, 846.

[3] M. Vallet-Regi, A. Ramila, R. P. del Real, J. Perez-Pariente, Chem. Mater. 2001, 13, 308.

[4] M. Vallet-Regi, F. Balas, D. Arcos, Angew. Chem., Int. Ed. 2007, 46, 7548.

[5] C.-Y. Lai, B. G. Trewyn, D. M. Jeftinija, K. Jeftinija, S. Xu, S. Jeftinija, V. S. Y. Lin, J. Am. Chem. Soc. 2003, 125, 4451.

[6] F. Torney, B. G. Trewyn, V. S. Y. Lin, K. Wang, Nat. Nanotechnol. 2007, 2, 295.

[7] S. Giri, B. G. Trewyn, M. P. Stellmaker, V. S. Y. Lin, Angew. Chem., Int. Ed. 2005, 44, 5038.

[8] N. K. Mal, M. Fujiwara, Y. Tanaka, Nature 2003, 421, 350.

[9] R. Casasus, E. Climent, M. D. Marcos, R. Martinez-Manez, F. Sancenon, J. Soto, P. Amoros, J. Cano, E. Ruiz, J. Am. Chem. Soc. 2008, 130, 1903.

[10] S. Saha, K. C. F. Leung, T. D. Nguyen, J. F. Stoddart, J. I. Zink, Adv. Funct. Mater. 2007, 17, 685.

[11] D. R. Radu, C.-Y. Lai, K. Jeftinija, E. W. Rowe, S. Jeftinija, V. S. Y. Lin, J. Am. Chem. Soc. 2004, 126, 13216.

[12] S. Angelos, Y.-W. Yang, K. Patel, J. F. Stoddart, J. I. Zink, Angew. Chem., Int. Ed. 2008, 47, 2222.

[13] C. Park, K. Oh, S. C. Lee, C. Kim, Angew. Chem., Int. Ed. 2007, 46, 1455.

[14] K. C. F. Leung, T. D. Nguyen, J. F. Stoddart, J. I. Zink, Chem. Mater. 2006, 18, 5919.

[15] K. Patel, S. Angelos, W. R. Dichtel, A. Coskun, Y.-W. Yang, J. I. Zink, J. F. Stoddart, J. Am. Chem. Soc. 2008, 130, 2382.

[16] T. D. Nguyen, Y. Liu, S. Saha, K. C. F. Leung, J. F. Stoddart, J. I. Zink, J. Am. Chem. Soc. 2007, 129, 626.

[17] E. Johansson, E. Choi, S. Angelos, M. Liong, J. I. Zink, J. Sol-Gel Sci. Technol. 2008, 46, 313.

[18] S. Angelos, E. Choi, F. Voegtle, L. De Cola, J. I. Zink, J. Phys. Chem. C 2007, 111, 6589.

[19] J. Lu, E. Choi, F. Tamanoi, J. I. Zink, Small 2008, 4, 421.

[20] T. D. Nguyen, K. C. F. Leung, M. Liong, Y. Liu, F. Stoddart, J. I. Zink, Adv. Funct. Mater. 2007, 17, 2101.

[21] C. Park, K. Lee, C. Kim, Angew. Chem. Int. Ed. 2009, 48, 1275.

[22] G. Han, C.-C. You, B.-j. Kim, R. S. Turingan, N. S. Forbes, C. T. Martin, V. M. Rotello, Angew. Chem., Int. Ed. 2006, 45, 3165.

[23] I. H. El-Sayed, X. Huang, M. A. El-Sayed, Cancer Lett. 2006, 239, 129.

Figure captions

Figure 1. (a) TEM micrograph of MSN, the MCM-41 type mesoporous structure is clearly visualized with the light-colored parallel stripes and the hexagonally packed spots. **(b)** TEM micrograph of the PR-AuNPs-capped MSN shows the aggregation (dark spots) of the PR-AuNPs on the exterior surface of MSN.

Figure 2. (a) Controlled release profile of fluorescein-loaded PR-AuNPs-MSN after UV irradiation (▲), in dark (**X**), and the control sample, fluorescein-loaded MSN without the AuNPs cap (◆). Micrographs of human fibroblast cells containing paclitaxel-loaded PR-AuNPs-MSN before **(b)** and after **(c)** UV irradiation.

Figure 3. Cell viability study of the paclitaxel-loaded PR-AuNPs-MSN material with Human fibroblast **(a)** and liver **(b)** cells. All samples were UV-irradiated (365 nm) for 10 min. The concentration of material used was 10 μg/mL. Dark-gray and light-gray bars represent samples without and with irradiation, respectively.

Figure 1

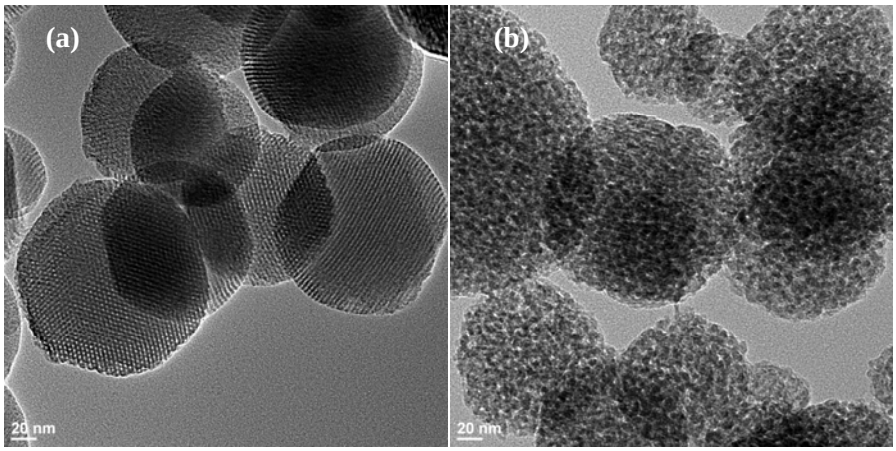

Figure 2

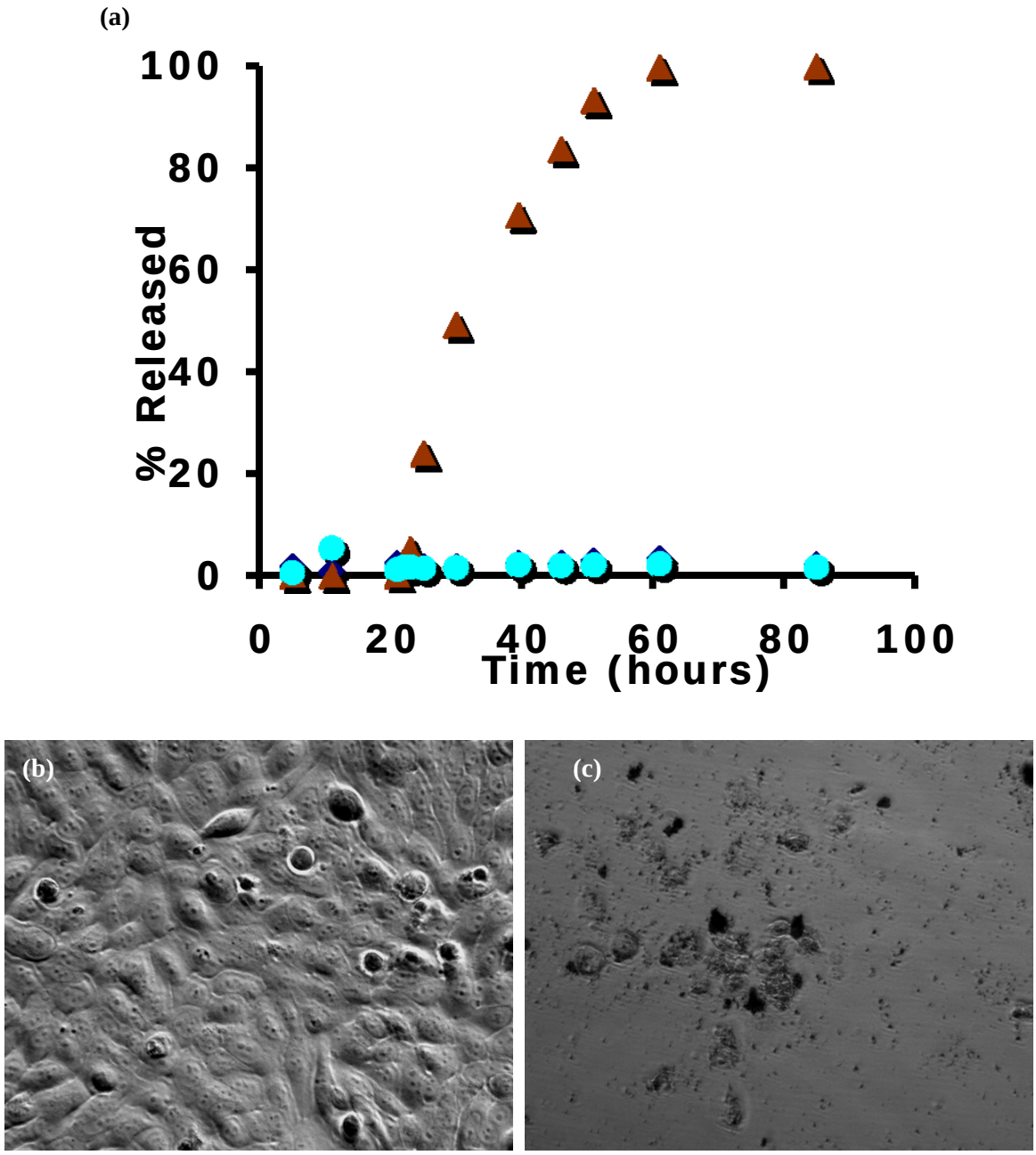

Figure 3

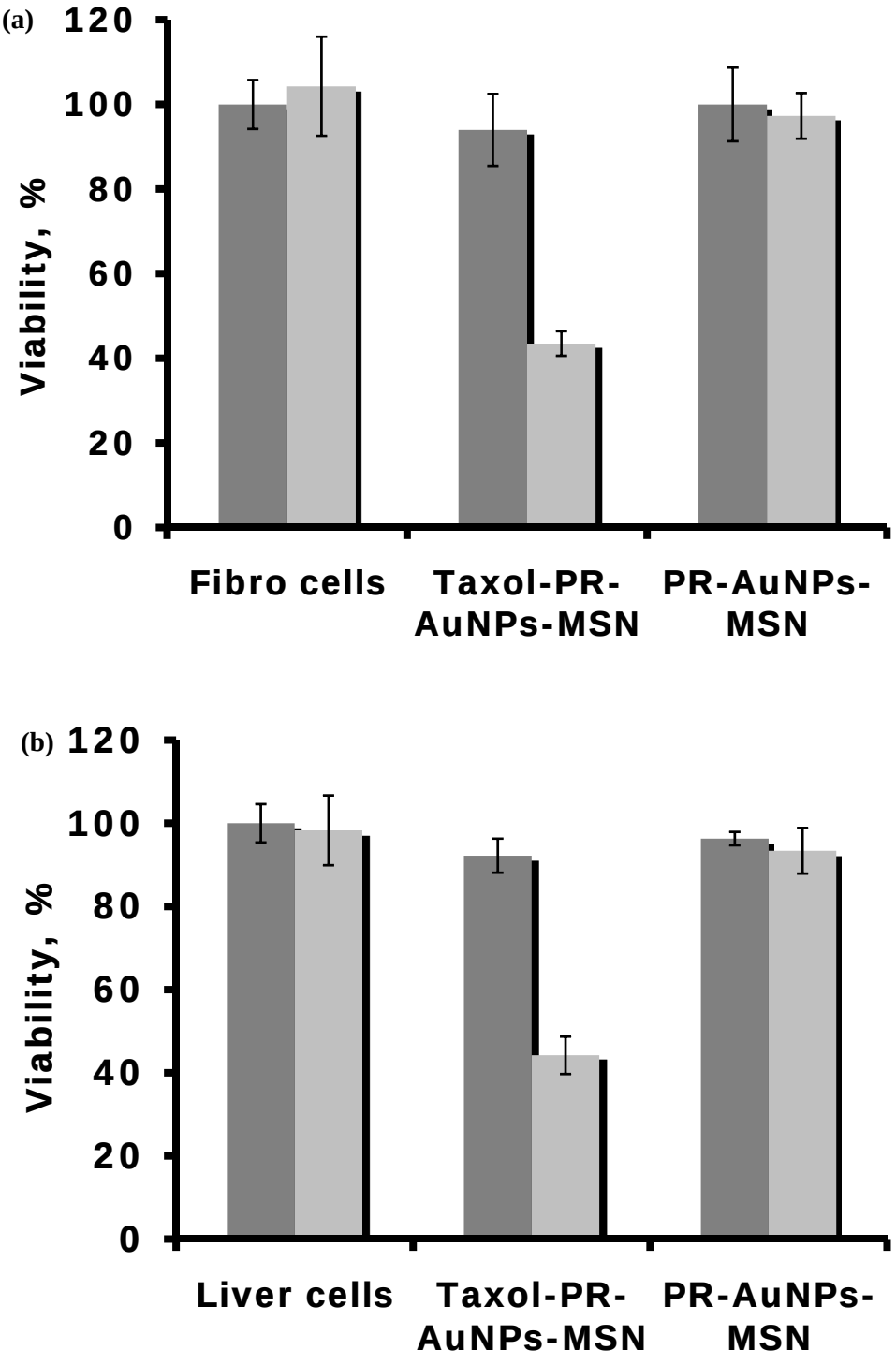
(a)
120
100
80
60
40
20
0
Viability, %
Fibro cells
Taxol-PR-AuNPs-MSN
PR-AuNPs-MSN
(b)
120
100
80
60
40
20
0
Viability, %
Liver cells
Taxol-PR-AuNPs-MSN
PR-AuNPs-MSN

Scheme captions

Scheme 1. Schematic illustration of the photo-induced intracellular controlled release of PR-AuNPs-MSN. Upon UV irradiation, the photo-labile linker on the PR-AuNPs was cleaved, changing the surface charge property (ζ-potential) of these gold nanoparticles from positive to negative. The charge repulsion between the AuNPs and MSN would then uncap the mesopores and allowed the release of guest molecules.

Scheme 1

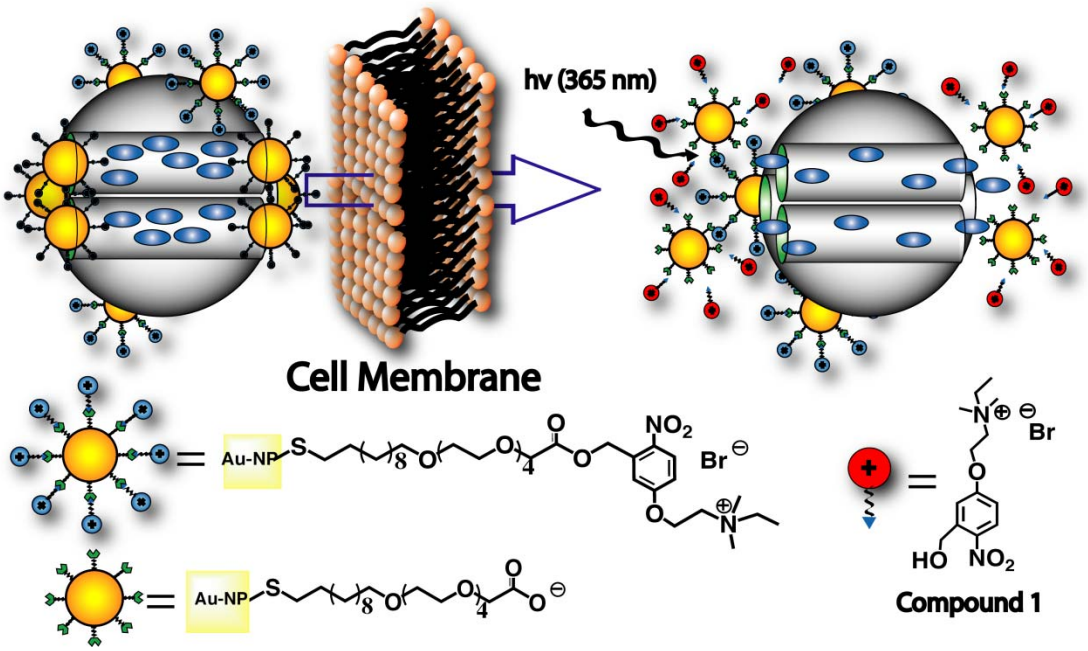

Appendix: Supporting information

Reagents and materials. Tetraethylorthosilicate (TEOS) was purchased from Gelest, Inc. Cetyltrimethylammonium bromide, trifluoroacetic acid, triisopropylsilane, 5-(2'-dimethylaminoethoxy)-2-nitrobenzyl alcohol, bromoethane, 1-ethyl-3-(3-dimethylaminopropyl)carbodiimide, fluorescein, and paclitaxel were purchased from Sigma-Aldrich, Inc. Donor Equine serum was purchased from HyClone, Inc. *L*-alanyl-*L*-glutamine, gentamicin sulfate, and penicillin-streptomycin solution were purchased from Mediatech, Inc. All chemicals were used as received.

Synthesis of negatively charged Gold Nanoparticles (NC-AuNPs). Following a literature procedure (Scheme S1),[1,2] Compound 1 (750 mg) were dissolved in dichloromethane (DCM), followed by the addition of trifluoroacetic acid (TFA, 2 mL, 26.9 mmol) and triisopropylsilane (1.5 mL, 7.32 mmol). The solution was stirred at room temperature for 12 h. Then the solvent was removed under vacuum. The as-synthesized compound (1.0 g) and 150 mg of Au-NPs[3] were dissolved in 25 mL of DCM. The mixture was stirred at room temperature for 3 days. After that, the solvent was removed under reduce pressure to afford the "protected" NC-AuNPs. The solid product obtained was added to 20 mL of MeOH:THF (1:1), followed by the addition of 6 mL of aqueous lithium hydroxide (1.0 M). This dispersion was stirred at room temperature for 9h. Finally, the solids obtained were centrifugated and washed several times to afford NC-AuNPs.

Synthesis of ethyl-[2-(3-hydroxymethyl-4-nitro-phenoxy)-ethyl]-dimethyl-ammonium bromide (2). The synthetic procedure was modified from a literature-reported method,[1] 5-(2'-Dimethylamino-ethoxy)-2-nitrobenzyl alcohol (400 mg, 1.665 mmol) was dissolved in DCM (40 mL) and bromoethane (5.5 mL, 74 mmol) was added slowly. This solution was

stirred at room temperature under dark conditions for 48 h. Then, the solvent and the excess of bromoethane were removed under vacuum to afford the desired product. ^{1}H-NMR (400 MHz, DMSO-d_6): δ 8.17 (d, J = 12.4 Hz, 1H), 7.38 (d, J = 4.0 Hz, 1H), 7.09 (dd, J = 12.4, 4.0 Hz, 1H), 4.85 (s, 2H), 4.58 (t, J = 6.8 Hz, 2H), 3.78 (t, J = 6.8 Hz, 2H), 3.46 (q, J = 9.6 Hz, 2H), 3.10 (s, 6H), 1.27 (t, J = 9.6 Hz, 3H). ^{13}C NMR (400 MHz. DMSO-d_6): 162.5, 142.9, 140.5, 128.1, 114.3, 113.6, 62.9, 61.9, 60.8, 60.3, 50.9, 8.7 MS(ESI): m/z[M-Br]$^{+}$: 269; [M-Br]$^{++}$: 268.

Synthesis of photo-responsive AuNPs (PR-AuNPs). NC-AuNPs (50 mg) and 1-ethyl-3-(3-dimethylaminopropyl) carbodiimide (EDC; 63.3 mg; 0.330 mmol) were added to 15 mL of nanopure water and stirred for 10 min. To this solution, 57.6 mg of Compound 2 (0.165 mmol) were added. The final mixture was stirred for 72 h under dark conditions. Finally, the solid product was washed several times with dry methanol, and dried under high vacuum.

Synthesis of mesoporous silica nanoparticles (MSN). The detailed synthetic procedure for the preparation and purification of MSN was described in our previous reports.[4,5]

Characterization of materials. Surface analysis of MSN was performed by nitrogen sorption isotherms in a Micromeritics TriStar surface area and porosity analyzer. The powder diffraction patterns of MSN were measured by Scintag XDS-2000 powder diffractometer using Cu Kα irradiation. Particle morphology was investigated by using Tecnai G^2 F20 transmission electron microscopy operating at 200 kV.

ζ-potential measurements. The ζ-potential of MSN, NC-AuNPs, PR-AuNPs, were measured in a Malvern Nano HT Zetasizer. Each material was tested five times. Solutions (500 μg/mL) of each material in PBS buffer (10 mM, pH 7.4) were prepared. After sonication of the suspension for 10 min the ζ-potential was measured.

Loading experiments. MSN (20.0 mg) was added to 10 mL of a previously prepared fluorescein solution (25 μM; PBS solution: 10 mM, pH 7.4). This suspension was stirred for 24 h. Then, PR-AuNPs (20.0 mg) were added to the suspension, the mixture was stirred for another 24 h. After that, the material was centrifuged, washed several times with PBS buffer (at least 10) to get rid of any fluorescein physisorbed, and dried under high vacuum. The supernatant and all the washings solutions were collected and the amount of fluorescein washed was measured using fluorescent spectroscopy (FluoroMax-2, λ_{ex}: 488 nm, λ_{em}: 515 nm). The loading of fluorescein was calculated with the difference between the original and the washed amount of fluorescein.

Releasing experiments. Fluorescein-loaded PR-AuNPs-MSN material (10.0 mg) was redispersed in 3 mL of PBS solution. This dispersion was stirred for 21h at room temperature. The amount of fluorescein leaked from the material was measured by fluorescent microscopy (FluoroMax-2, λ_{ex} 488 nm, λ_{em}: 515 nm). Then, the solution was irradiated for 10 min either with a hand-held low power (0.49 mW/cm^2, Radiometer DSE-100H/L) UV lamp (Spectroline® Model ENF-240C, 365 nm) or a HBO mercury short arc lamp (3.0 mW/cm^2, Radiometer DSE-100H/L) filtered through a 530 nm filter ((Brightline® FF01). After that, the solution was stirred for more than 40h and the release of fluorescein was monitored by fluorescent spectroscopy at different periods of time.

Loading of paclitaxel into MSN. A solution of paclitaxel (1.5 mg) in DMSO (1.5 mL) was added to MSN (10.0 mg). This mixture was let in contact for 24h. After that, the paclitaxel physisorbed MSN was washed at least three times with DMSO and finally dried under high vacuum.

Capping of paclitaxel-physisorbed MSN with PR-AuNPs. PR-AuNPs (5 mg) and paclitaxel-physisorbed MSN (5 mg) were added to 1 mL of PBS solution (10 mM, pH 7.4). The dispersion was stirred for 24 h. Then the material was centrifuged and washed at least twice with DMSO and PBS solution. The material was dried under high vacuum and kept in dark until the in vitro experiments were carried out.

Cell viability study of paclitaxel-physisorbed PR-AuNPs-MSN in human liver and fibroblast cells. Liver or Fibroblast cells were seeded in 24-well plates at the concentration of $1x10^5$ cells/mL and were incubated for 24h in D-10 medium (Dubelcco Modified Eagle's Medium plus fetal bovine serum, *L*-alanyl-*L*-glutamine, gentamicin sulfate, and penicillin-streptomycin solution). Then, the D-10 medium was replaced by a dispersion of paclitaxel-physisorbed PR-AuNPs-MSN in D-10 medium (10 μg/mL). The Liver/Fibroblast cells were incubated with this dispersion for 12 h. After that, the plates were photo irradiated for 10 min with a hand-held low power (0.49 mW/cm^2) UV lamp (365 nm). As a control experiment, a plate of Liver and Fibroblast cells containing the paclitaxel-physisorbed PR-AuNPs-MSN material was kept in dark during the same time. Both Liver and Fibroblast cells samples were incubated for another 36 h. Finally, the cytotoxicity of the samples was evaluated by means of Guava test and flow cytometry.

References

[1] Han, G.; You, C.-C.; Kim, B.-j.; Turingan, R. S.; Forbes, N. S.; Martin, C. T.; Rotello, V. M. Angew. Chem., Int. Ed. 2006, 45, 3165-3169.

[2] Houseman, B. T.; Mrksich, M. J. Org. Chem. 1998, 63, 7552-7555.

[3] Brust, M.; Walker, M.; Bethell, D.; Schiffrin, D. J.; Whyman, R. J. Chem. Soc., Chem. Commun. 1994, 801-2.

[4] Radu, D. R.; Lai, C.-Y.; Jeftinija, K.; Rowe, E. W.; Jeftinija, S.; Lin, V. S. Y. J. Am. Chem. Soc. 2004, 126, 13216-13217.

[5] Lai, C.-Y.; Trewyn, B. G.; Jeftinija, D. M.; Jeftinija, K.; Xu, S.; Jeftinija, S.; Lin, V. S. Y. J. Am. Chem. Soc. 2003, 125, 4451-4459.

Table S1. Structural properties of MSN and PR-AuNPs-MSN. The BET surface area, pore size and volume of the AuNPs capped MSN decreased dramatically in comparison with the one measured for MSN.

Property	**MSN**	**PR-AuNPs-MSN**
Surface Area (m^2/g)	1082.5	124.6
Pore Volume (cm^3/g)	1.2286	0.2058
Pore Size (nm)	3.0	---

Table S2. ζ-potential measurements of MSN, NC-AuNPs, and PR-AuNPs.

Material	**ζ-potential (mV)**
MSN	-23.8 ± 1.8
NC-AuNPs	-33.4 ± 1.3
PR-AuNPs	+4.2 ± 1.4

Figure captions

Figure S1. Transmission electron micrographs (TEM) of AuNPs. The size of the nanoparticles is between 4-7 nm (Scale bar: 5 nm).

Figure S2. Powder X-ray diffraction patterns of MSN (◆) and PR-AuNPs-MSN (■). The original material exhibited hexagonal type mesoporous structure characteristic of MCM-41. The PXRD shows a clear decrease in the intensity of the MCM-41 type peaks after capping with PR-AuNPs.

Figure S3. N_2 sorption isotherms of MSN (◆) and PR-AuNPs-MSN (■). **(a)** BET nitrogen sorption isotherms, and **(b)** BJH pore size distribution. The blocking of the MSN pores by PR-AuNPs was confirmed by the N_2 adsorption/desorption isotherms. A change in the shape of the isotherm from type IV to type I after capping and the disappearing of the maximum peak in the BJH pore size distribution were observed.

Figure S4. (a) Scanning electron micrograph (SEM) and energy dispersive X-ray (EDX) analysis of PR-AuNPs-MSN. **(b)** Long-angle XRD. The dark spots in the SEM micrograph were confirmed as AuNPs by EDX method and its crystallinity was corroborated by long-angle XRD.

Figure S5. FTIR spectra of PR-AuNPs. The FT-IR spectra of PR-AuNPs confirmed the success of the coupling reaction between NC-AuNPs and the cationic *o*-nitrobenzyl alcohol (see compound 2 in Scheme S2). We observed, the characteristic peaks for aromatic C-H (3056, and 3017 cm^{-1}), aliphatic C-H (2924, and 2853 cm^{-1}), ester (1748 cm^{-1}), and aromatic-nitro (1501 cm^{-1} and 1324/1275 cm^{-1}) stretching vibrations.

Figure S6. Micrographs of liver cells containing placlitaxel-loaded PR-AuNPs-MSN; **(a)** before, and **(b)** after irradiation.

Figure S7. (a) Controlled release profile of fluorescein-loaded PR-AuNPs-MSN after UV irradiation at ~365 nm (◆), and ~530 nm (■). **(b)** UV changes of PR-AuNPs-MSN upon irradiation at ~365 nm (▲/λ = 304 nm) and ~530 nm (◆/λ = 304 nm). Irradiation led to a decrease in absorption at 304 nm, as an indication of the breakage of the photo-labile ester bond.

Figure S1

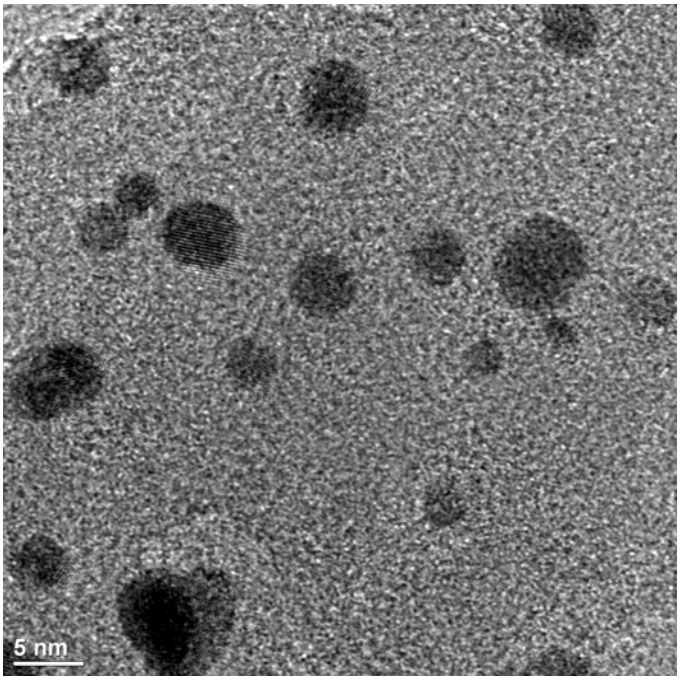

Figure S2

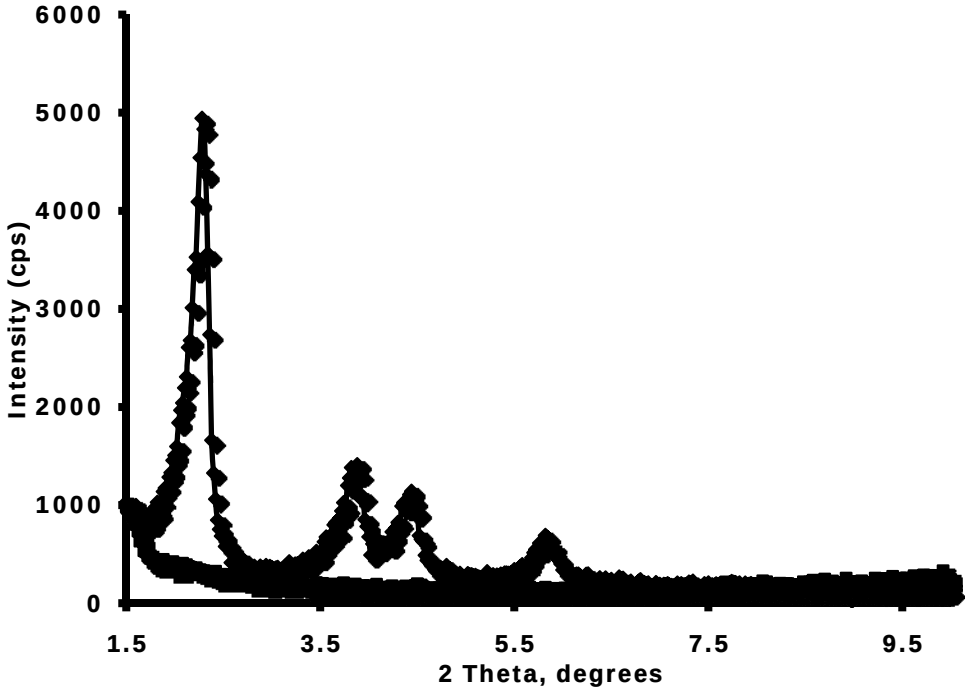
6000
5000
4000
3000
2000
1000
0
Intensity (cps)
1.5
3.5
5.5
7.5
9.5
2 Theta, degrees

Figure S3

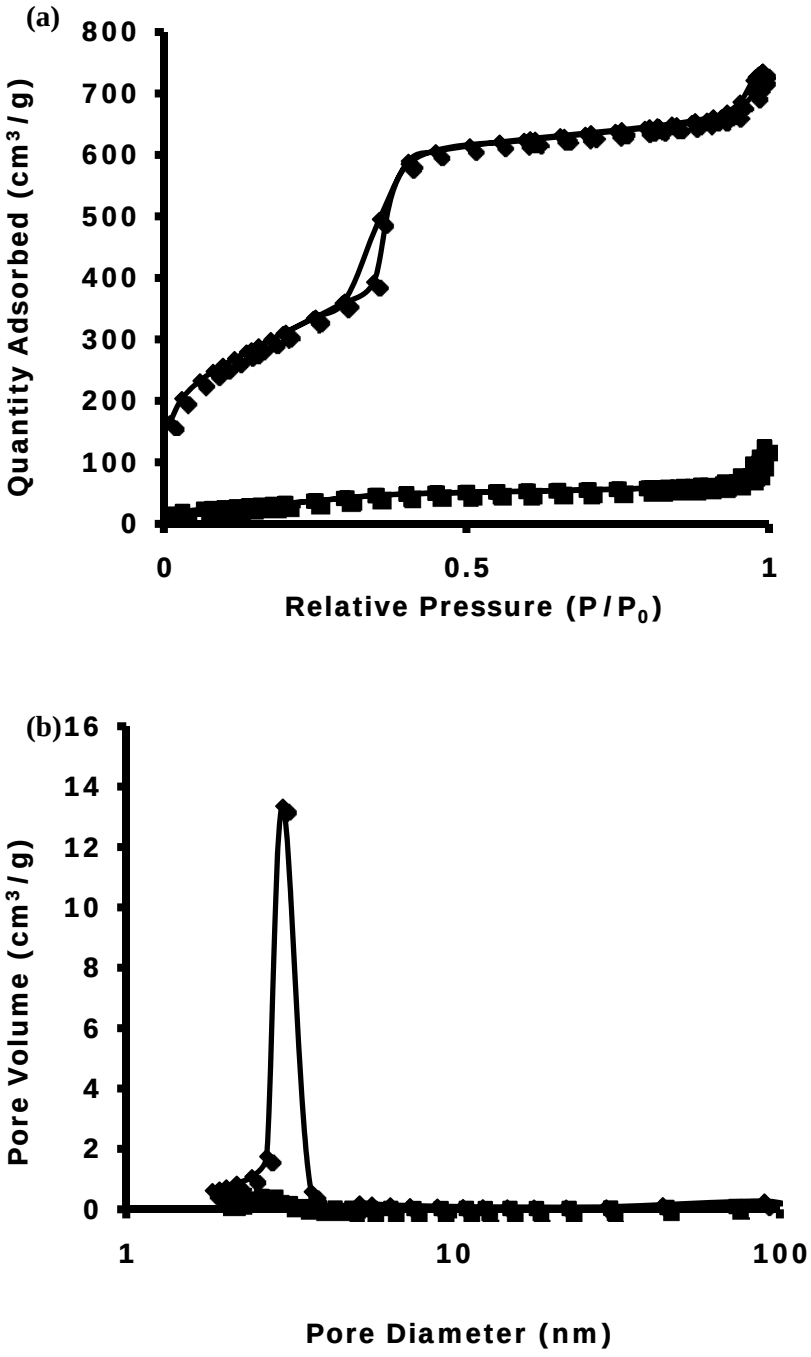
(a)
800
700
600
500
400
300
200
100
0
Quantity Adsorbed (cm³/g)
0
0.5
1
Relative Pressure (P/P0)
(b)16
14
12
10
8
6
4
2
0
Pore Volume (cm³/g)
1
10
100
Pore Diameter (nm)

Figure S4

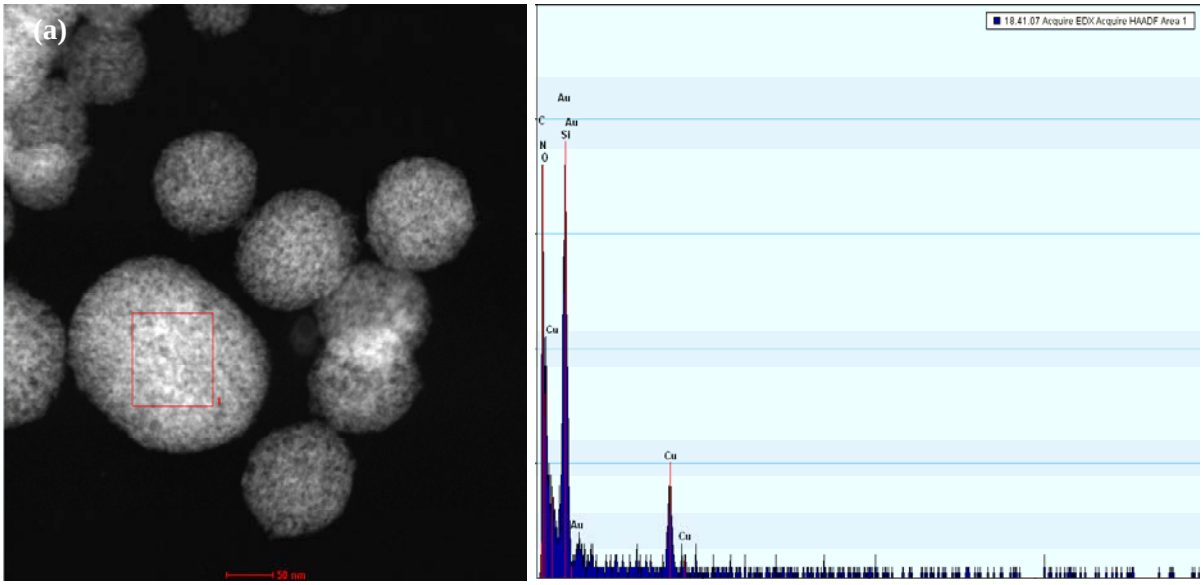
(a)
18.41.07 Acquire EDX Acquire HAADF Area 1
Au
C
Au
Si
N
O
Cu
Cu
Au
Cu

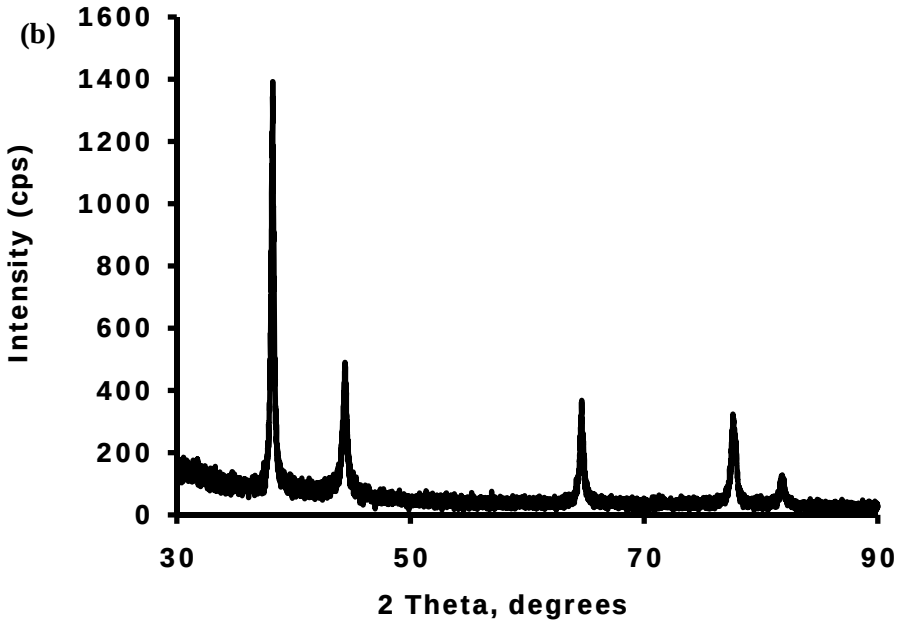
(b)
1600
1400
1200
1000
800
600
400
200
0
Intensity (cps)
30
50
70
90
2 Theta, degrees

Figure S5

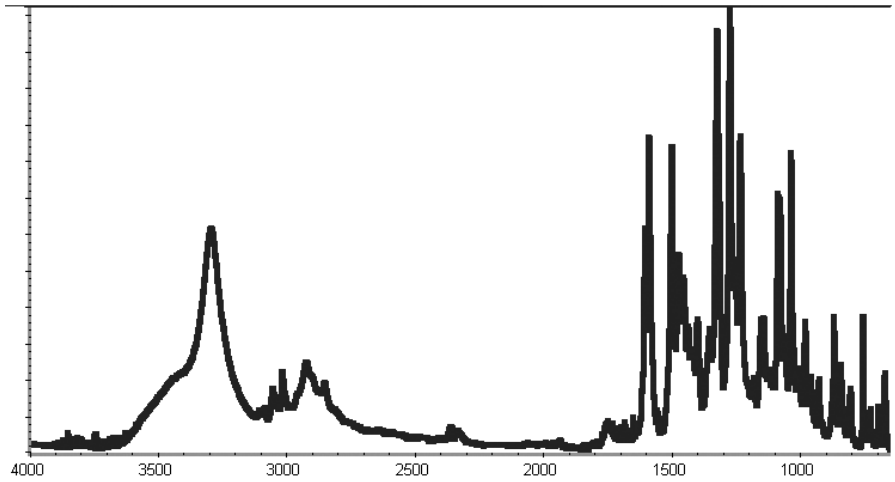

Figure S6

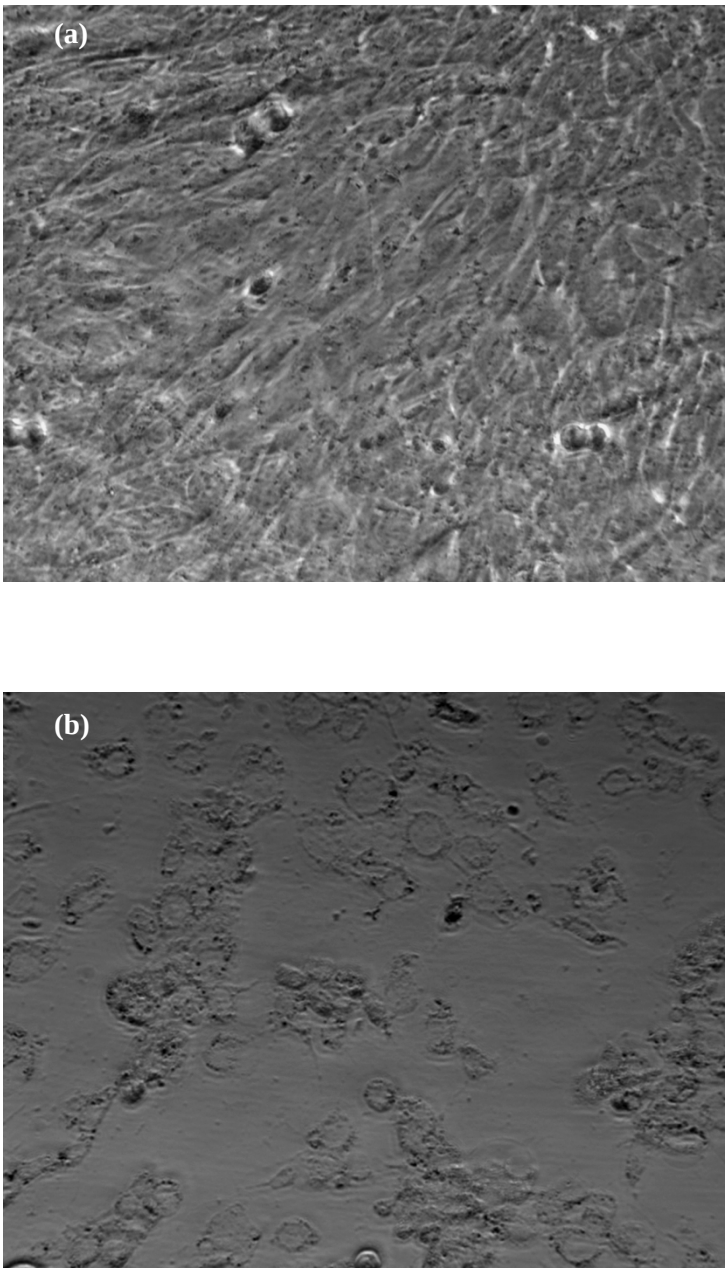

Figure S7

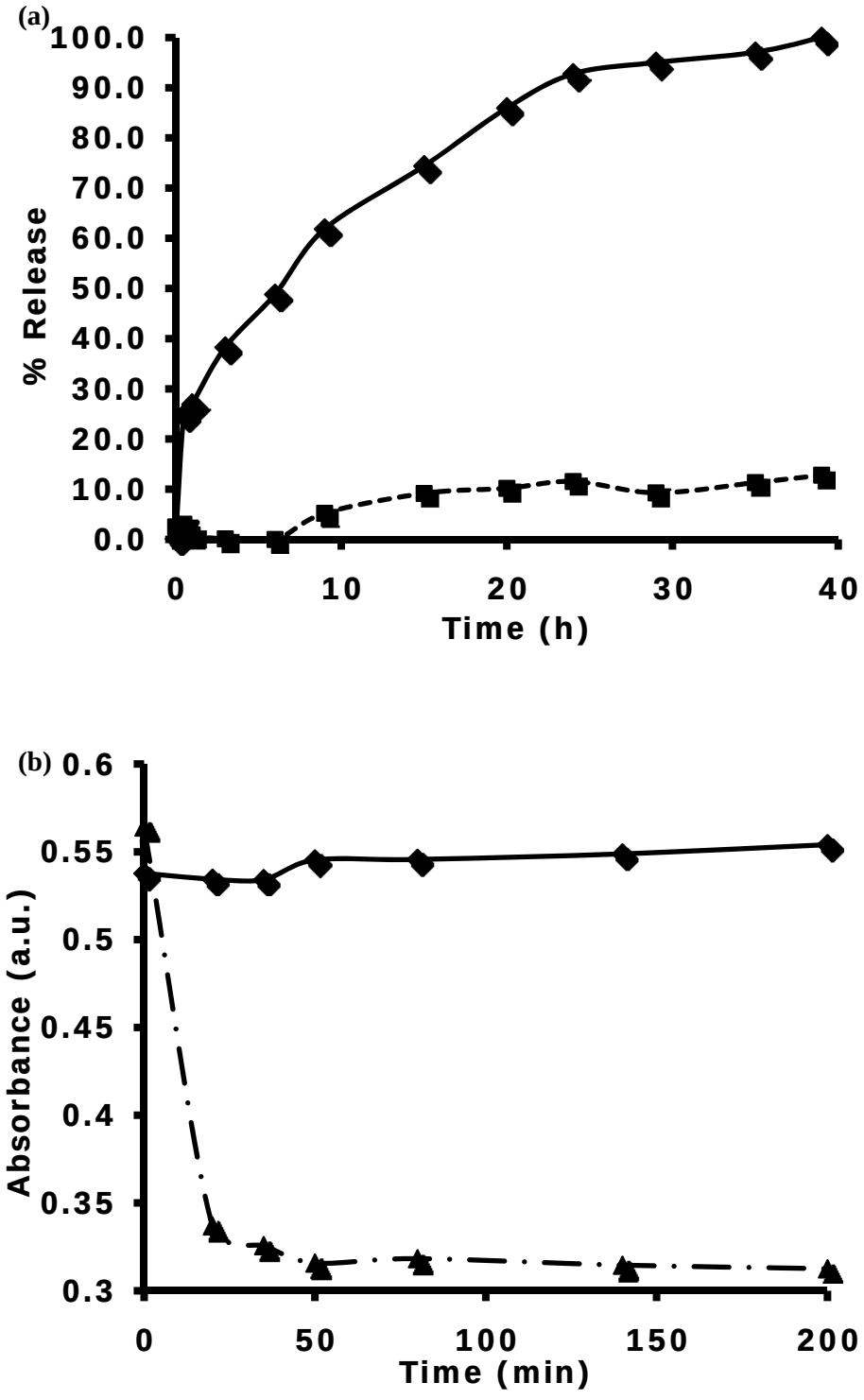
(a)
100.0
90.0
80.0
70.0
60.0
50.0
40.0
30.0
20.0
10.0
0.0
% Release
0
10
20
30
40
Time (h)
(b)
0.6
0.55
0.5
0.45
0.4
0.35
0.3
Absorbance (a.u.)
0
50
100
150
200
Time (min)

Scheme captions

Scheme S1. Synthesis of negatively-charged AuNPs (NC-AuNPs). **(a)** Compound 1 was deprotected from the protecting group (trityl thioether) using TFA/triisopropylsilane in DCM. **(b)** A Murray place-exchange reaction between AuNPs and the deprotected compound 1 was carried out to afford the ester-NC-AuNPs. **(c)** Finally, the ester-NC-AuNPs was saponified with aqueous lithium hydroxide in THF/MeOH to afford the NC-AuNPs.

Scheme S2. Synthesis of photo-responsive AuNPs (PR-AuNPs). NC-AuNPs were reacted with compound 2 in presence of EDC to afford PR-AuNPs.

Scheme 1

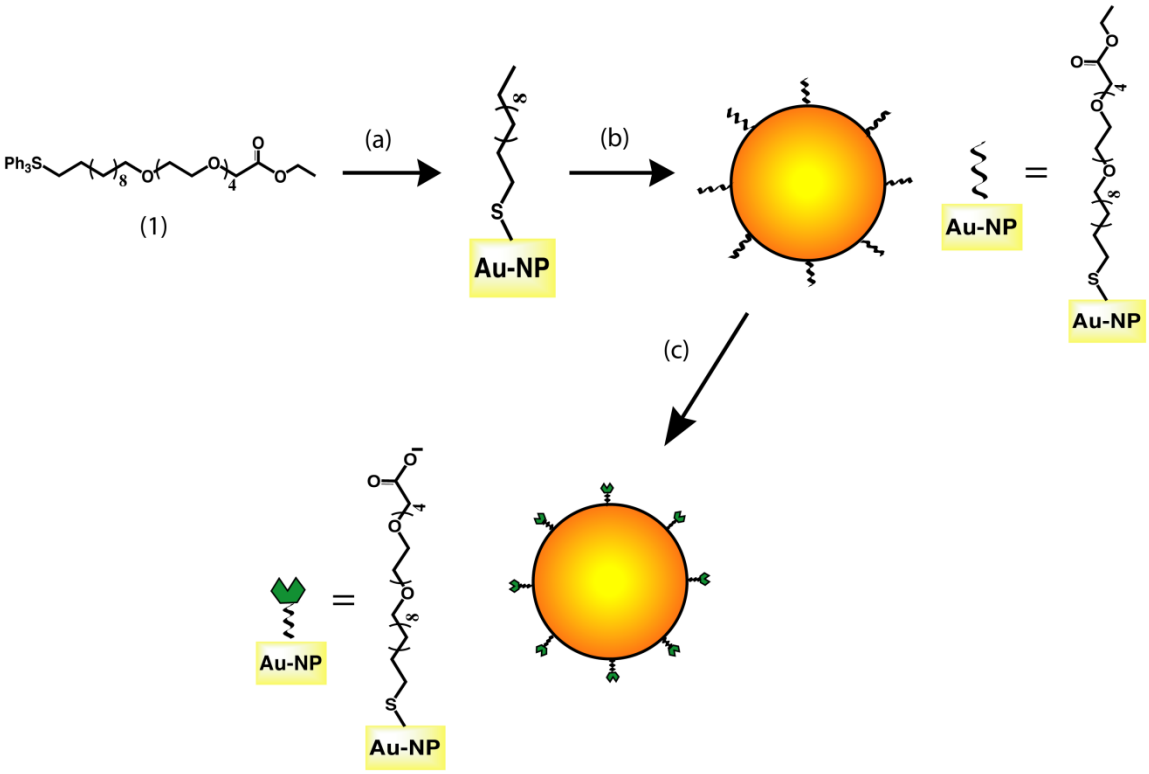

Scheme 2

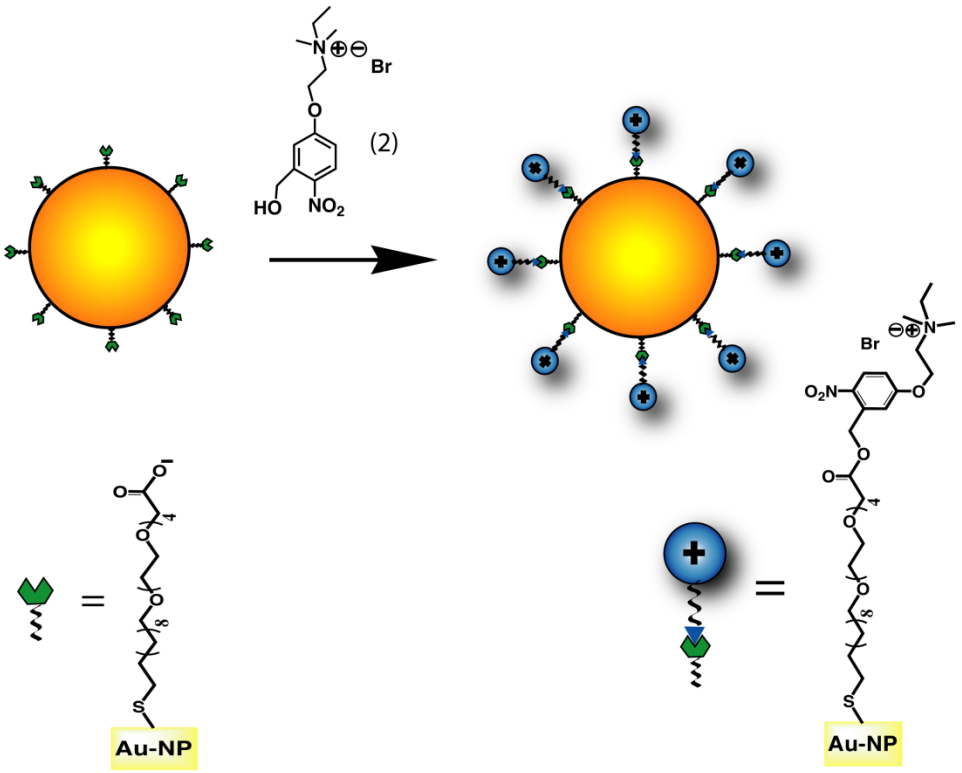

CHAPTER 4. CELL-INDUCED INTRACELLULAR CONTROLLED RELEASE OF MEMBRANE IMPERMEABLE CYSTEINE FROM MESOPOROUS SILICA NANOPARTICLE-BASED DRUG DELIVERY SYSTEM

A paper published on **Chemical Communications**
2009, 3219 - 3221
Renato Mortera, Juan L. Vivero-Escoto, Igor I. Slowing, Edoardo Garrone, Barbara Onida, and Victor S.-Y. Lin

Abstract

A mesoporous silica nanoparticle-based (MSN) intracellular cysteine delivery system that could be induced and regulated by cell-produced natural antioxidants was synthesized. A large amount of cysteine molecules were covalently attached to the silica surface of MSN through cleavable disulfide linkers. These cysteine-containing nanoparticles were efficiently endocytosed by human cervical cancer cells HeLa. These materials exhibit 450 times higher cell growth inhibition capability than that of the conventional N-acetylcysteine pro-drug.

Introduction

Intracellular thiols are of vital importance for controlling the homeostasis of live cells.[1] For example, glutathione (GSH) is one of the agents responsible for the reducing milieu of various cell types. Recent studies have highlighted the key role of GSH in several physiological processes, such as DNA synthesis, microtubular-related processes, immune functions, and protection against oxidative damages induced by free radicals and other toxicants.[1, 2] The low intracellular concentration of GSH has been attributed to several chronic inflammation disorders, which often leads to cancerous,[3] neurodegenerative,[4] and

cardiovascular[5] maladies. A variety of therapeutic methods in promoting GSH biosynthesis have been developed for the treatment of these diseases.[6-8]

The success of these approaches hinges upon the availability of intracellular cysteine (Cys). However, Cys is toxic and unstable in the extracellular media.[9, 10] To circumvent this problem, the current state-of-the-art approach is to chemically alter the structures of Cys, so that the stability and membrane permeability could be enhanced. Among these different cysteine-derivatives, N-acetylcysteine (NAC) is one of the most widely administered pro-drugs due to the rapid absorption upon oral ingestion and the high stability in the extracellular media.[9, 11] Despite these advantages, the intracellular release of cysteine from NAC is mediated by a specific enzyme-catalyzed process.[9] In many cases, a large quantity (extracellular concentration larger than 20 mM) of NAC is necessary.[9] Also, recent reports have demonstrated that high concentrations (>1 mM) of NAC would cause severe damage on cellular DNAs.[12, 13] Therefore, the pursuit of alternative intracellular cysteine delivery systems that allow rapid transport of active and controllable amounts of Cys into cytoplasm continues to be a vigorous research area.

Recent developments in designing surface-functionalized mesoporous silica nanoparticles (MSNs) have shown promising potential in utilizing these materials for the controlled-release of different kinds of biogenic molecules, such as pharmaceutical drugs, DNA's, proteins, and imaging agents.[14-18] To the best of our knowledge, however, there is no prior report on the application of these mesoporous silica materials for intracellular controlled release of cysteine. The simple impregnation or physisorption of Cys inside of the mesoporous silica matrix would suffer from rapid leaching of cysteine in water before the cellular uptake of the amino acid-silica composite.

Herein, we report on the synthesis and characterization of an MSN-based intracellular cysteine delivery system (MSN-S-Cys), where the release could be triggered by cell-produced antioxidants, including nicotinamide adenine dinucleotide hydride (NADH), dihydrolipoic acid (DHLA), and glutathione.[19] As depicted in Figure 1, we investigated the efficacy of using this MSN-S-Cys for intracellular controlled release of cysteine inside human cervical cancer cells HeLa. The performance of this MSN-S-Cys system was compared with NAC in solution, Cys chemically attached via a thioether bond (MSN-Cys) to MSN and Cys physisorbed to MSN (MSN+Cys). We note that the direct comparison with solution Cys was not possible because of its high instability.[10]

Results and Discussion

To construct the MSN-S-Cys system, we first prepared a mercaptopropyl-functionalized mesoporous silica nanoparticle (MSN-SH) material via a co-condensation method that we have previously reported.[14, 20] The synthesis of MSN-SH is detailed in the Supporting Information (SI). As depicted in Scheme 1, the mercaptopropyl groups of MSN-SH were first treated with 2,2'-dipyridyl disulfide to yield a 2-pyridinyldisulfanylpropyl functionality. A consequent disulfide exchange reaction with *L*-cysteine gave rise to the desired MSN-S-Cys material (Scheme 1). The loading efficiency of MSN-S-Cys was determined to be 0.45 mmol/g of MSN, respectively, by means of HPLC and UV/Vis spectroscopy (Table S2 of the SI).

The honeycomb-like hexagonal mesoporous structure of these surface functionalized MSN materials were confirmed by powder X-ray diffraction (XRD) spectroscopy, N_2 isotherms (Figure S1-S2 and Table S1 of the SI), and transmission electron microscopy (TEM image of Figure 1). The results of dynamic light scattering (DLS) analysis of MSN-S-

Cys and MSN+Cys revealed that both materials formed stable suspension in water with average particle diameters of 395 and 390 nm, respectively. The surface charge properties of these mesoporous silica nanospheres in aqueous solution were also measured. The values of zeta potential (ζ) of MSN-S-Cys (-20.1 mV) and MSN+Cys (-19.2 mV) are summarized in Table S2 of the SI.

To test the efficacy of using MSN as the delivery carrier for cysteine, we evaluated the release kinetics of cysteine in PBS from MSN-S-Cys material, where Cys molecules are covalently anchored on the mesoporous silica matrix. The amount of Cys release was measured by HPLC, as described in the SI. We investigated four disulfide-reducing antioxidants, dithiothreitol (DTT),[21] DHLA, NADH, and glutathione, as the chemical triggers for the controlled release of cysteine molecules from MSN-S-Cys. As shown in Figure 2, no leaching of Cys in PBS solution prior to the addition of reducing agents was observed; in contrast, the release of Cys from the physisorbed sample was immediate (Figure S3 of the SI). As depicted in Figure 2 (inset), within 30 minutes upon the addition of NADH, DTT, DHLA and GHS, approximately 99, 90, 70 and 60% of mesopore-loaded Cys was released, respectively. The different rates of release could be attributed to the different reducing power between each reducing agent. It is interesting to note that the amount of cysteine release was clearly controlled by the quantity of reducing agent added to the solution as shown in the plot of percent release of Cys versus the concentrations of DTT and glutathione (Figure 3).

We and others have demonstrated previously that MSN materials could be efficiently endocytosed by a variety of cell types.[17, 22-24] To analyze the intracellular controlled release properties, we introduced these Cys-containing nanoparticles to human cervical cancer cells

HeLa. As illustrated in Figure 4, the cell proliferation was evaluated 48 hours after the addition of 100 μg/mL of the following MSN samples (MSN+Cys, MSN-Cys and MSN-S-Cys) and NAC in solution at concentrations of 0.1 mM and 20 mM. Approximately 50% of cell growth was inhibited in the case of MSN-S-Cys. It is interesting to note that NAC at the concentration of 0.1 mM was ineffective in causing any cell growth inhibition and a high concentration (20 mM) is required to reach the same level of inhibition of MSN-S-Cys. This finding is consistent with the results reported in literature, where a minimum concentration of 15 mM is required for NAC to be therapeutically active.[25] In contrast to the high dosage requirement of NAC, our results suggested that MSN-S-Cys is indeed a superior drug delivery system in inhibiting cell growth of HeLa. Apparently, the actual amounts of cysteine molecules in the systems of MSN-S-Cys and NAC for inhibiting 50% of the cell growth of HeLa are very different. After comparing the amount of Cys and NAC present (0.14/60 μmol) we found that MSN-S-Cys is approximately 444 times more effective in delivering the membrane impermeable amino acid, cysteine, than the conventional NAC approach. These results further suggest that the cellular uptake process for HeLa to internalize MSN-S-Cys must be quite efficient. We note that the MSN+Cys material, like the thioether-functionalized MSN material (MSN-Cys), did not show any significant effect on the cell growth inhibition (Figure 4).

To further examine the cellular uptake of MSN-S-Cys and the intracellular release of Cys, we labeled Cys and MSN with two different fluorescent dyes, fluorescein isothiocyanate (FITC; green emission) and tetramethylrhodamine isothiocyanate (TRITC; red emission), respectively, via a synthetic approach detailed in the SI. The endocytosis of this TRITC-MSN-S-Cys-FITC material by HeLa cells was monitored by fluorescence confocal

microscopy (Figure 5). The observed yellow spots (Figure 5a) represent the superimposed fluorescence of the TRITC-labeled MSN and the mesopore-encapsulated FITC-Cys. The observed green spots (Figure 5a and b) indicated that the FTIC-Cys molecules were indeed released from MSN-S-Cys. This result was further corroborated by externally introducing the cell membrane permeable glutathione monoester to enhance the intracellular release of Cys in HeLa cells (Figure S6 and 7 of the SI).[26]

Conclusions

In conclusion, we have demonstrated that mesoporous silica nanoparticles (MSN) can serve as an efficient carrier for the intracellular delivery of cysteine (400 times better than NAC). We found that the controlled release of cysteine from MSN-S-Cys could be induced and regulated by both artificial and cell-produced natural antioxidants. Also, our results indicated that the MSN-S-Cys particles could indeed penetrate the cell membrane of HeLa and effectively deliver cysteine intracellularly to inhibit the cell growth of these cancer cells. We envision that this MSN-based intracellular cysteine delivery system could serve as a new therapeutic method for many cysteine-related diseases and personal health care issues, such as HIV infection,[11] cancer,[11] aging,[27] and acetaminophen poisoning.[28] Further developments on the utilization of this design principle for constructing novel controlled release delivery systems could also bring impacts to other biomedical and biotechnological applications.

Acknowledgment

This work was supported by the U.S. National Science Foun-dation (CHE-0809521) and the U.S. DOE Ames Laboratory through the office of Basic Energy Sciences under Contract No. DE-AC02-07CH11358.

References

[1] S. C. Lu, Current Topics in Cellular Regulation, Vol 36 2000, 36, 95.

[2] M. E. Anderson, Chem.-Biol. Interact. 1998, 111-112, 1.

[3] K. Senthil, S. Aranganathan, N. Nalini, Clin. Chim. Acta 2004, 339, 27.

[4] Y. Gilgun-Sherki, E. Melamed, D. Offen, Neuropharmacology 2001, 40, 959.

[5] P. H. Black, L. D. Garbutt, J. Psychosom. Res. 2002, 52, 1.

[6] M. Costa, M. Ferreira, L. S. R. Asciuttia, L. J. da Silva, M. A. A. Rivera, S. Limbach, J. C. Guilland, M. Costa, G. S. F. Soares, Nutr. Clin. Metabol. 2007, 21, 4.

[7] A. L. Levonen, E. Vahakangas, J. K. Koponen, S. Yla-Herttuala, Circulation 2008, 117, 2142.

[8] R. M. Touyz, E. L. Schiffrin, in Atherosclerosis and Oxidant Stress: A New Perspective, 2008, pp. 51.

[9] M. E. Anderson, A. Meister, Methods in Enzymol. 1987, 143, 313.

[10] H. Sato, M. Tamba, T. Ishii, S. Bannai, J. Biol. Chem. 1999, 274, 11455.

[11] F. Santangelo, Curr. Med. Chem. 2003, 10, 2599.

[12] S. Oikawa, K. Yamada, N. Yamashita, S. Tada-Oikawa, S. Kawanishi, Carcinogenesis 1999, 20, 1485.

[13] S. Kawanishi, S. Oikawa, M. Murata, Antioxid. Redox Signaling 2005, 7, 1728.

[14] C. Y. Lai, B. G. Trewyn, D. M. Jeftinija, K. Jeftinija, S. Xu, S. Jeftinija, V. S. Y. Lin, J. Am. Chem. Soc. 2003, 125, 4451.

[15] J. Lu, E. Choi, F. Tamanoi, J. L. Zink, Small 2008, 4, 421.

[16] I. I. Slowing, B. G. Trewyn, S. Giri, V. S. Y. Lin, Adv. Funct. Mater. 2007, 17, 1225.

[17] I. I. Slowing, B. G. Trewyn, V. S. Y. Lin, J. Am. Chem. Soc. 2007, 129, 8845.

[18] M. Vallet-Regi, A. Ramila, R. P. del Real, J. Perez-Pariente, Chem. Mater. 2001, 13, 308.

[19] G. Liang, G. Du, J. Chen, Lett. Appl. Microbiol. 2008, 46, 507.

[20] S. Huh, J. W. Wiench, J. C. Yoo, M. Pruski, V. S. Y. Lin, Chem. Mater. 2003, 15, 4247.

[21] S. Giri, B. G. Trewyn, M. P. Stellmaker, V. S. Y. Lin, Angew. Chem. Int. Ed. 2005, 44, 5038.

[22] T. H. Chung, S. H. Wu, M. Yao, C. W. Lu, Y. S. Lin, Y. Hung, C. Y. Mou, Y. C. Chen, D. M. Huang, Biomaterials 2007, 28, 2959.

[23] J. Lu, M. Liong, J. I. Zink, F. Tamanoi, Small 2007, 3, 1341.

[24] I. I. Slowing, B. G. Trewyn, V. S. Y. Lin, J. Am. Chem. Soc. 2006, 128, 14792.

[25] S. Estany, J. R. Palacio, R. Barnadas, M. Sabes, A. Iborra, P. Martinez, J. Reprod. Immunol. 2007, 75, 1.

[26] R. Hong, G. Han, J. M. Fernandez, B.-j. Kim, N. S. Forbes, V. M. Rotello, J. Am. Chem. Soc. 2006, 128, 1078.

[27] W. Droege, Philos. Trans. R. Soc. London, Ser. B
2005, 360, 2355.

[28] A. L. Jones, J. Toxicol., Clin. Toxicol. 1998, 36, 277.

Figure captions

Figure 1. Schematic representation and TEM image (right) of an MSN-based intracellular delivery system of cysteine (MSN-S-Cys). The intracellular controlled-release mechanism of cysteine is controlled by the reductive cleavage of the disulfide linkage connecting Cys to MSN induced by natural cell-produced antioxidants.

Figure 2. Cysteine release profiles of MSN-S-Cys (30 mg) in 30 mL of PBS induced by NADH (△), DTT (■) DHLA (◆), and Glutathione (○). The percentage release of Cys over time using 1 mM reducing agents. No noticeable release was observed in the absence of reducing agents (▲).

Figure 3. Percent release of Cys vs. the concentrations of NADH (△), DTT (■) DHLA (◆), and Glutathione (○). All data were measured at 30 minutes after the addition of reducing agents.

Figure 4. Cell growth inhibition study: Amounts (%) of viable HeLa cells after exposing to 100 μg/mL of MSN+Cys, MSN-Cys, MSN-S-Cys, and solutions of NAC (0.1 and 20 mM) for 48 hours. The normal cell growth was shown in the entry (Crtl) without any addition of NAC, Cys, or MSN.

Figure 5. Confocal fluorescence micrographs of TRITC-MSN-S-Cys-FITC inside of HeLa cells. a) The green fluorescent spots indicating the intracellular locations of FTIC-Cys, whereas the yellow areas represent the superimposing fluorescence of TRITC-labeled MSN and FITC-Cys. b) Transmission micrograph of TRITC-MSN-S-Cys-FITC.

Figure 1

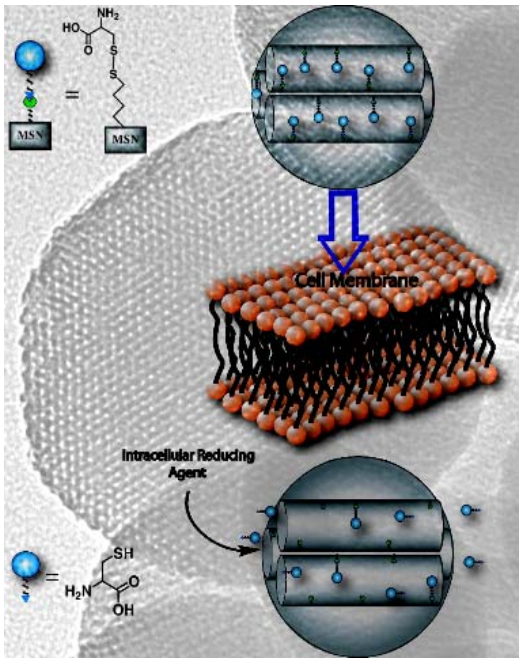
NH2
HO
O
S
S
MSN
MSN
Cell Membrane
Intracellular Reducing Agent
SH
H2N
O
OH

Figure 2

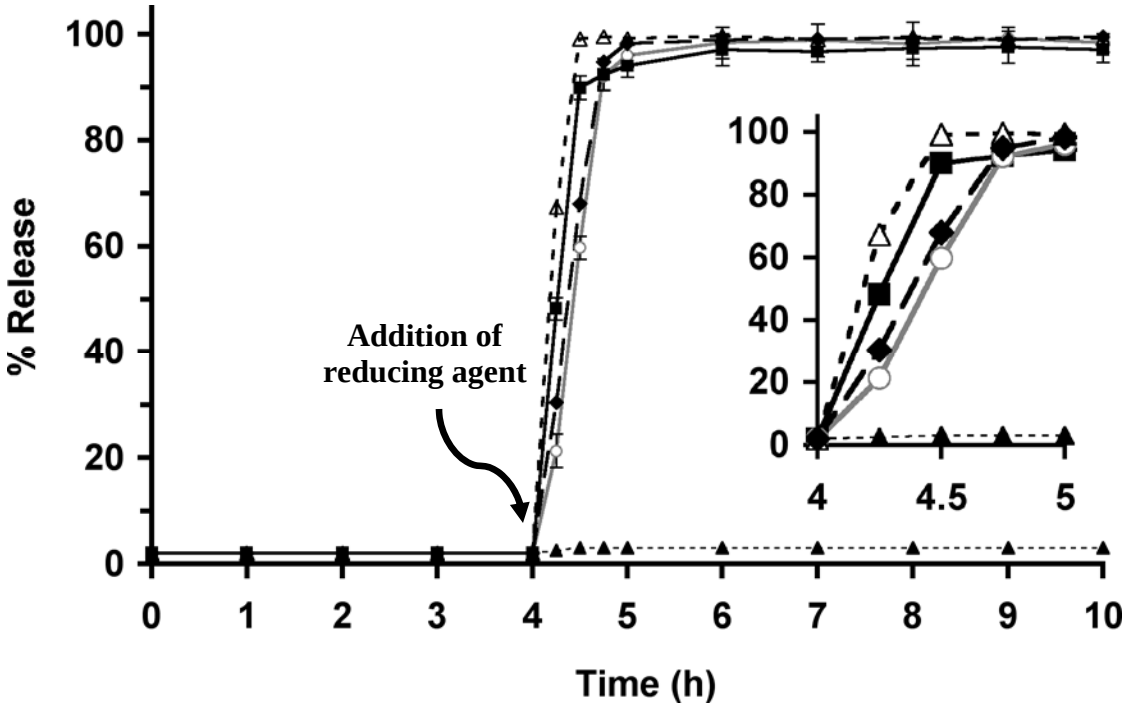
% Release
Time (h)
Addition of
reducing agent
0
20
40
60
80
100
0
1
2
3
4
5
6
7
8
9
10
4
4.5
5

Figure 3

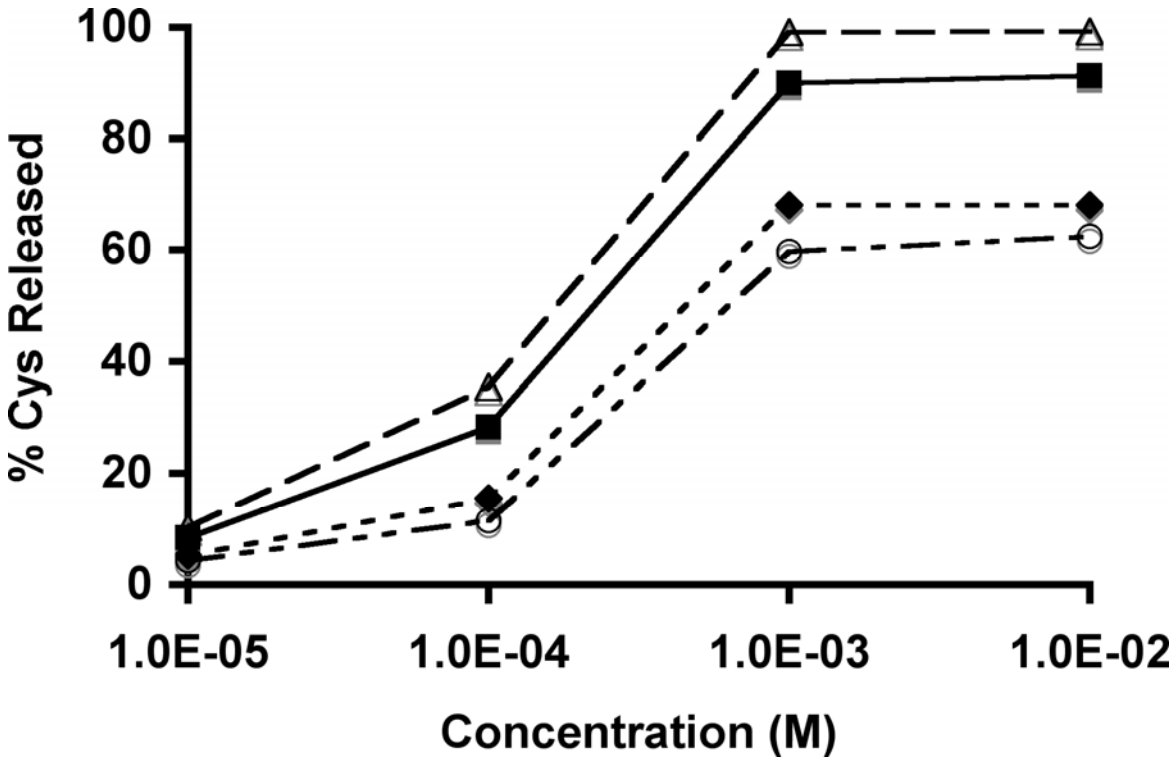
100
80
60
40
20
0
% Cys Released
1.0E-05
1.0E-04
1.0E-03
1.0E-02
Concentration (M)

Figure 4

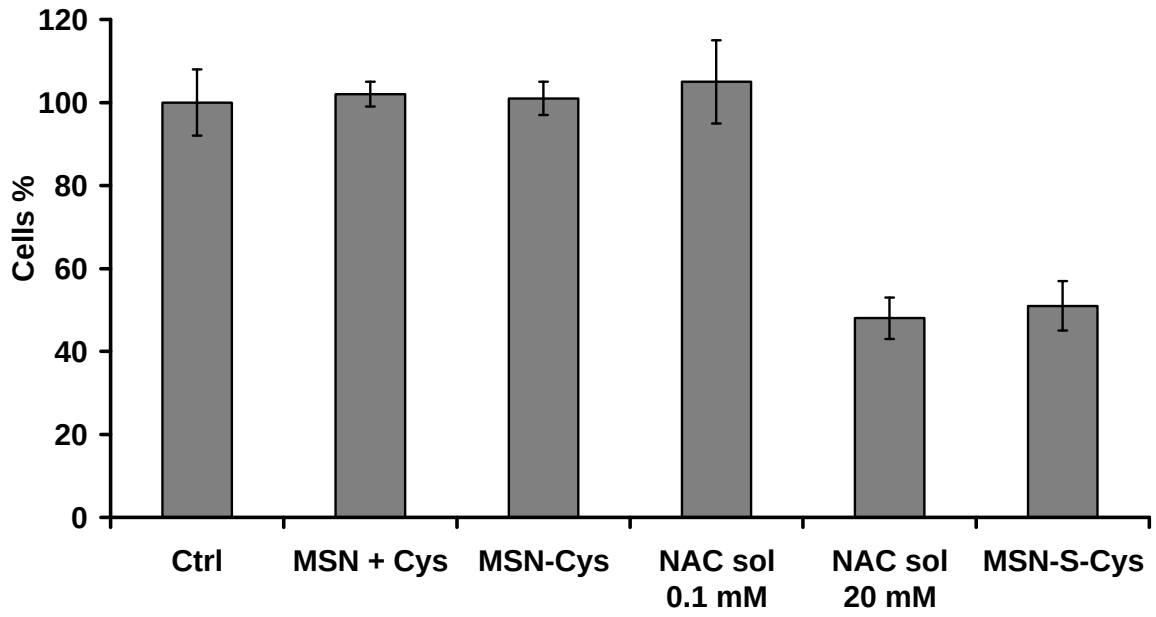
120
100
80
60
40
20
0
Cells %
Ctrl
MSN + Cys
MSN-Cys
NAC sol 0.1 mM
NAC sol 20 mM
MSN-S-Cys

Figure 5

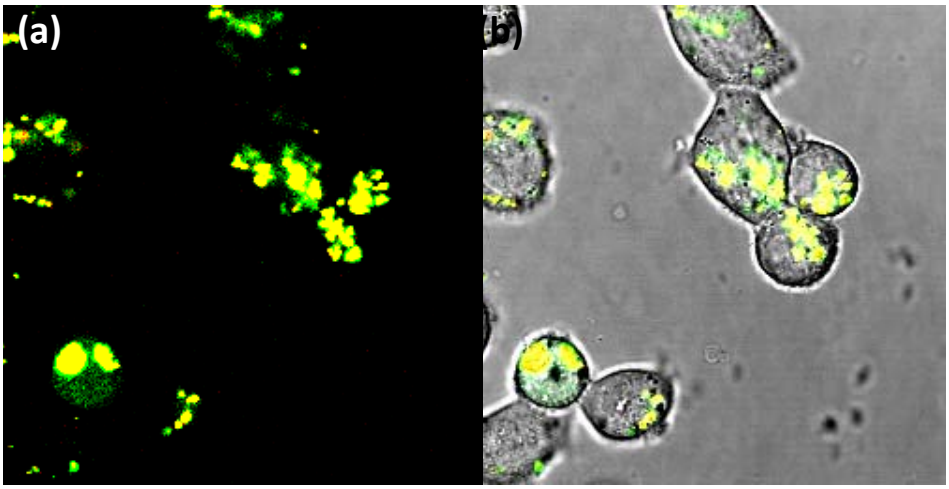

Scheme captions

Scheme 1. Synthetic scheme of MSN-S-Cys. The detailed reaction condition of a) is described in the Supporting Information. Reactions b) and c) were performed in PBS (pH 7.4) at room temperature for 8 hours.

Scheme 1

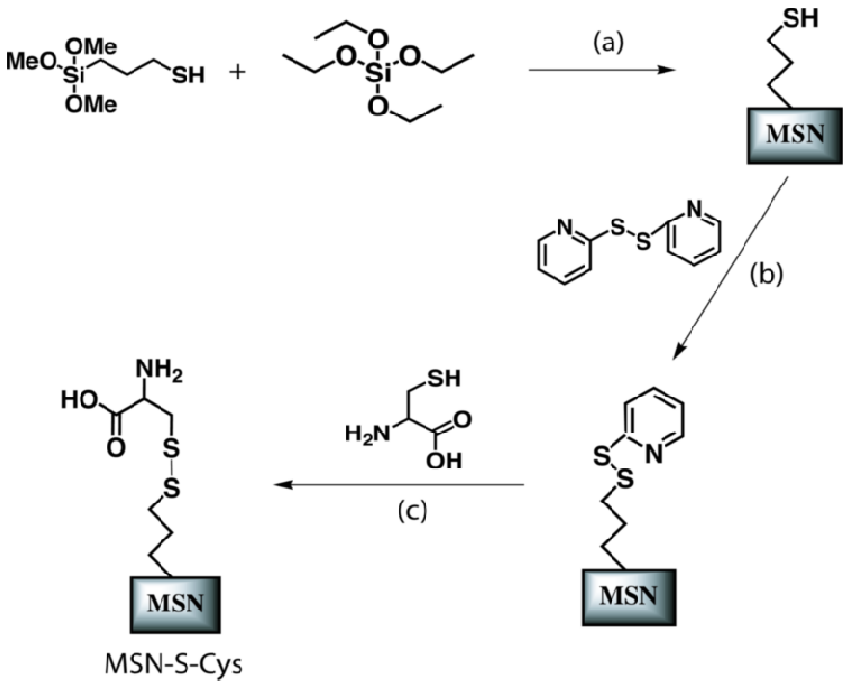
MeO
OMe
Si
OMe
SH
+
O
O
Si
O
O
(a)
SH
MSN
N
S
S
N
(b)
S
N
S
MSN
SH
H2N
O
OH
(c)
NH2
HO
O
S
S
MSN
MSN-S-Cys

Appendix: Supporting information

Reagents and Materials: Tetraethylorthosilicate (TEOS) was purchased from Gelest. N-hexadecyltrimethylammonium bromide (CTAB), 3-mercaptopropyl trimethoxysilane (MP-TMS), 3-aminopropyl trimethoxysilane (AP-TMS), 2,2'-dipyridyl disulfide (Aldrithiol-2), dithiothreitol (DTT), cysteine (Cys), glutathione (GSH), nicotinamide adenine dinucleotide hydride (NADH), dihydrolipoic acid (DHLA), fluorescein isothiocyanate (FITC), N-acetylcysteine (NAC), fluorescein isothiocyanate (FITC), tetramethylrhodamine isothiocyanate (TRITC), and trifluoroacetic acid (TFA) were purchased from Aldrich. Methanol, hydrochloric acid, tetrahydrofuran and acetonitrile were purchased from Fischer. All chemicals were used as received. Nanopure water (18.1 MHz), prepared from a Barnstead E-pure water purification system, was employed throughout all the experiments.

Synthesis of MCM-41-type mesoporous silica nanoparticles with mercaptopropyl functionality (MSN-SH): Following the procedure previously reported,[1] 1.0 g of n-hexadecyltrimethylammonium bromide (CTAB) was dissolved in 480 mL nanopure water and 3.5 mL NaOH(aq) (2.0 M). The solution was stirred for 1 h at 353 K, followed by the dropwise addition of 5 mL of tetraethylorthosilicate (22.5 mmol, TEOS). Immediately after the injection of TEOS, 1 mL of 3-mercaptopropyl trimethoxysilane (5.4 mmol, MPTMS) was introduced to the solution mixture. After stirring for 2 h at 353 K, the resulting solid product was filtered, dried under high vacuum. The CTAB surfactant was removed by extraction with a solution of 0.5 mL HCl (37.4%) and 50 mL of methanol for 6 h at 333 K.

Characterization of MSN systems: Powder X-ray diffraction patterns were collected with a Scintag XRD 2000 X-ray diffractometer using CuKα radiation (2-theta: 1.5°-10°). Nitrogen sorption measurements at 77 K were performed using a Micromeritics TriStar sorptometer;

BET specific surface areas have been calculated in the relative pressure range 0.05-0.15 and pore size has been evaluated following the BJH method.[2] A JEOL 840A Scanning Electron Microscopy, a Tecnai G^2 F20 transmission electron microscopy operating at 200 kV and a Malvern NANO ZS90 Zetasizer were used to determine the mesoporous particle morphology and ζ potential.

Physisorption of cysteine on the mesopore surface of MSN (MSN+Cys): MSN particles (100 mg) were dispersed in a PBS solution of Cys (1 mM). The suspension was stirred for 20 h at RT. The resulting material was washed several times with PBS solution and dried under high vacuum. The amount of Cys absorbed by MSN was quantified by HPLC as detailed below.

Preparation of cysteine-functionalized MSN via a disulfide linkage (MSN-S-Cys): MSN-SH particles (200 mg) were treated with a solution of 2,2'-dipyridyl disulfide (88 mg) in 200 mL PBS. After stirring for 8 h at RT, the resulting 2-pyridinyldisulfanylpropyl-functionalized MSN product was isolated and washed with copious methanol and PBS buffer. The purified material was then introduced to a 200 mL PBS solution of Cys (48 mg) to yield the desired MSN-S-Cys product.[3, 4] The amount of Cys bonded to the surface of MSN was quantified by UV/Vis spectroscopy and HPLC as detailed below.

Preparation of cysteine-functionalized MSN via thioether bond (MSN-Cys): Following a experimental procedure previously reported in the literature[1,3] 1.0 g of CTAB was dissolved into 480 ml of nanopure water and 3.5 ml of NaOH(aq) (2.0 M) and stirred for 1h at 353 K. Then, 5 ml of TEOS and 1 ml of allyltrimethoxysilane were then added drop wise. After stirring for 2 hours at 353 K, the products were filtered, washed, and dried under vacuum. To wash CTAB out from this material, 500 mg of the as-made MSN were dispersed in a solution

of 0.5 ml HCl (37.4%) and 50 ml of methanol and stirred for 6h at 333 K. The material was washed several times with methanol and dried under high vacuum. Following the well known radical reaction between alkenes and thio compounds,[5] 200 mg of this sample were subsequently added to Cys (0.4 mmol) and azobisisobutyronitrile (6 mg, AIBN) in 30 ml of dry tetrahydrofuran (THF) for 24 hours in nitrogen conditions with vigorous stirring and UV light irradiation(λ~350 nm).

Controlled release of cysteine: The release profiles were measured by soaking 30 mg of Cys-containing MSN sample in 30 mL PBS solution (10 mM, pH 7.3) at RT. Every 15 min, the sample was centrifuged and aliquots (0.5 mL) were taken to quantify the amount of Cys released from MSN by HPLC. Four different disulfide-reducing agents (NADH, DHLA, DTT, and GSH) were used as triggers for the release of cysteine in the case of MSN-S-Cys.

Cys quantification: ***HPLC method.*** A Hitachi Organizer high-performance liquid chromatographic system controlled with a Hitachi L-7100 pump, a Hitachi L-7200 autosampler, a Hitachi L-7455 Diode Array Detector and a Hitachi L-7300 Column Oven was employed to evaluate the amount of Cys loaded and released by the samples. The mobile phase was 99.9% of nanopure water and 0.1% TFA. It was pumped through a Supelco Discovery®C18 column with a flow-rate of 0.2 mL/min at RT. The detector was set at 320 nm and the peak ascribable to Cys in PBS solution appeared between 8.54 and 8.59 minutes. In the case of release with reducing agents both the peaks of GSH (19.1-19.5 minutes) and DTT (24.9-25.3 minutes) did not overlap with the Cys signal. To determine the Cys loaded by the materials the difference in the concentration of Cys in PBS solution before and after contact with the samples was calculated. The calibration curves have been determined using PBS solutions of Cys in the range of 0.01 mM – 5 mM.

UV-Vis method. The MSN-SH sample was treated in PBS firstly with 2,2'-dipyridyl disulfide and subsequently with Cys. This reaction afforded 2-thiopyridone as byproduct. The concentration of this molecule was used to quantify the surface coverage of chemically accessible thiol groups in MSN-SH and the amount of Cys linked to MSN in MSN-S-Cys by means of a HP 8453 UV-VIS system (λ = 354 nm). The calibration curve has been calculated using PBS solutions of 2-thiopyridone in the 0.01 mM – 0.1 mM concentration range.

Synthesis of MSN+Cys, MSN-SH, and MSN-S-Cys labeled with FITC: 200 mg of as-made MSN-SH or MSN sample were treated at first with a solution of 3-aminopropyl trimethoxysilane (0.23 mL) in 30 mL of dry toluene at 370 K for 24h. Then this material was added to a solution of FITC (7.75 mg) in 200 ml of methanol and stirred at RT for 24h. The CTAB was washed out in acid media as is described above. In the case of MSN+Cys and MSN-S-Cys, Cys was linked to FITC labeled-MSN via disulfide bond, as reported above.

Synthesis of TRITC-MSN-S-Cys-FITC: FITC (39.8 mg, 100 μmol) were added to 100 mg of MSN-S-Cys in dry DMSO and stirred for 12h. The product was collected by centrifugation and washed several times with DMSO, MeOH and water, and finally dried under high vacuum. Then, TRITC (1 mg, 2.25 μmol) was reacted with AP-TMS (10 μL, 56 μmol) in DMSO (1.0 mL) for 6h at room temperature. To this solution 50 mg of previously prepared MSN-S-Cys-FITC material dispersed in 4 mL of DMSO were added and the final mixture was allowed to react for 24 h at 353 K. The final product was recovered by centrifugation and washed several times with DMSO and water, and dried under high vacuum.

Synthesis of TRITC-MSN-Cys-FITC: FITC (39.8 mg, 100 μmol) were added to 100 mg of MSN-Cys in dry DMSO and stirred for 12h. The product was collected by centrifugation and washed several times with DMSO, MeOH and water, and finally dried under high vacuum. TRITC (1 mg, 2.25 μmol) was reacted with AP-TMS (10 μL, 56 μmol) in DMSO (1.0 mL) for 6h at room temperature. To this solution 50 mg of previously prepared MSN-Cys-FITC material dispersed in 4 mL of DMSO were added and the final mixture was allowed to react for 24 h at 353 K. The final product was recovered by centrifugation and washed several times with DMSO and water, and dried under high vacuum.

Intracellular toxicity of MSN-S-Cys in HeLa cells: HeLa cells were seeded in six-well plates with a density of 1 x 10^5 cells ml^{-1} in 3 mL of D-10 medium (Dubelcco Modified Eagle's Medium with horse serum, *L*-alanyl-*L*-glutamine, gentamicin sulfate and penicillin-streptomycin solution), and incubated at 310 K with a 5% CO_2 atmosphere for 24 hours. Then, the cells were seeded with different concentration of NAC solution (ranging from 0.05 to 100 mM), MSN-SH, MSN + Cys, and MSN-S-Cys samples (ranging from 25 to 100 μg mL^{-1}) in D-10 serum for other 48 hours. After the incubation each well was washed with PBS and the cells were trypsinized, centrifuged, and re-suspended in D-10 medium. Viability was determined by the Guava ViaCount cytometry assay (Guava Technologies, Inc.).

Intracellular toxicity of MSN-S-Cys in HeLa cells in presence of GSH monoester:[6,7] HeLa cells were seeded in six-well plates with a density of 1 x 10^5 cells ml^{-1} in 3 mL of D-10 medium (Dubelcco Modified Eagle's Medium with horse serum, L-alanyl-L-glutamine, gentamicin sulfate and penicillin-streptomycin solution), and incubated at 310 K with a 5% CO_2 atmosphere for 24 hours. Then, the cells were seeded with MSN-S-Cys (100 μg mL^{-1}) in D-10 serum for other 24 hours. The cells medium was replaced by GSH monoester in D-10

serum (10 mM and 20 mM) and incubated for 2 h. After that, the cells were washed with PBS and D-10 serum was added and incubated for other 22h. After the incubation each well was washed with PBS and the cells were trypsinized, centrifuged, and re-suspended in D-10 medium. Viability was determined by the Guava ViaCount cytometry assay (Guava Technologies, Inc.).

Measurement of the internalization of MSN-SH, MSN + Cys, and MSN-S-Cys in HeLa cells by flow cytometry: HeLa cells were seeded at the density of 1 x 10^5 cells per well in six-well plates in 3 mL D-10 medium. After incubation for 48 hours, the D-10 medium was replaced by 3 mL of FITC labeled material suspensions at different concentrations (1, 10, 25, 50, and 100 μg mL^{-1}) in the serum-free DMEM medium for 12 h. All the tests were run in triplicate. The cells were washed with medium, harvested by trypsinization and, after centrifugation, re-suspended in 0.4% trypan blue PBS solution in order to be analyzed by flow cytometry with a Becton-Dickinson FACSCanto cytometer with a DB-FACS Diva software. To distinguish the true fluorescence generated by the endocytosed FITC-labeled material from the natural autofluorescence of cells, a threshold of fluorescence intensity was established by performing the flow cytometry analysis on the cells incubated without FITC-labeled material. The threshold was set at an intensity of fluorescence slightly above the highest value observed for control samples (HeLa cells only). The number of cells with endocytosed FITC-labeled material was determined by counting those that show fluorescence intensity higher than the threshold.

Confocal fluorescence microscopy measurements: HeLa cells were seeded at the density of 5 x 10^4 cells per well in six-well plates in 3 mL of D-10 medium. After incubation for 24 h, the D-10 medium was replaced by 3 mL of either TRITC-MSN-S-Cys-FITC or TRITC-

MSN-Cys-FITC material (15 μg mL^{-1}) in fresh D-10 medium for 12 h. Then the cell medium was replaced by a solution of GSH monoester in D-10 serum (10 mM) for 2 h. The cells were washed with PBS and the cells were incubated in D-10 medium for other 10h. In the case of the samples that were not treated with GSH monoester, the cells in presence of material were incubated for 24h. Finally, the cell-plates were then washed with PBS and 3 mL of D-10 medium were added to each well. An aqueous solution of Hoechst 33258 (5 μg/mL) was added to the wells and they were let to rest for 30 min at RT. After replacing the Hoechst-staining solution with D-10 serum, the TRITC-MSN-S-Cys-FITC/ TRITC-MSN-Cys-FITC materials inside of HeLa cells were visualized by means of a Leica TCS NT confocal fluorescence microscope system with 100x oil immersion objective.

References

[1] C. Y. Lai, B. G. Trewyn, D. M. Jeftinija, K. Jeftinija, S. Xu, S. Jeftinija, and V. S. Y. Lin, J. Am. Chem. Soc., 2003, 125, 4451.

[2] E. P. Barrett, L. G. Joyner, and P. P. Halenda, J. Am. Chem. Soc., 1951, 73, 373.

[3] V. S. Y. Lin, C. Y. Lai, J. G. Huang, S. A. Song, and S. Xu, J. Am. Chem. Soc., 2001, 123, 11510.

[4] G. Saito, J. A. Swanson, and K. D. Lee, Adv. Drug Delivery Rev., 2003, 55, 199.

[5] A. Kumar and Akanksha, Tetrahedron, 2007, 63, 11086.

[6] M. E. Anderson and A. Meister, Anal. Biochem., 1989, 183, 16.

[7] A. Agarwal, S. Gupta, and R. K. Sharma, RB&E, 2005, 3, 28.

Table S1. Specific Surface Area (SSA), mesopore volume (Vp), pore size (DBJH), d_{100}, cell parameter (a), ζ potential (ζ) and average particles diameter (D) values for MSN materials.

	SSA_{BET} (m^2/g)	V_p (cm^3/g)	D_{BJH} (nm)	d_{100} (nm)	a (nm)	ζ (mV)	D (nm)
MSN	1093	1.014	3.02	3.98	4.59	-30.5	380
MSN-SH*	1012	0.578	2.20	3.83	4.43	-28.8	390

*EC50 of MSN-SH = 4.3 μg/mL

Table S2. Amount of pharmacological agent (Cys), ζ potential (ζ) and average particles diameter (D) of different MSN systems:

	Cys (mmol g^{-1})	ζ (mV)	D (nm)	EC_{50} (μg/mL)
MSN + Cys	0.41 *	-19.2	390	4.0
MSN-S-Cys	0.45 *	-20.1	395	3.6

* Evaluated by means of HPLC.
* Evaluated by means of UV after aldrithiol-2 reaction.

Figure captions

Figure S1. Characterization of MSN sample. a) XRD pattern, b) nitrogen sorption isotherms at 77 K, c) BJH pore size distribution and d) SEM picture. The material exhibited hexagonal type of mesoporous structure characteristic of MCM-41 with a pore size of 3.02 nm and particle size of 380 nm.

Figure S2. Characterization of MSN-SH sample. a) XRD pattern, b) nitrogen sorption isotherms at 77 K, c) BJH pore size distribution and d) SEM picture. The material exhibited hexagonal type of mesoporous structure characteristic of MCM-41 with a pore size of 2.2 nm and particle size of 390 nm.

Figure S3. Percent release of mesopore-adsorbed cysteine from MSN+Cys material in PBS solution (10 mM, pH 7.3). The profile showed a fast release kinetics of Cys from MSN+Cys, in less than 60 min roughly 95% of Cys was released in PBS solution.

Figure S4. Proliferation of HeLa cells treated for 48 hours with different concentrations of MSN + Cys (dark gray boxes), MSN-SH (black boxes), and MSN-S-Cys (light gray boxes). Graph shows the percentage of cells after each treatment, pointing out the role played by the Cys released inside the cell membrane from MSN-S-Cys.

Figure S5. Proliferation of HeLa cells treated for 48 hours with solutions at different concentrations of NAC (dark gray boxes) compared to HeLa control (white boxes). Graph shows the percentage of cells after each treatment, stressing a noticeable reduction of viability above 10 mM solution.

Figure S6. Confocal fluorescence images of HeLa cells loaded with TRITC-MSN-Cys-FITC (a-e), TRITC-MSN-S-Cys-FITC (f-j), and TRITC-MSN-S-Cys-FITC in presence of GSH monoester (k-o). (a, f, and k) green fluoresecnece of FITC labeled Cys, (b, g, and l) red

fluorescence of the endocytosed TRITC-labeled MSN, (c, h, and m) yellow spots corresponding to the overlapped image of green (Cys-FITC) and red (TRITC-MSN) micrographs, (d, i, and n) superimposed micrographs of green (Cys-FITC) and red (TRITC-MSN) images in presence of nuclei-staining dye Hoechst 33258, and (e, j, and o) overlapped image of green (Cys-FITC) and red (TRITC-MSN) with transmission image.

Figure S7. Cell proliferation inhibition of HeLa cells as a function of the concentration of glutathione monoester (GSH*). The glutathione monoester dose-dependent perfomance in the cell proliferation inhibition confirm its influence in the intracellular release of Cys from MSN-S-Cys.

Figure S1

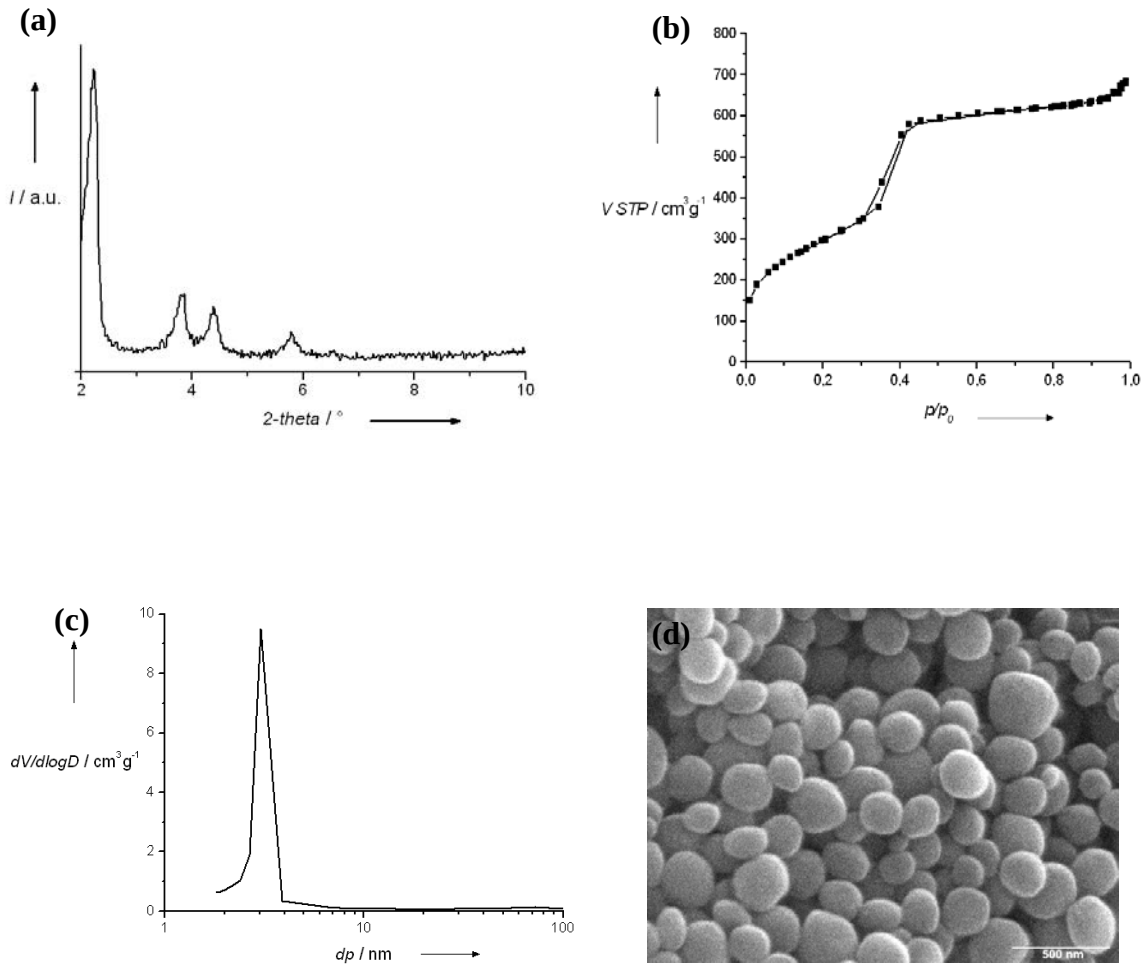

Figure S2

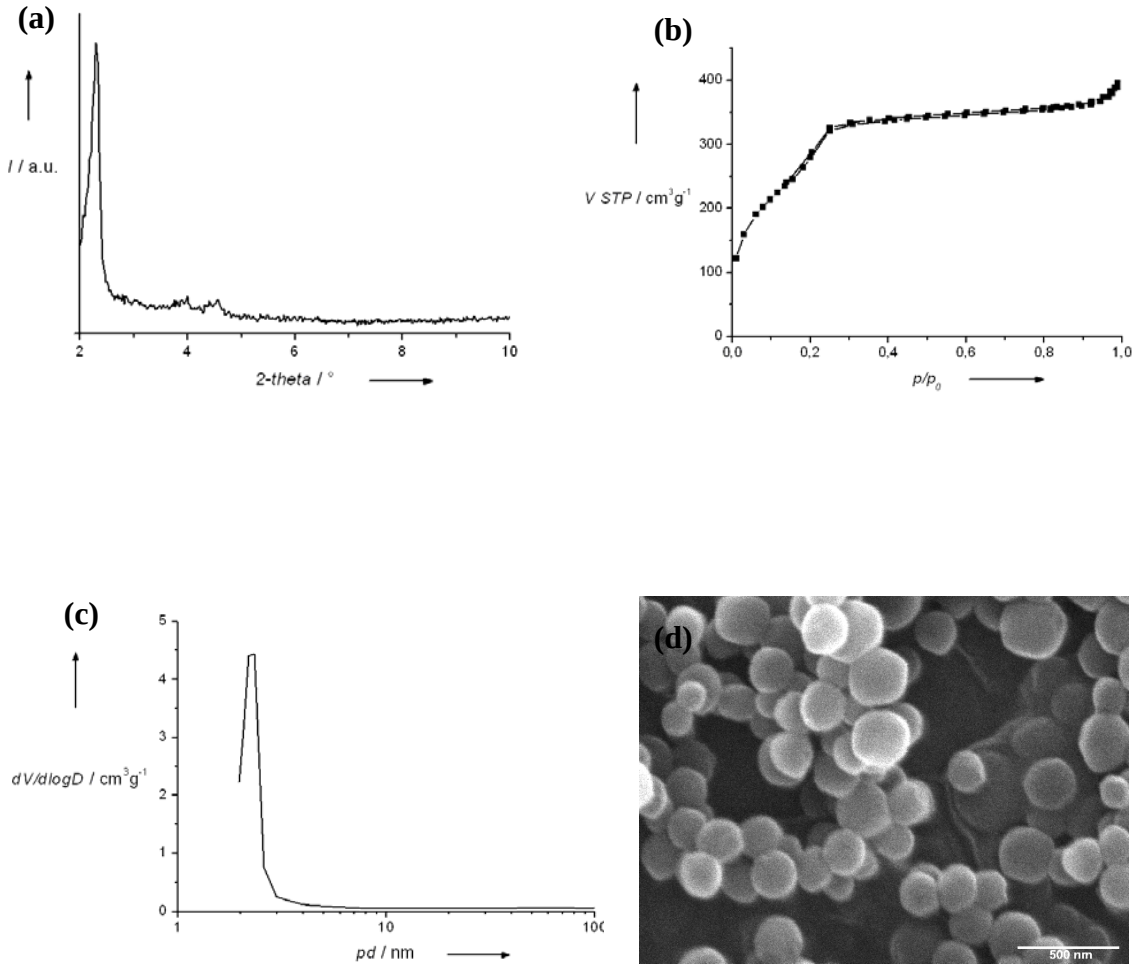

Figure S3

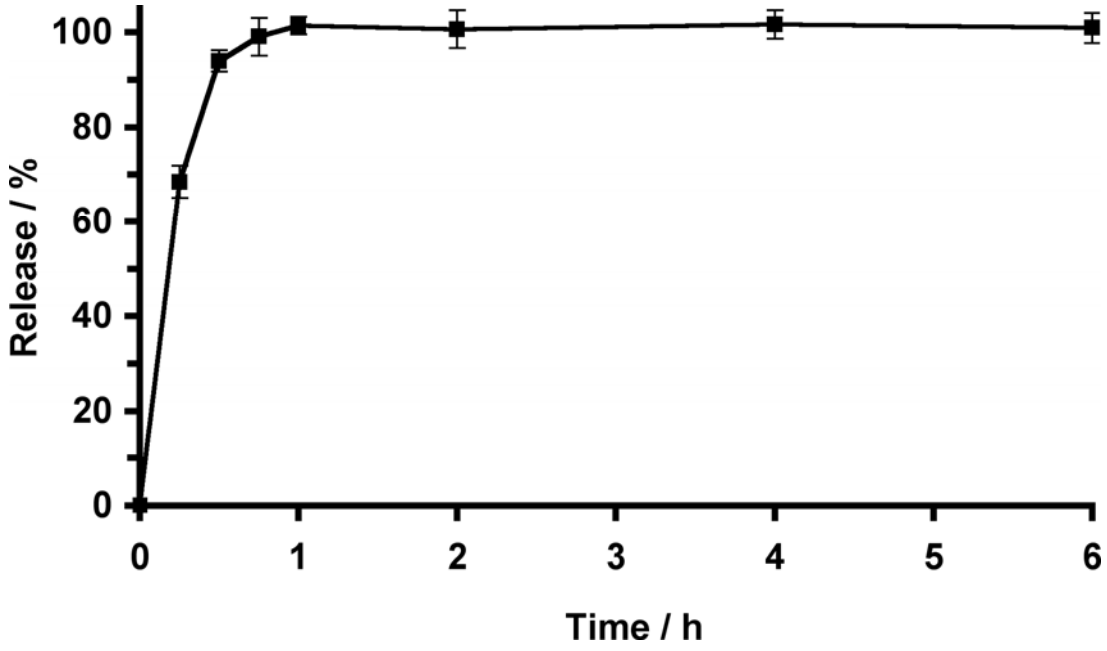

Figure S4

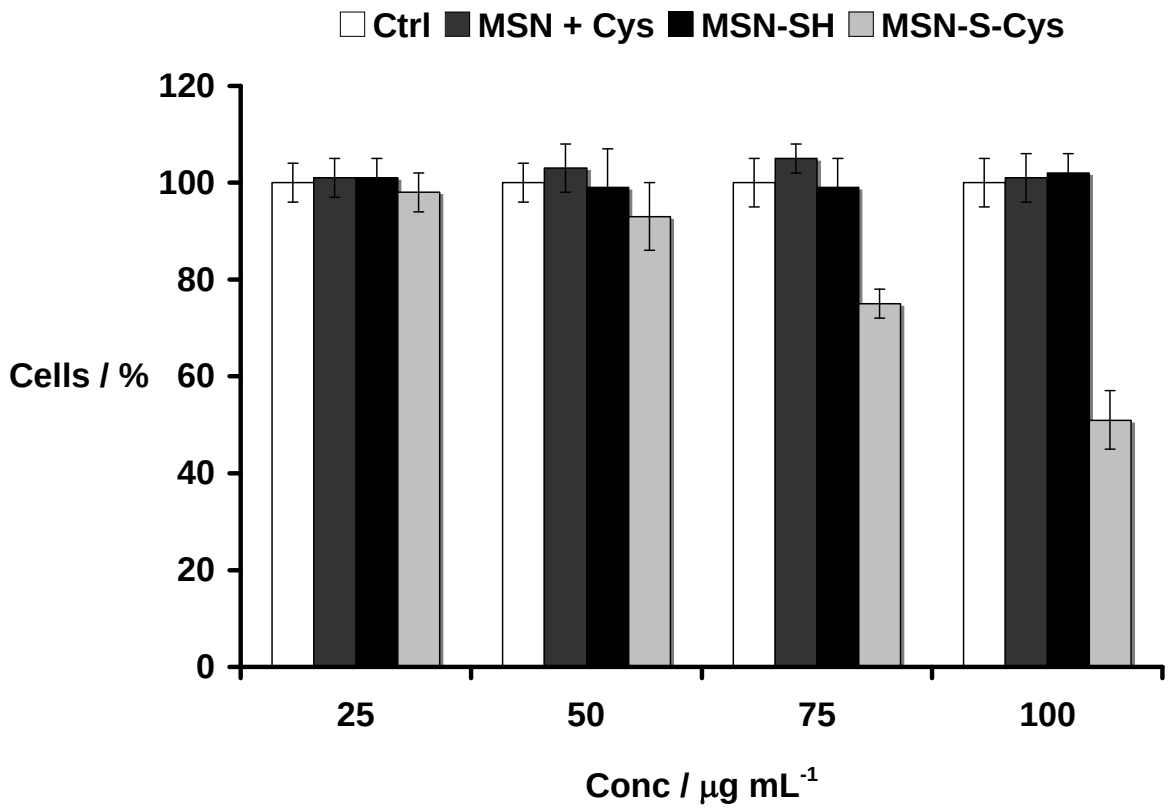
Ctrl
MSN + Cys
MSN-SH
MSN-S-Cys
120
100
80
60
40
20
0
Cells / %
25
50
75
100
Conc / μg mL-1

Figure S5

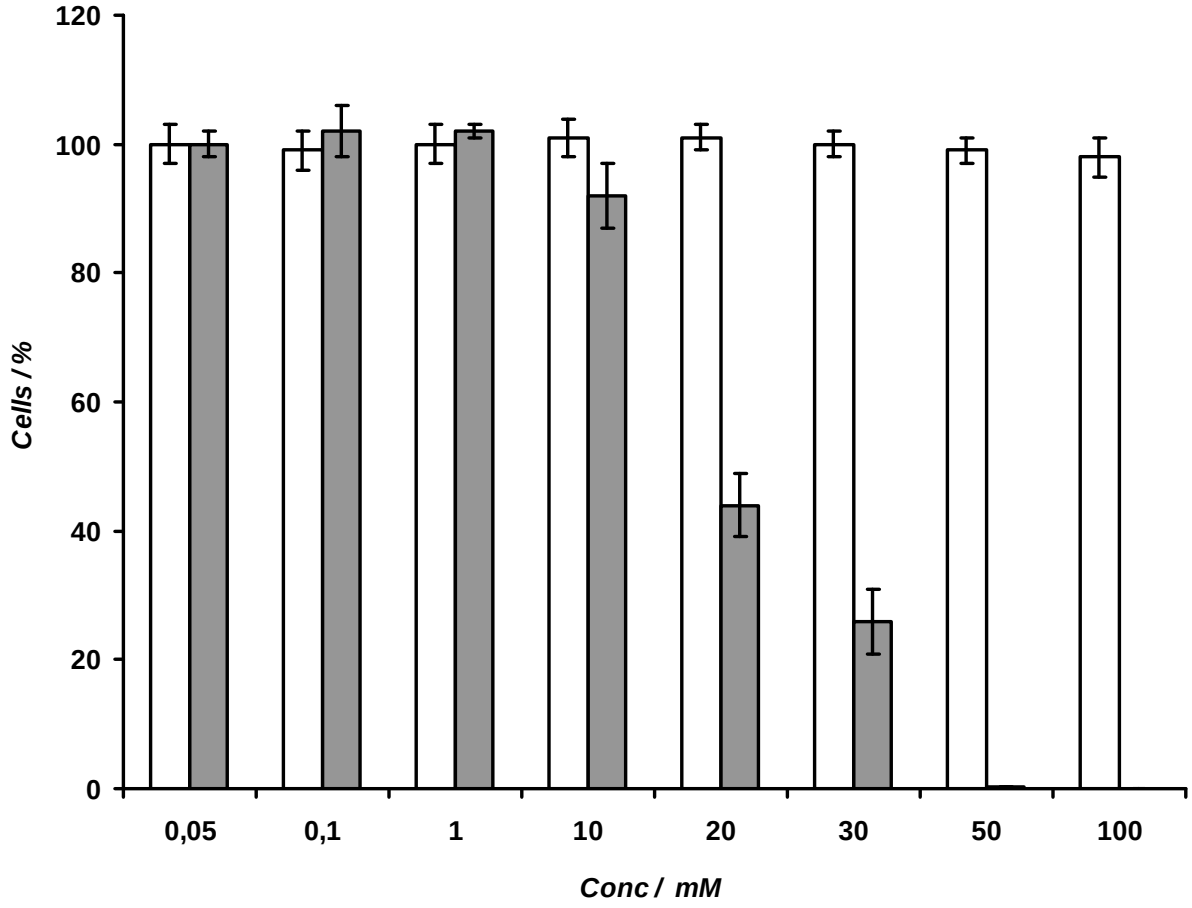

Figure S6

TRITC-MSN-Cys-FITC (Control)

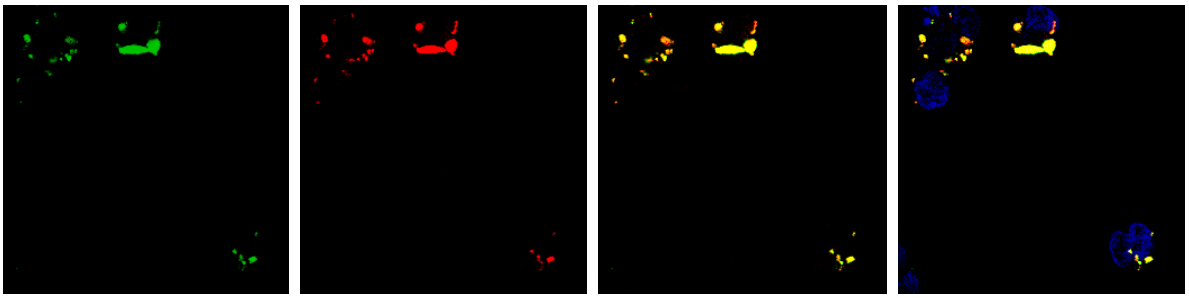

TRITC-MSN-Cys-FITC

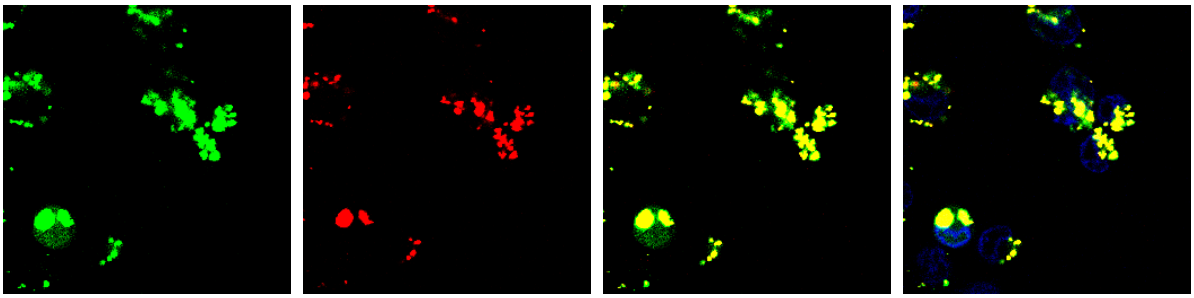

TRITC-MSN-S-Cys-FITC in presence of GSH monoester (10 mM)

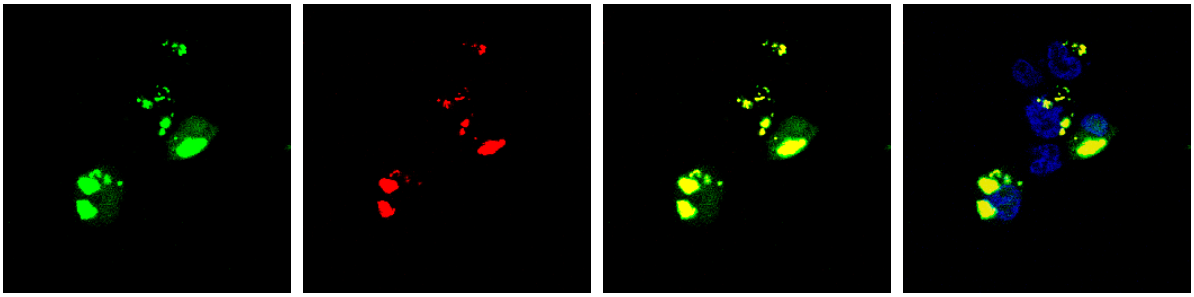

Figure S7

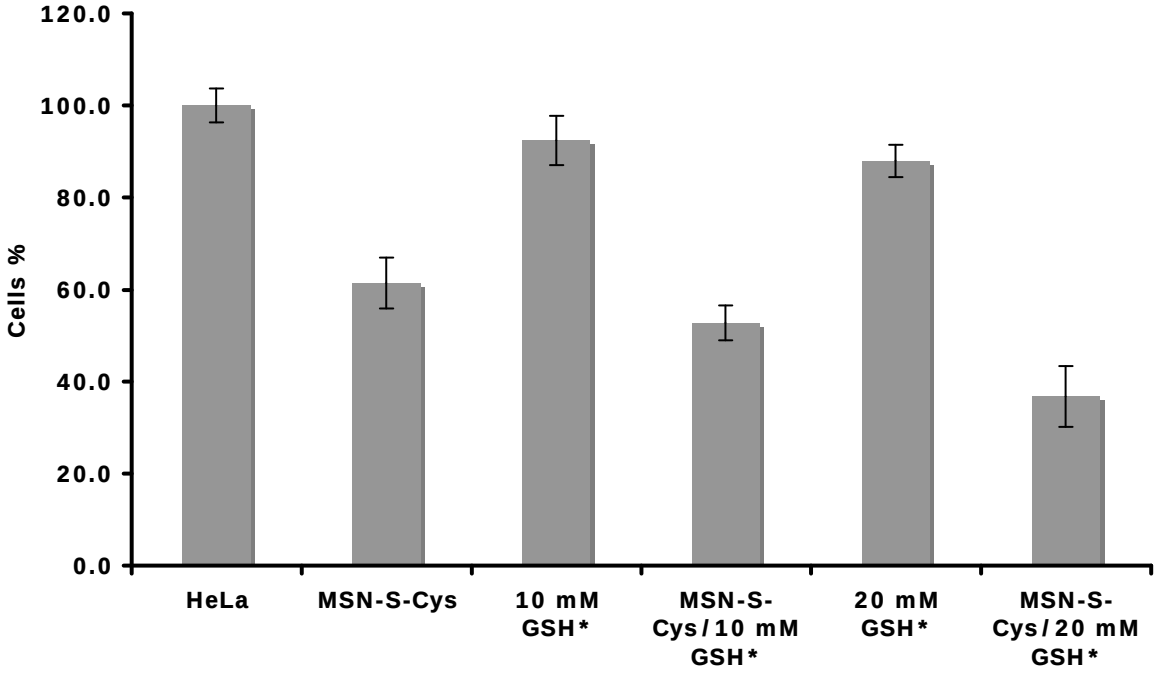
120.0
100.0
80.0
60.0
40.0
20.0
0.0
Cells %
HeLa
MSN-S-Cys
10 mM GSH*
MSN-S-Cys/10 mM GSH*
20 mM GSH*
MSN-S-Cys/20 mM GSH*

CHAPTER 5. TUNING THE CELLULAR UPTAKE AND CYTOTOXICITY PORPERTIES OF OLIGONUCLEOTIDE INTERCALATOR-FUNCTIONALIZED MESOPOROUS SILICA NANOPARTICLES WITH HUMAN CERVICAL CANCER CELLS (HeLa)

A manuscript submitted to **Biomaterials**

Juan L. Vivero-Escoto, Igor I. Slowing, and Victor S.-Y. Lin

Abstract

A series of organically functionalized, MCM-41 type mesoporous silica nanoparticle materials (PAP-LP-MSN and AP-PAP-MSN) with different pore sizes (5.7 nm and 2.5 nm, respectively) were synthesized and characterized. We selectively decorated the exterior particle surface of PAP-LP-MSN and the interior pore surface of AP-PAP-MSN with an oligonucleotide intercalating phenanthridinium functionality. While phenanthridinium itself is a cell membrane impermeable molecule, we demonstrated that both these phenanthridinium-immobilized PAP-LP-MSN and AP-PAP-MSN materials could indeed be internalized by live human cervical cancer cells (HeLa). We discovered that the PAP-LP-MSN nanoparticles with the phenanthridium groups located on the exterior surface were able to bind to cytoplasmic oligonucleotides, such as messenger RNAs, of HeLa cells resulting in sever cell growth inhibition. In contrast, the cytotoxicity of AP-PAP-MSN, where the same oligonucleotide intercalating molecules were anchored inside the pores, was significantly lowered upon the endocytosis by HeLa cells. We envision that this approach of combining the selective functionalization of the two different surfaces (exterior particle and interior pore surfaces) with morphology control of mesoporous silica nanoparticles would lead to a new

generation of nanodevices with tunable biocompatibility and cell membrane trafficking properties for many biomedical applications.

Introduction

Recent advancements on the synthesis of mesoporous silica nanoparticles (MSNs) have attracted much attention for their unique structural features, such as high total surface area (> 800 m^2/g), tunable pore diameter (2-10 nm), and narrow particle size distribution[1-5]. In contrast to other non-porous solid nanoparticles, MSNs offer two different surfaces, i.e., the exterior particle and interior pore surfaces. The chemical accessibility to these surfaces of MSNs could be tuned by varying the pore diameters and particle sizes of these materials. By taking advantage of this characteristic of MSNs, one can manipulate how these materials interact with cell membranes, subcellular organelles, and biological macromolecules, such as proteins and oligonucleotides, for drug/gene delivery and bio-sensor applications [6-15]. For example, we recently reported on the different hemolytic properties of MSN and amorphous silica with live red blood cells (RBC) [16]. We demonstrated that, contrary to the known cytotoxicity of amorphous silica towards RBC, MSN exhibits a high biocompatibility at concentrations adequate for pharmacological applications. We discovered that the hemolytic property of silica is related to the amount of silanol groups accessible to the cell membrane. The low hemolytic activity of MSN was attributed to the fact that most of the silanol groups are “hidden” inside the mesoporous channels that are not accessible to the cell membrane of RBC [16].

In addition to the interaction between cell membrane and the intrinsic silanol functionality of MSN, we also examined the efficiency and mechanism for the endocytosis and escape of endosomal entrapment of several MSN materials with their exterior particle

surface derivatized with various organic molecules [17, 18]. Our results showed that the presence of these different organic functional groups on the exterior particle surface of MSN indeed had a pronounced effect on the endocytic efficiency and pathways of MSNs with live human cancer cells [17, 18]. However, to the best of our knowledge, no prior study reported in the literature on how the properties of cell membrane trafficking and intracellular behaviors would be altered if the same organic functional groups would be immobilized on the interior pore surface of MSN.

In this study, we report on a strategy that combines the pore and particle morphology control with the organic functionalization of MSN to decorate a selective (interior or exterior) surface of the mesoporous nanoparticles with an oligonucleotide-intercalating functionality, namely phenanthridium (PAP). The endocytosis efficiencies and the interactions with intracellular oligonucleotides of these PAP-functionalized MSNs with different chemical accessibility were investigated. In general, molecules with the phenanthridinium group, such as ethidium bromide (EtBr) and propidium iodide (PI), are excluded from healthy viable cells because of their low permeability through the plasmic membrane. However, it has been reported in the literature that these molecules can penetrate damaged plasmic and nuclear membranes of animal cells [19, 20]. They are genotoxic and mutagenic because of their strong binding affinity to nuclear DNAs and RNAs via intercalation, and thereby blocking the gene replication and transcription processes [21-26]. Ideally, if one could find ways to carry these strong oligonucleotide intercalators through the intact plasmic membrane of a healthy live cell, while preventing them from entering the nucleus, it would be possible to design a phenanthridinium-based system for the selective sequestration of cytoplasmic oligonucleotides, i.e., messenger RNAs.

Herein, we describe the synthesis and characterization of two N-[3-(3,8-diamino-6-phenyl-5-phenanthridinium)propyl]-3-aminopropyl-functionalized, MCM-41 type mesoporous silica nanoparticle materials (PAP-LP-MSN and AP-PAP-MSN) that have the same average particle size (300 nm) and different pore diameters (5.7 and 2.5 nm, respectively). The large particle sizes of both materials prevent them from entering the nuclei of live mammalian cells, suggesting that the endocytosed particles would likely to be interacting only with cytoplasmic species. In the case of PAP-LP-MSN, the oligonucelotide intercalating PAP groups are located on the external surface of MSN. In contrast, AP-PAP-MSN contains the same intercalator functionality inside of the mesopores, preventing any possibility of interaction with oligonucleotides that are too large in size to penetrate the 2.5 nm pores.

As depicted in Figure 1, we examined the cell membrane permeability of the two phenanthridinium-functionalized MSN materials with live human cervical cancer cells (HeLa). Interestingly, we discovered that PAP-LP-MSN and AP-PAP-MSN were efficiently endocytosed by HeLa cells. In contrast to the free phenanthridinium molecules that can penetrate the nuclear membrane, these organically functionalized MSN particles were not able to enter the nucleus and remained in the cytoplasm because of the large particle size. Furthermore, our results indicated that phenanthridinium-functionalized MSNs (PAP-LP-MSN) was able to sequester and bind to cytoplasmic oligonucleotides to inhibit the expression of a green fluorescent protein introduced by an extraneous plasmid DNA vector (pEGFP1-C1). We envision that the further developments of these organically functionalized MSN materials can lead to a new generation of nanodevices for the manipulation of many intracellular biochemical processes.

Results and Discussion

To construct the PAP-LP-MSN and AP-PAP-MSN oligonucleotide intercalating systems, we first synthesized mesoporous silica nanoparticle materials (LP-MSN and MSN) according to the procedure that we have reported previously [6, 12, 27]. LP-MSN and MSN materials exhibited a MCM-41 type of hexagonally packed, channel-like mesoporous structure with a monodisperse particle size distribution. The average pore diameter for LP-MSN was expanded to 5.7 nm in comparison to MSN (2.5 nm) without compromising the hexagonal honeycomb mesoporous structure and the spherical particle morphology.

As depicted in Scheme S1 of the Supporting Information (SI), we functionalized the as-synthesized, CTAB-containing LP-MSN and MSN materials with an aminopropyl group by grafting an organoalkoxysilane, aminopropyltrimethoxysilane (AP-TMS), onto the exterior surfaces of these particles in refluxing toluene. The resulting AP-LP-MSN and AP-MSN materials were isolated and purified as described in the materials and methods section. We then reacted the commercially available 3,8-diamino-6-phenylphenanthridine with ethyl chloroformate in dry pyridine to yield the "ethoxycarbonyl-protected" 3,8-bisethoxycarbonylamino-6-phenyl-phenanthridine (Compound 1) as shown in Scheme S2 of the SI. Compound 1 was subsequently converted to a 3,8-bis-ethoxycarbonylamino-5-(3'-propylbromine)-6-phenyl-phenanthridium bromide (Pht-Br) by reacting with 1,3-dibromopropane in refluxing anhydrous THF. The Pht-Br was reacted with the aforementioned AP-LP-MSN materials to covalently anchor the desired phenanthridium functionality on the exterior surface of these mesoporous silica nanoparticles. The resulting phenanthridium functionalized PAP-LP-MSN materials were washed extensively with methanol and DMSO to remove any physisorbed phenanthridium derivatives. Finally, the

surfactant CTAB was removed via a previously reported acidic extraction method [12]. The ethoxycarbonyl protecting group of the phenanthridium functionality of PAP-LP-MSN was also removed during this acid extraction process.

In the case of AP-PAP-MSN material, the surfactant CTAB was removed from AP-MSN via acid extraction method as depicted in Scheme S3 of the SI. We then reacted in situ AP-TMS and Pht-Br in dry toluene, the resulting organo-silane derivative (PAP-TMS) was grafted in the internal surface of AP-MSN by refluxing in toluene as described above. Finally the material was washed in acidic conditions to remove the protecting group of the phenanthridium functionality of AP-PAP-MSN.

The mesoporous structures of the PAP-LP-MSN and AP-PAP-MSN materials were characterized by powder X-ray diffraction (XRD) spectroscopy, transmission electron microscopy (TEM), and nitrogen sorption isotherms (BET method for surface area and BJH method for pore size distribution). The powder XRD measurements of both PAP-LP-MSN and AP-PAP-MSN materials exhibited diffraction patterns characteristic of the MCM-41 type hexagonal mesoporous structure with three pronounced (100), (110), and (200) peaks (Figure S1 of the SD). The honeycomb-like mesoporous structure was further confirmed by transmission electron microscopy (TEM) as depicted in Figure 2. The light-colored spots representing the openings of the mesopores of PAP-LP-MSN and AP-PAP-MSN were packed in a hexagonal symmetry forming the typical MCM-41 type mesoporous structure. Moreover, we observed that these materials are monodisperse particles with an average particle diameter of 200 and 320 nm for AP-PAP-MSN and PAP-LP-MSN, respectively (Table S1 of the SI). The N_2 adsorption/desorption isotherms of the PAP-LP-MSN material revealed a type-IV BET isotherm, which is representative of a cylindrical, channel-like

mesoporous structure. The total surface area was found to be 705 m^2/g. Also, the BJH analysis of PAP-LP-MSN indicated a narrow pore size distribution with an average pore diameter of 57 Å (Figure S2 and Table S1 of the SI). In the case of AP-PAP-MSN, the material also exhibited a high BET surface area of 669 m^2/g and a BJH pore diameter of 25 Å (Figure S3 and Table S1 of the SI).

The presence of phenanthridium functional group on the surface of PAP-LP-MSN was confirmed by ^{13}C and ^{29}Si CP-MAS NMR spectroscopy (Figure S4 of the SI). The amounts of phenanthridium functionality on the surfaces of the PAP-LP-MSN and AP-PAP-MSN were determined to be 0.238 and 0.465 mmol/g, respectively by UV/Vis as described in the materials and methods section.

We have demonstrated in our previous reports that the MSN materials can be efficiently endocytosed by various cell types, but cannot penetrate the nucleus membrane of live cells because of their large particle sizes [6, 17]. By immobilizing the phenanthridium functionality on the surface of MSN particles, we anticipated that the PAP-LP-MSN and AP-PAP-MSN materials would be able to penetrate the plasmic membrane of live cells. To verify this hypothesis, we measured the effective concentrations (EC_{50}) via flow cytometry for the endocytosis of PAP-LP-MSN and AP-PAP-MSN by live human cervical cancer cells (HeLa) (Figure 3). The observed EC_{50} values, 23.7 and 6.6 μg/mL, for PAP-LP-MSN and AP-PAP-MSN, respectively, are within the same order of magnitude with that of pure inorganic MSN material (12.0 μg/mL). The results confirmed that these materials could indeed be internalized by live HeLa cells.

To locate these materials intracellularly, we applied fluorescence confocal microscopy to examine the red fluorescence emitting from the phenanthridium groups of

PAP-LP-MSN nanoparticles that were endocytosed by HeLa cells. A series of fluorescence images of different cross-sections of PAP-LP-MSN-containing HeLa cells were obtained by changing the focal depth every 1.2 μm vertically. As depicted in Figure 4, DAPI-stained nuclei was clearly observed by exciting the cells with a UV laser at wavelengths from 340 to 365 nm (Figure 4b). Red fluorescence was observed within the cell bodies of these HeLa cells upon excitation at 568 nm (Figure 4c), which strongly indicates that PAP-LP-MSN materials were indeed endocytosed by HeLa cells. The overlapped image of both micrographs allows us to conclude that even though PAP-LP-MSN materials are inside of the cell, they were not able to penetrate the nucleus (Figure 4d).

As described previously, phenanthridium compounds, such as ethidium bromide (EtBr) are genotoxic and mutagenic [21, 22]. The lethal concentration (LC_{50}) value of ethidium bromide with different cell types was determined to be ranging from 0.12 to 5.13 mg/L (0.3 to 13 μM) (30, 31). In contrast to the free molecular ethidium bromide that cannot effectively penetrate intact cellular membrane, the phenanthridium functionality is covalently attached to the surface of mesoporous silica nanoparticles in the cases of PAP-LP-MSN and AP-PAP-MSN. As described above, both PAP-LP-MSN and AP-PAP-MSN could be efficiently uptaken by HeLa cells. Presumably, the levels of cytotoxicity of PAP-LP-MSN material should be significantly higher than that of EtBr due to the higher membrane permeability. To examine the cytotoxicity of PAP-LP-MSN and AP-PAP-MSN, we conducted a cell viability (Guava) test of these materials with live HeLa cells. As illustrated in Figure 5, the cell growth inhibition effects of both materials are dosage dependent and the corresponding levels of cytotoxicity of PAP-LP-MSN (LC_{50} = 66 mg/L; 15.75 μM) and AP-PAP-MSN (LC_{50} > 100 mg/L; 28.2 μM) are not higher than those of free phenanthridium

molecules. It is interesting to note that, in the case of PAP-LP-MSN, the LC_{50} value is at least twice higher than AP-PAP-MSN material (Figure 5), even the amount of phenanthridium group grafted is almost twice smaller in PAP-LP-MSN (0.238 mmol/g) than AP-PAP-MSN (0.465 mmol/g). These results suggested that our phenanthridium-functionalized PAP-LP-MSN material could perhaps bind to those oligonucleotides that are present in the cytoplasm and could not access and intercalate to the nuclear oligonucleotides. But in the case of AP-PAP-MSN the cytotoxicity should be lower because even the phenantridium group is efficiently internalized into HeLa cells the group is grafted inside the pores of the material, which avoid most of the contact with cytoplasmic oligonucleotides.

To verify the above mentioned hypothesis and to investigate the mechanism of cell growth inhibition, we stained the RNA molecules of live HeLa cells (5×10^4 cells in 3 mL D-10 medium) with a green fluorescent RNA marker (SYTO RNA®Select™; 500 nM) in the presence of PAP-LP-MSN (40 μg/mL). The endocytosis of PAP-LP-MSN into these RNA-stained HeLa cells was monitored by fluorescence confocal microscopy (Figure 6). The observed green fluorescent spots of SYTO®RNASelect™ in Figure 6a represent the locations of intracellular RNAs, whereas the red fluorescent areas are the positions of PAP-LP-MSN particles inside the HeLa cells (Figure 6b). Interestingly, after 22 hours of incubation, most of the cytoplasmic RNAs were localized in specific spots inside the cell body. By superimposing the green (SYTO®RNASelect™) and the red (PAP-LP-MSN) fluorescence images, we found that both cytoplasmic RNAs and PAP-LP-MSN particles coincided at the same spots as illustrated by the orange-colored (red + green) fluorescent spots in Figure 6c. This result strongly suggested that the intracellular RNA molecules were sequestered and bound to the PAP-LP-MSN particles.

To investigate whether there was the same effect with AP-PAP-MSN, the material was introduced to the RNA-stained HeLa cells and the endocytosis of these nanoparticles was monitored and analyzed by fluorescence confocal microscopy. As depicted in Figure 7a-c, the AP-PAP-MSN particles could indeed be internalized by live HeLa cells. In contrast to the case of PAP-LP-MSN, the cytoplasmic RNAs were not localized in a few spots as depicted by the green fluorescent areas in Figure 7a. On the other hand, the AP-PAP-MSN particles appear to be localized inside the cells as represented by the red fluorescent spots shown in Figure 7b. The majority of RNA molecules apparently were not sequestered by the AP-PAP-MSN material since there were only a few orange-colored spots that could be observed in the overlapped micrograph (Figure 7c). By comparing this result with those of PAP-LP-MSN (Figure 7d-f) and the RNA-stained HeLa cells (Figure 7g-i), it was obvious that a high level of RNA-binding could be achieved by anchoring the phenanthridium groups on the exterior surface of MSN. In addition, we have conducted a control experiment, where the RNA marker and non-functional MSN or LP-MSN were mixed and introduced to HeLa cells, and the same confocal fluorescence studies were performed on these samples. As shown in Figure S5 of the SI, we found no localized green fluorescence spots inside the cells indicating that the cytoplasmic oligonucleotides were not sequestered to the locations of MSN or LP-MSN nanoparticles. These results clearly indicated that the binding between the RNAs and these MSN nanoparticles depends on the accessibility of the phenanthridium functionality to the targeted oligonucleotides and not due to some non-specific surface adsorption between oligonucleotide and silica.

To rule out the possibility that the spots of orange-colored fluorescence were the outcome of the surface adsorption of the green fluorescent RNA marker on the red

fluorescent PAP-LP-MSN, and not from the intercalation of phenanthridium to the RNA, we examined the binding between the PAP-LP-MSN material and yeast tRNA in PBS buffer (pH 7.4) by fluorescence emission spectroscopy. The suspension of these species was excited at a wavelength of 450 nm and the intensity of fluorescence emission λ_{max} (520 nm) of phenanthridium was measured. Upon the introduction of green fluorescent RNA marker to the suspension of PAP-LP-MSN, we did not observe any increase of the fluorescence intensity of the phenanthridium group at 520 nm. As was previously reported in the literature [28-30], the fluorescence intensity of phenanthridium increases upon intercalation to the base-pairs of oligonucleotides. As shown in Figure S6 of the SI, the fluorescence intensity at 520 nm was significantly enhanced when the yeast tRNA was added to the suspension of PAP-LP-MSN. This result confirmed that PAP-LP-MSN could indeed bind to the yeast tRNA molecules via intercalation.

To further confirm that the PAP-LP-MSN materials could sequester and bind to cytoplasmic oligonucleotides, we introduced an extraneous plasmid DNA (pEGFP-C1) that is encoding for an enhanced green fluorescence protein (EGFP) to HeLa cells via a gene transfection method that we have developed and reported previously[6]. We cultured and transfected two batches of HeLa cells with the pEGFP-C1 DNA for 2 h. As we previously demonstrated, the endocytosis of this gene transfection system into the HeLa cells took place within 1 h [6]. In one of the two cultures, we introduced PAP-LP-MSN, while the cells in the other culture was used as the control sample without PAP-LP-MSN. The expression of EGFP in both cultures was evaluated using fluorescence microscopy after 32 h of the introduction of PAP-LP-MSN. Figure 8a shows the successful expression of EGFP (green spots) in the control sample. In contrast, no expression of EGFP was observed in the culture

where the PAP-LP-MSN was added (Figure 8b). The result clearly indicated that PAP-LP-MSN material was able to inhibit the gene transfection and the expression of EGFP.

Conclusions

We have demonstrated that, by covalently immobilized the oligonucleotide intercalator phenantridium group on either the exterior particle or interior pore surface of mesoporous silica nanoparticles materials, the cell membrane impermeable PAP functionality could be brought into the cytoplasm of live HeLa cells efficiently. We found that the endocytosis efficiency of AP-PAP-MSNs is higher than that of PAP-LP-MSNs, which is consistent with our previous observation, i.e., the more positively charged MSN particles are more cell membrane permeable[17]. While the amounts of PAP on the surface of PAP-LP-MSN is only 50% of that of AP-PAP-MSNs, our result indicated that the PAP-LP-MSNs material could indeed bind to intracellular oligonucleotides leading to significant inhibition of protein biosynthesis and cell growth. In contrast, the same intercalator group anchored on the interior surface of AP-PAP-MSN did not exhibit any interaction with cytoplasmic oligonucleotides. The pronounced difference in the intracellular behavior of these MSN materials could be attributed to the size discrimination effect preventing the oligonucleotides from accessing the PAP groups inside of AP-PAP-MSN. We envision that this approach of combining the selective surface functionalization with morphology control of mesoporous silica nanoparticles would lead to new intracellular nanodevices with tunable biocompatibility and cell membrane trafficking properties. These materials could play a key role in manipulating various intracellular processes for many biomedical and biotechnological applications.

Acknowledgment

This research was supported by NSF Career Award (CHE-02239570), CMS-0409625, and US DOE (AL-03-380-011 and W-7405-Eng-82). The authors thank Dr. C.-W. Wu for experimental assistance in TEM measurement of the materials and helpful discussions.

References

[1] B. G. Trewyn, I. I. Slowing, S. Giri, H.-T. Chen, V. S. Y. Lin, Acc. Chem. Res. 2007, 40, 846.

[2] S. Giri, B. G. Trewyn, V. S. Y. Lin, Nanomedicine 2007, 2, 99.

[3] S. Angelos, E. Johansson, J. F. Stoddart, J. I. Zink, Adv. Funct. Mater. 2007, 17, 2261.

[4] I. I. Slowing, B. G. Trewyn, S. Giri, V. S. Y. Lin, Adv. Funct. Mater. 2007, 17, 1225.

[5] M. Vallet-Regi, F. Balas, D. Arcos, Angew. Chem., Int. Ed. 2007, 46, 7548.

[6] D. R. Radu, C.-Y. Lai, K. Jeftinija, E. W. Rowe, S. Jeftinija, V. S. Y. Lin, J. Am. Chem. Soc. 2004, 126, 13216.

[7] S. Giri, B. G. Trewyn, M. P. Stellmaker, V. S. Y. Lin, Angew. Chem., Int. Ed. 2005, 44, 5038.

[8] S. Angelos, Y.-W. Yang, K. Patel, J. F. Stoddart, J. I. Zink, Angew. Chem., Int. Ed. 2008, 47, 2222.

[9] R. Casasus, E. Climent, M. D. Marcos, R. Martinez-Manez, F. Sancenon, J. Soto, P. Amoros, J. Cano, E. Ruiz, J. Am. Chem. Soc. 2008, 130, 1903.

[10] F. Torney, B. G. Trewyn, V. S. Y. Lin, K. Wang, Nature Nanotechnol. 2007, 2, 295.

[11] N. K. Mal, M. Fujiwara, Y. Tanaka, Nature 2003, 421, 350.

[12] C.-Y. Lai, B. G. Trewyn, D. M. Jeftinija, K. Jeftinija, S. Xu, S. Jeftinija, V. S. Y. Lin, J. Am. Chem. Soc. 2003, 125, 4451.

[13] K. Patel, S. Angelos, W. R. Dichtel, A. Coskun, Y.-W. Yang, J. I. Zink, J. F. Stoddart, J. Am. Chem. Soc. 2008, 130, 2382.

[14] R. Mortera, J. Vivero-Escoto, I. I. Slowing, E. Garrone, B. Onida, V. S. Y. Lin, Chem. Commun. 2009, 3219.

[15] J. L. Vivero-Escoto, I. I. Slowing, C.-W. Wu, V. S. Y. Lin, J. Am. Chem. Soc. 2009, 131, 3462.

[16] I. I. Slowing, C.-W. Wu, J. L. Vivero-Escoto, V. S. Y. Lin, Small 2009, 5, 57.

[17] I. Slowing, B. G. Trewyn, V. S. Y. Lin, J. Am. Chem. Soc. 2006, 128, 14792.

[18] T.-H. Chung, S.-H. Wu, M. Yao, C.-W. Lu, Y.-S. Lin, Y. Hung, C.-Y. Mou, Y.-C. Chen, D.-M. Huang, Biomaterials 2007, 28, 2959.

[19] J. A. Steinkamp, B. E. Lehnert, N. M. Lehnert, J. Immunol. Methods 1999, 226, 59.

[20] B. L. Sailer, A. J. Nastasi, J. G. Valdez, J. A. Steinkamp, H. A. Crissman, Cytometry 1996, 25, 164.

[21] J. T. Macgregor, I. J. Johnson, Mutat. Res. 1977, 48, 103.

[22] J. McCann, E. Choi, E. Yamasaki, B. N. Ames, Proc. Natl. Acad. Sci. U. S. A. 1975, 72, 5135.

[23] H. Ihmels, D. Otto, Top. Curr. Chem. 2005, 258, 161.

[24] M. Okamaoto, T. Ohsato, K. Nakada, K. Isobe, J. N. Spelbrink, J.-I. Hayashi, N. Hamasaki, D. Kang, Curr. Genet. 2003, 43, 364.

[25] V. D. Vacquier, J. Brachet, Nature 1969, 222, 193.

[26] W. H. Elliott, Biochem. J. 1963, 86, 562.

[27] I. I. Slowing, B. G. Trewyn, V. S. Y. Lin, J. Am. Chem. Soc. 2007, 129, 8845.

[28] J. B. LePecq, C. Paoletti, J. Mol. Biol. 1967, 27, 87.

[29] M. J. Waring, J. Mol. Biol. 1965, 13, 269.

[30] E. Nordmeier, J. Phys. Chem. 1992, 96, 6045.

Figure captions

Figure 1. Schematic representation of the endocytosis of AP-PAP-MSN/PAP-LP-MSN into HeLa cells and binding to cytoplasmic oligonucleotides.

Figure 2. Transmission electron micrographs (TEM) of AP-PAP-MSN (a, b) and PAP-LP-MSN (c, d). The typical hexagonal array of MCM-41 type mesoporous structure is visualized by the parallel strips and the light-colored spots in the micrographs.

Figure 3. Cell uptake of PAP-LP-MSN (■) and AP-PAP-MSN (◆) as a function of their concentration.

Figure 4. Confocal fluorescence images of HeLa cells with PAP-LP-MSN inside the cell body. (a) Phase contrast of the cells, (b) DAPI-stained nuclei, (c) red fluorescence of the endocytosed PAP-LP-MSN, and (d) the overlapped image of blue (nuclei) and red (PAP-LP-MSN) spots.

Figure 5. Cell growth inhibition of HeLa as a function of the concentration of AP-PAP-MSN (light-grey bars), and PAP-LP-MSN (dark-grey bars).

Figure 6. Confocal fluorescence images of HeLa cells with PAP-LP-MSN inside the cell body in the presence of RNA-staining dye (SYTO®RNASelect™) after 22 h of incubation. (a) SYTO®RNASelect™ stained cells, (b) red fluorescence of the endocytosed PAP-LP-MSN, and (c) the overlapped image of green (SYTO®RNASelect™) and red (PAP-LP-MSN) spots.

Figure 7. Confocal fluorescence images of HeLa cells loaded with AP-PAP-MSN (a-c), PAP-LP-MSN (d-f), and control (g-i) in the presence of SYTO®RNASelect™. (a, d, and g) SYTO®RNASelect™ stained cells, (b, e, and h) red fluorescence of the endocytosed PAP-

LP-MSN, and (c, f, and i) the overlapped image of green (SYTO®RNASelect™) and red (PAP-LP-MSN) spots.

Figure 8. Fluorescence images of HeLa cells transfected by the pEGFP-C1 DNA vector-coated G4-PAMAM-MSN system. (a) Phase contrast image of the cells and (b) Fluorescent image of the cells expressed the enhanced green fluorescent proteins (EGFP). (c) Phase contrast image and (d) fluorescent image of the cells treated with PAP-LP-MSN.

Figure 1

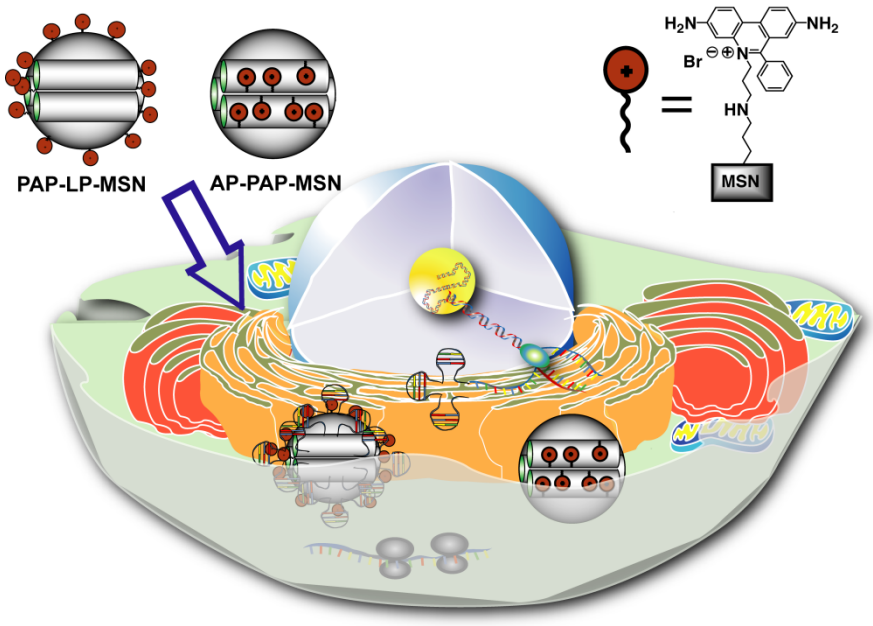

Figure 2

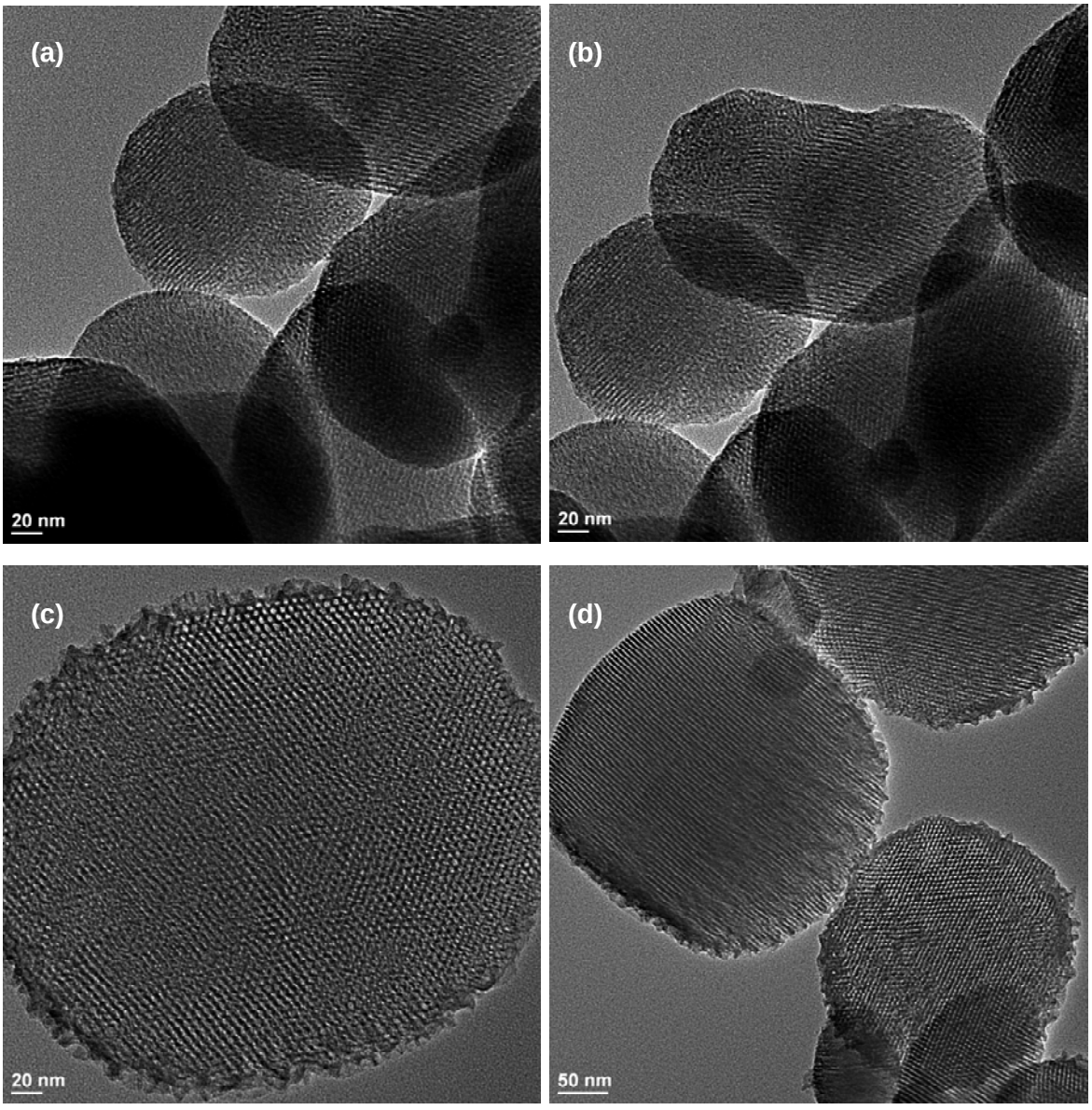

Figure 3

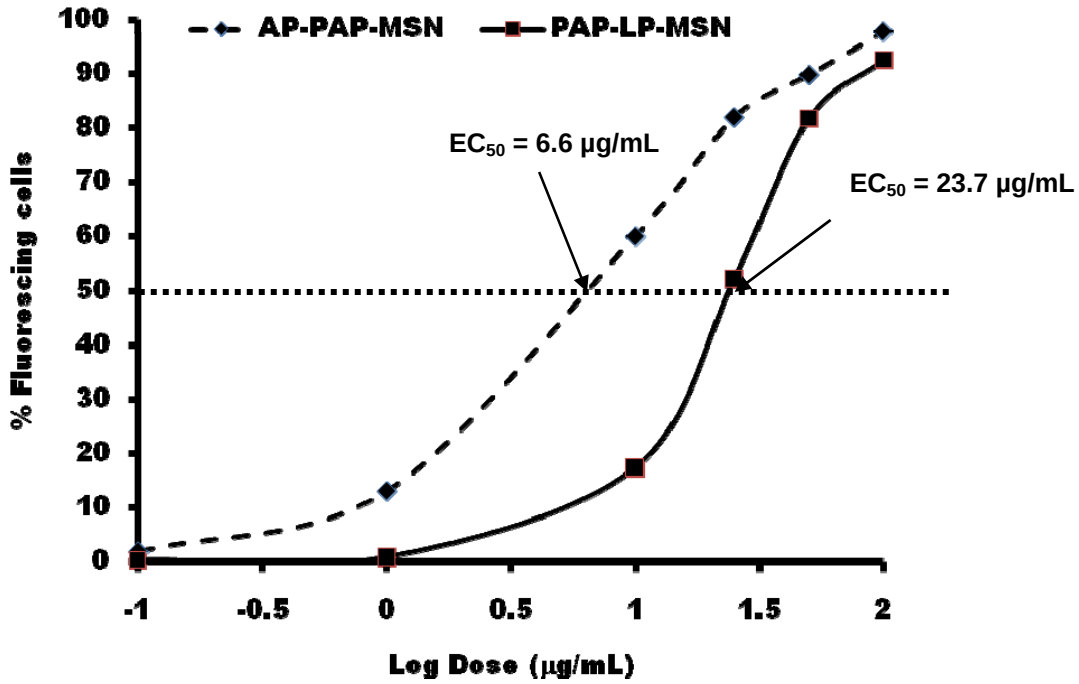
AP-PAP-MSN
PAP-LP-MSN
EC50 = 6.6 µg/mL
EC50 = 23.7 µg/mL
% Fluorescing cells
Log Dose (µg/mL)
100
90
80
70
60
50
40
30
20
10
0
-1
-0.5
0
0.5
1
1.5
2

Figure 4

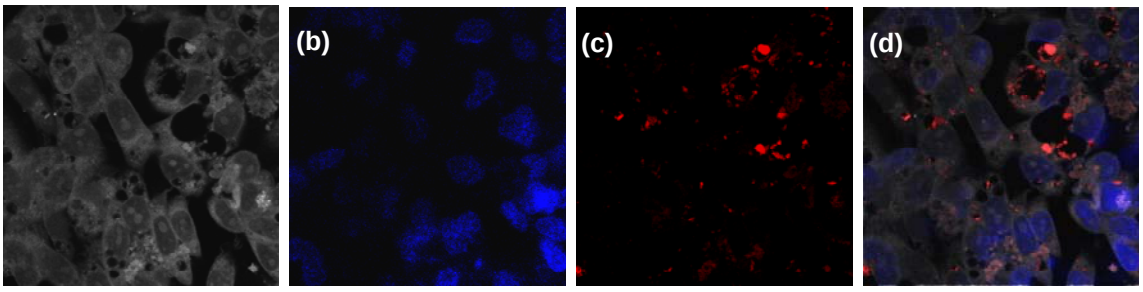

Figure 5

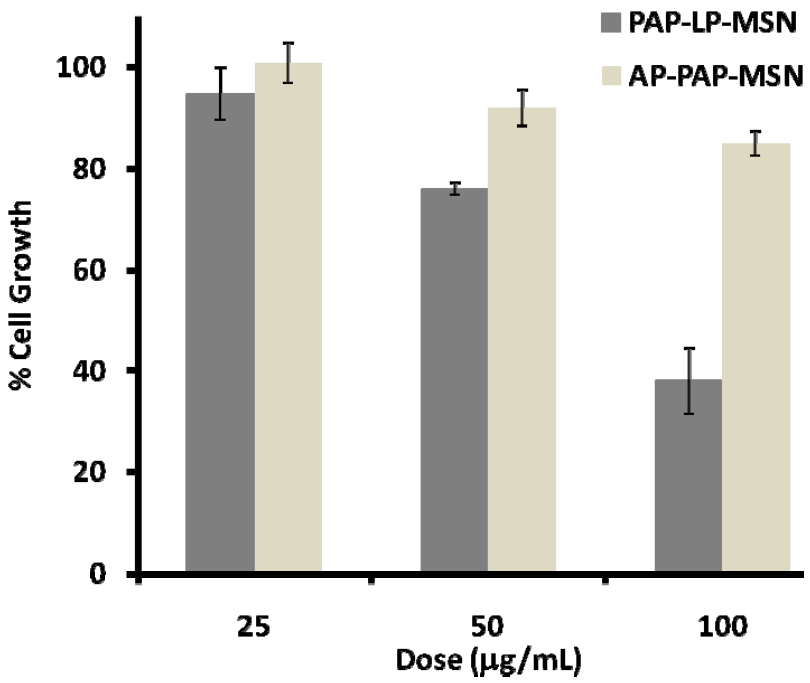
PAP-LP-MSN
AP-PAP-MSN
% Cell Growth
100
80
60
40
20
0
25
50
100
Dose (µg/mL)

Figure 6

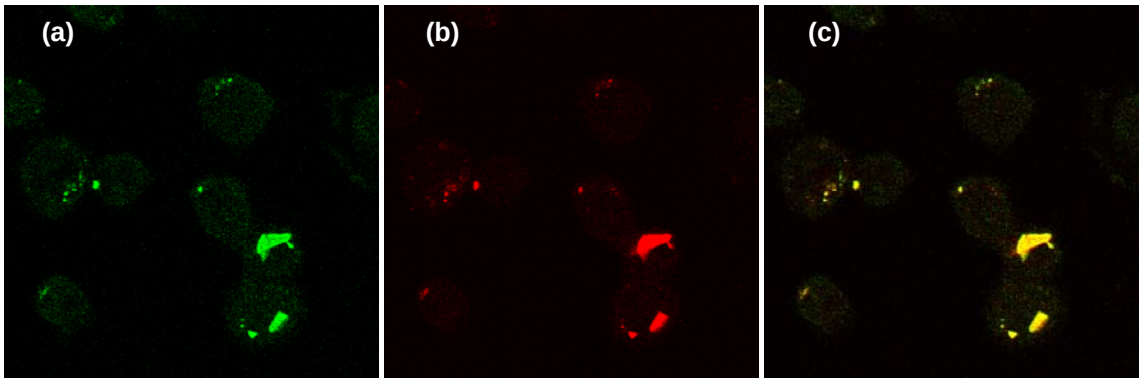

Figure 7

AP-PAP-MSN

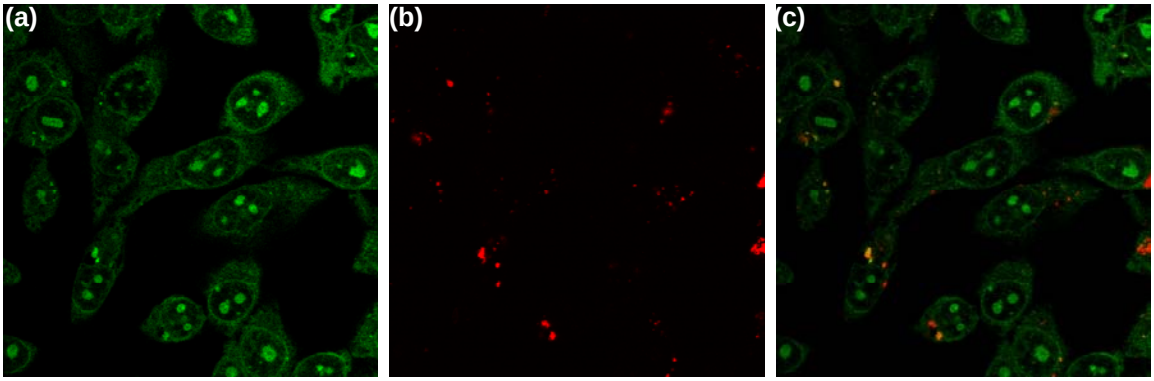

PAP-LP-MSN

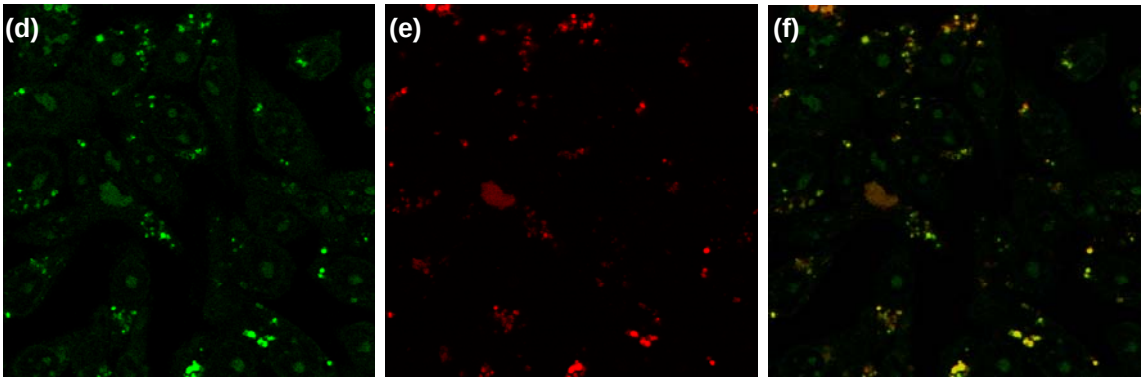

Control

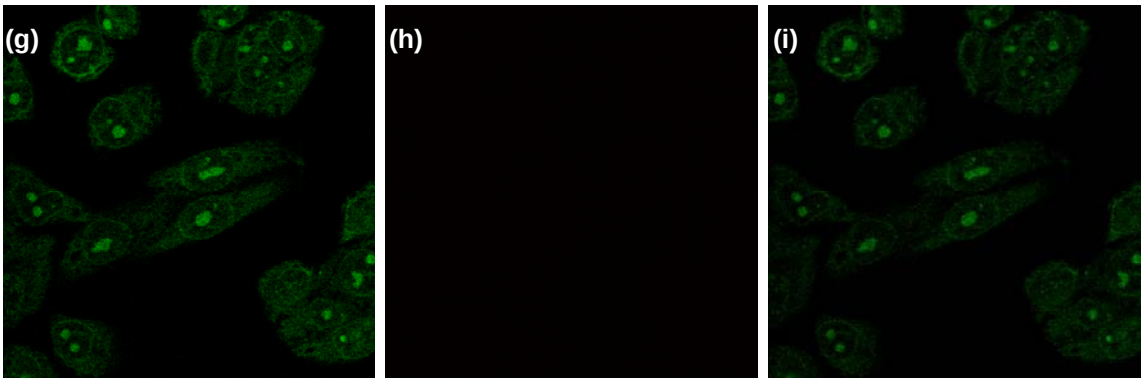

Figure 8

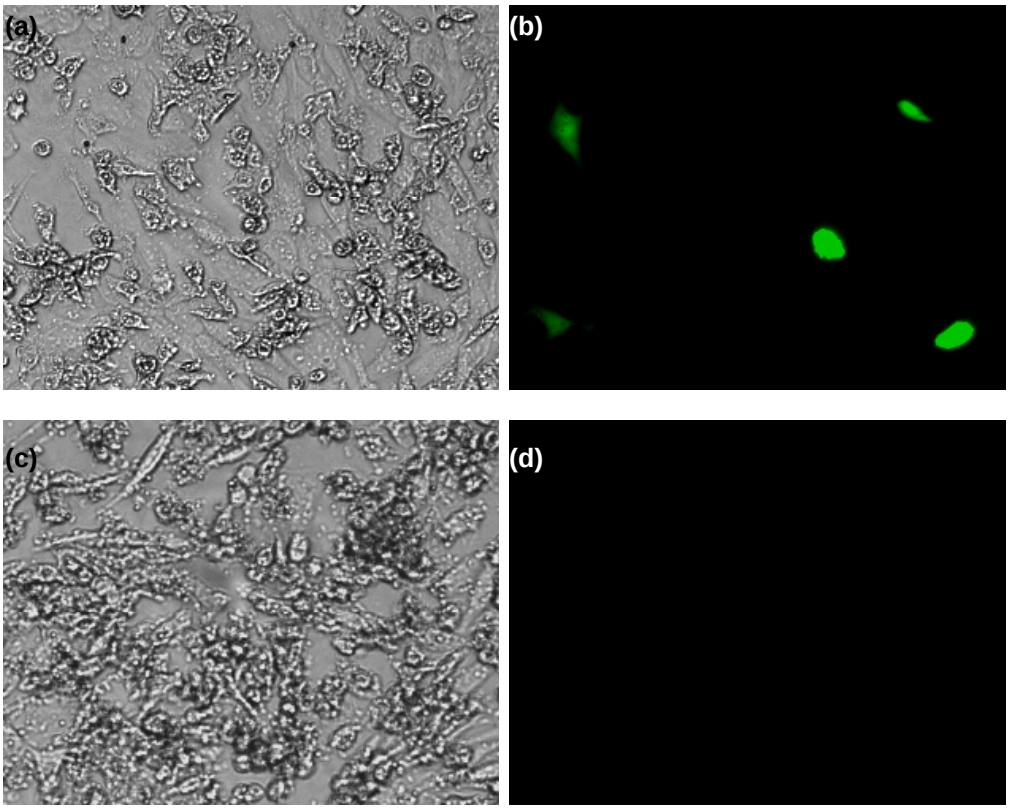

Appendix: Supporting information

Reagents and materials. Tetraethylorthosilicate (TEOS) was purchased from Gelest. Ethyl chloroformate was purchased from Acros. Cetyltrimethylammonium bromide, pyridine (anhydrous), 3-aminopropyltrimethoxysilane (AP-TMS), 3,8-diamino-6-phenyl-phenanthridine, 1,3-dibromopropane, 4,6-Diamidino-2-phenylindole dihydrochloride (DAPI), and PAMAM dendrimer (Generation 4) were purchased from Aldrich. SYTO®RNASelect™ RNA marker, and yeast tRNA were purchased from Invitrogen, Inc. Plasmid DNA encoding EGFP (Living Colors® pAcGFP1-C1 Vector) was purchased from Clontech. Donor Equine serum was purchased from HyClone. L-alanyl-L-glutamine, gentamicin sulfate, and penicillin-streptomycin solution were purchased from Mediatech, Inc. All chemicals were used as received.

Synthesis of mesoporous silica nanoparticles (MSN and LP-MSN). The detailed synthetic procedures for the preparation and purification of these materials were described in our previous reports[1,2,3].

Synthesis of 3,8-bis-ethoxycarbonylamino-6-phenyl-phenanthridine. The synthetic procedure was modified from a literature-reported method[4]. 3,8-Diamino-6-phenylphenanthridine (2.0 g, 7.01 mmol) was dissolved in dry pyridine (14.4 mL, 178.04 mmol), followed by the addition of ethyl chloroformate (1.44 mL, 15.08 mmol) at 25 °C. The dark red solution was slowly stirred at room temperature for 5 h, and then poured into cool water. The yellow precipitates were isolated to yield the desired 3,8-bis-ethoxycarbonylamino-6-phenyl-phenanthridine. ^{1}H-NMR (400 MHz, DMSO-d_6): δ 10.04 (s, 1H, NH, 3-Etoc), 10.00 (s, 1H, NH, 8-Etoc), 8.73 (d, J = 9.2 Hz, 1H, H1), 8.63 (d, J = 9.2 Hz, 1H, H10), 8.32 (s,1H, H7), 8.22 (d, J = 1.2 Hz, 1H, H4), 7.96 (d, J = 7.6 Hz, 1H, H9), 7.81

(dd, J = 9.2 Hz, J = 2.0 Hz, 1H, H2), 7.72-7.57 (m, 5H, 6-Ph), 4.19 (q, J = 6.8 Hz, 2H, CH2, 3-Etoc), 4.11 (q, J = 7.2 Hz, 2H, CH2, 8-Etoc), 1.28 (t, J = 6.8 Hz, 3H, CH3, 3-Etoc), 1.22 (t, J = 7.2 Hz, 2H, CH2, 8-Etoc). ^{13}C NMR (400 MHz, DMSO-d_6): δ 161.0, 154.3, 154.2, 143.8, 140.0, 138.6, 130.3, 129.3, 128.9, 125.1, 123.8, 123.4, 119.6, 119.2, 116.9, 115.7, 61.1 (CH2, 3, and 8-Etoc), 15.2 (CH3, 3-Etoc), 15.1 (CH3, 8-Etoc). MS (ESI): m/z $[M]^+$, 429.2; $[M+1]^+$, 430.2

Synthesis of 3,8-bis-ethoxycarbonylamino-5-(3'propylbromine)-6-phenyl phenanthridium bromide (Pht-Br). Following a literature procedure[5], 3,8-bis-ethoxycarbonylamino-6-phenyl-phenanthridine (400 mg, 0.93 mmol) was dissolved in 20 mL of dry THF. 1,3-Dibromopropane (3.6 mL) was added to the solution. The reaction mixture was refluxed for 9 days at 65 °C. The resulting solid product was filtered, washed with copious THF and dried under high vacuum to yield the purified Pht-Br. ^{1}H-NMR (400 MHz, DMSO-d_6): δ 10.37 (s, 1H, NH, 3-Etoc), 10.23 (s, 1H, NH, 8-Etoc), 8.90 (d, J = 9.0 Hz, 1H, H1), 8.81 (d, J = 9.0 Hz, 1H, H10), 8.57 (s,1H, H7), 8.38 (s, 1H, H4), 8.15 (d, J = 7.6 Hz, 1H, H9), 7.85 (d, J = 9.2 Hz, 1H, H2), 7.80-7.74 (m, 5H, 6-Ph), 4.69 (m, 2H, H1'), 4.19 (q, J = 6.8 Hz, 2H, CH2, 3-Etoc), 4.10 (q, J = 7.2 Hz, 2H, CH2, 8-Etoc), 3.56 (t, J = 6.2 Hz, 2H, H3'), 2.46 (m, 2H, H2'), 1.28 (t, J = 6.8 Hz, 3H, CH3, 3-Etoc), 1.20 (t, J = 7.2 Hz, 2H, CH2, 8-Etoc). ^{13}C NMR (400 MHz, DMSO-d_6): δ 161.7, 154.3, 154.1, 142.8, 142.4, 141.6, 140.1, 131.9, 131.0, 129.4, 128.2, 127.6, 124.5, 124.3, 121.6, 120.1, 116.7, 115.6, 61.5 (CH2, 3-Etoc), 61.4 (CH2, 8-Etoc), 47.5 (C1'), 33.2 (C3'), 31.2 (C2'), 15.2 (CH3, 3-Etoc), 15.1 (CH3, 8-Etoc). MS (TOF MS EI): m/z $[M]^+$, 551.4

Synthesis of the exterior grafted amino propyl MSN (AP-MSN and AP-LP-MSN). The CTAB-containing MSN or LP-MSN (1.0 g) and 1.0 mL (5.73 mmol) of

aminopropyltrimethoxysilane (AP-TMS) were added to 100 mL dry toluene. This reaction mixture was refluxed for 24 h. The resulting aminopropyl-grafted, CTAB-containing AP-MSN or AP-LP-MSN was washed with copious water and methanol, and dried under high vacuum. To remove CTAB, 1.0 g of CTAB-containing AP-MSN or AP-LP-MSN was added to a solution of 1.0 mL of HCl (37%) in 100 mL of methanol. This mixture was refluxed at 60 °C for 6h. The resulting solid was washed with methanol and water; and finally dried under high vacuum to afford AP-MSN or AP-LP-MSN

Synthesis of "ethoxycarbonyl-protected" phenanthridium aminopropyl LP-MSN (PAP-LP-MSN). AP-LP-MSN (250 mg) and Pht-Br (75 mg, 0.118 mmol) were added to 50 mL of dry toluene. The mixture was refluxed for 24 h. The solid product was filtered, washed several times with methanol and DMSO. The material was then dried under high vacuum. The amount of Pht-Br grafted to the MSN material was determined by measuring the solution concentrations of Pht-Br before and after the reaction. The UV/Vis absorption profiles of Pht-Br in methanol and DMSO were carefully calibrated (MeOH: λ = 440 nm, ε = 833.33 M^{-1}, R^2 = 0.993; DMSO: λ = 435 nm, ε = 1000 M^{-1}, R^2 = 0.999). To remove the ethoxycarbonyl-protecting group, 200 mg of the as-synthesized PAP-LP-MSN material was refluxed for 6 h in a solution of concentrated hydrochloric acid (0.2 mL) in 20 mL of methanol, followed by washing with copious deionized water and methanol. The isolated solid was dried under high vacuum.

Synthesis of the interior grafted phenanthridium aminopropyl MSN (AP-PAP-MSN). We first prepared the phenanthridium-aminopropyltrimethoxysilane (PAP-TMS) by reacting Pht-Br (63.1 mg, 0.10 mmol) with AP-TMS (20 μL, 0.113 mmol) and triethylamine (14 μL, 0.10 mmol) in 10 mL of refluxing toluene for 24 h. This solution was added to 40 mL of dry

toluene containing 250 mg of AP-MSN. The mixture was refluxed for 48 h under nitrogen. The resulting AP-PAP-MSN material was isolated through filtration and washed with copious methanol and DMSO. Finally, the product was acid washed to deprotect the PAP functionality. The purified final product was dried under high vacuum.

Characterization of materials. Surface analysis of the aforementioned materials was performed by nitrogen sorption isotherms in a Micromeritics TriStar surface area and porosity analyzer. The powder X-Ray diffraction patterns of these mesoporous materials were measured by a Scintag XDS-2000 powder diffractometer using Cu Kα irradiation. Solid-state ^{13}C and ^{29}Si crossed polarization magic angle spinning NMR (CP-MAS NMR) measurements of PAP-LP-MSN were obtained from a Bruker MSL-300 spectrometer equipped with a Bruker 4 mm rotor MAS probe. Particle morphology was investigated by using a Tecnai G^2 F20 transmission electron microscopy operating at 200 kV.

Cytotoxicity measurements. Viability assays of the HeLa cells in the presence and absence of PAP-LP-MSN and AP-PAP-MSN were studied by Guava ViaCount assay (Guava Technologies, Inc.). HeLa cells were first seeded in six-well plates with a density of 1×10^5 cells/mL in 3 mL of D-10 medium (Dubelcco Modified Eagle's Medium plus horse serum, *L*-alanyl-*L*-glutamine, gentamicin sulfate, and penicillin-streptomycin solution), and set in an incubator at 37 °C in a 5% CO_2 atmosphere for 24 h. After that, the media of the wells was replaced with freshly prepared D-10 media containing different concentrations of PAP-LP-MSN and AP-PAP-MSN materials ranging from 0 to 100 μg/mL, and the wells were set back into the incubator at 37 °C and 5% CO_2 for 2 days. The plates were then removed from the incubator, the media of each well was discarded, each well was washed with phosphate saline buffer (PBS) and the cells were trypsinized, centrifuged, and re-suspended in D-10 medium.

The cells in the re-suspended media were then counted and their viability was determined by the Guava ViaCount cytometry assay.

Confocal fluorescence microscopy measurements. HeLa cells were seeded at the density of 5×10^4 cells per well in six-well plates in 3 mL D-10 medium with coverslips at the bottom of the wells. After incubation for 24 h, the D-10 medium was replaced by 3 mL of PAP-LP-MSN or AP-PAP-MSN (50 μg/mL) in the serum-free DMEM medium for 24 h. The cell-plated coverslips were then washed with PBS and soaked for 30 min in 3 mL of 4',6-diamidino-2-phenyindole dihydrochloride (DAPI; 5.7 μM) and formaldehyde (3.7%) in 100 mM PBS buffer pH 7.44. The DAPI-stained coverslips were examined by a Leica TCS NT confocal fluorescence microscope system with a 100x oil immersion objective. DAPI-stained nuclei fluorescence micrographs were observed by exciting the cells with a UV laser at wavelengths from 340 to 365 nm. The red fluorescent PAP-LP-MSN and AP-PAP-MSN materials inside of the HeLa cells were visualized by excitation at 568 nm with a Krypton laser.

Imaging PAP-LP-MSN and AP-PAP-MSN inside HeLa cells in presence of SYTO®RNASelect™. HeLa cells were seeded at the density of 5×10^4 cells per well in six-well plates in 3 mL D-10 medium with coverslips at the bottom of the wells. After incubation for 24 h, the D-10 medium was replaced by 3 mL of PAP-LP-MSN or AP-PAP-MSN (40 μg/mL) in the D-10 medium for 22 h. The cell-plated coverslips were then washed with PBS twice and fixed by soaking them in 3 mL of methanol pre-chilled at 20 °C for 10 min. Methanol was then removed and the coverslips were washed twice with PBS. The cells were treated with SYTO®RNASelect™ green fluorescent cell stain (3 mL, 500 nM) in PBS and incubated for 20 min at room temperature. The staining solution was then removed and

the cells were rinsed twice with PBS. Finally, an aqueous solution of DAPI (6 μM) was added to the wells containing the coverslips and they were let to rest for 30 min at room temperature. After rinsing with PBS, the DAPI and RNASelect-stained coverslips were placed in microscope slides and examined by a Leica TCS NT confocal fluorescence microscope system with a 100x oil immersion objective. The green fluorescent SYTO®RNASelect™ marker was excited at 488 nm with an Argon Laser. The red fluorescent PAP-LP-MSN and AP-PAP-MSN materials inside of HeLa cells were visualized by excitation at 568 nm with a Krypton laser. PAP-LP-MSN/AP-PAP-MSN is considered to be bound to the intracellular RNAs when the green and the red spots are co-localized to give an orange color.

Binding study of PAP-LP-MSN and yeast tRNA. PAP-LP-MSN (2.0 mg) was introduced to 1.0 mL of PBS solution (pH= 7.4, 10 mM), followed by the addition of 5 μL yeast tRNA (10 mg/mL). The fluorescence emission of the mixture was measured by FluoroMax-2 fluorimeter (λ_{ex}= 450 nm).

Binding study of PAP-LP-MSN and RNA marker dye. PAP-LP-MSN (2.0 mg) was introduced to 1.0 mL of PBS solution (pH= 7.4, 10 mM), followed by the addition of 20 μL DMSO solution of SYTO®RNASelect™ marker (0.2 μM). The fluorescence emission of the mixture was measured by FluoroMax-2 fluorimeter (λ_{ex}= 450 nm).

Influence of PAP-LP-MSN on the expression of enhanced green fluorescence protein (EGFP) in HeLa cells. Modified from our previously reported procedure[1], 0.5 μg of a plasmid DNA (pEGFP-C1) that is encoding for an enhanced green fluorescence protein (Clontech) was added to a 100 μL suspension of G4-PAMAM-MSN (10 μg) that was prepared by dispersing MSN (1.0 mg) and G4-PAMAM (0.13 mL) in 1.0 mL of PBS (10

mM, pH 7.4) for 8 h at 25 °C. The mixture was stirred for 4h at 4 °C. From this mixture, 36 μL of the suspension were added to HeLa cells cultured on 48-well plates. HeLa cells were seeded at the density of 5×10^4 cells per well in 500 μL D-10 medium. After incubation for 24 h, the D-10 medium was replaced by 500 μL of a DMEM solution containing the transfection agent. After 2 h of incubation with the transfection agent at 37 °C, the mixture containing residual pEGFP DNA vector and G4-PAMAM-MSN complex was removed by washing the transfected cells with PBS buffer. The medium was replaced by 500 μL of PAP-LP-MSN (40 μg/mL) in the D-10 medium for 8 h. The suspension of PAP-LP-MSN was then removed and the wells were washed with PBS buffer, followed by adding 500 μL of the D-10 medium to the wells. The culture was continued for another 24 h to allow the incorporation of gene. The expression of pEGFP was monitored by using a LEICA DMIRE2 fluorescent microscope.

Measurement of the internalization of PAP-LP-MSN and AP-PAP-MSN in HeLa cells by flow cytometry. HeLa cells were seeded at the density of 5×10^4 cells per well in six-well plates in 3 mL D-10 medium with coverslips at the bottom of the wells. After incubation for 48 h, the D-10 medium was replaced by 3 mL of PAP-LP-MSN or AP-PAP-MSN suspensions at concentrations 1, 10, 25, 50, and 100 μg/mL) in the serum-free DMEM medium for 12 h. All the tests were run in triplicate. The cells were washed with medium and harvested by trypsinization. After centrifugation, the cells pellets were re-suspended in DMEM medium, and analyzed by flow cytometry with a Becton-Dickinson FACSCanto cytometer and DB-FACS Diva software. To distinguish the true fluorescence generated by the loaded MSN from the natural auto-fluorescence of cells, a threshold of fluorescence intensity was established by performing the flow cytometry analysis on HeLa cells incubated

without any PAP-LP-MSN or AP-PAP-MSN. The threshold was set at an intensity of fluorescence slightly above the highest value observed for control samples (HeLa cells only). The number of cells with endocytosed PAP-LP-MSN or AP-PAP-MSN was determined by counting the cells showing fluorescence intensity higher than the threshold.

References

[1] D. R. Radu, C.-Y. Lai, K. Jeftinija, E. W. Rowe, S. Jeftinija, V. S. Y. Lin, J. Am. Chem. Soc. 2004, 126, 13216.

[2] C.-Y. Lai, B. G. Trewyn, D. M. Jeftinija, K. Jeftinija, S. Xu, S. Jeftinija, V. S. Y. Lin, J. Am. Chem. Soc. 2003, 125, 4451.

[3] I. I. Slowing, B. G. Trewyn, V. S. Y. Lin, J. Am. Chem. Soc. 2007, 129, 8845.

[4] Watkins TI. Trypanocides of the phenanthridine series. I. The effect of changing the quaternary grouping in dimidium bromide. J. Chem. Soc. 1952:3059-64.

[5] Huber R, Amann N, Wagenknecht H-A. Synthesis of DNA with Phenanthridinium as an Artificial DNA Base. J. Org. Chem. 2004;69(3):744-751.

Table S1. Structural Properties of MSN materials

Sample	BET Surface Area (m^2/g)	BET Pore Volume (mL/g)	BJH Pore Diameter (Å)	Zeta-Potential (mV)	Particle size DLS (nm)
PAP-LP-MSN	705	1.034	57	1.3 ± 0.4	200 ± 40
AP-PAP-MSN	669	0.684	25	10.5 ± 1.5	320 ± 35

Figure captions

Figure S1. Powder X-ray diffraction patterns. (a) PAP-LP-MSN, and (b) AP-PAP-MSN. The two materials exhibited hexagonal type mesoporous structure characteristic of MCM-41.

Figure S2. N_2 sorption isotherms of PAP-LP-MSN. (a) BET nitrogen sorption isotherms, and (b) BJH pore size distribution.

Figure S3. N_2 sorption isotherms of AP-PAP-MSN. (a) BET nitrogen sorption isotherms, and (b) BJH pore size distribution.

Figure S4. (a) Solid state ^{13}C CP-MAS NMR spectra of PAP-LP-MSN, and (b) Solid state ^{29}Si CP-MAS NMR spectra of PAP-LP-MSN.

Figure S5. Confocal fluorescence images of HeLa cells (a-c), and HeLa cells loaded with MSN (d-f), and LP-MSN (g-i) in presence of SYTO®RNASelect™. (a, d, and g) Phase constrast of cells, (b, e, and h) SYTO®RNASelect™ stained cells, and (c, f, and i) red fluorescence of the endocytosed of MSN and LP-MSN.

Figure S6. Fluorescence emission spectra of PAP-LP-MSN (blue line) and PAP-LP-MSN with yeast tRNA (red line). (Excitation wavelength = 450 nm)

Figure S1

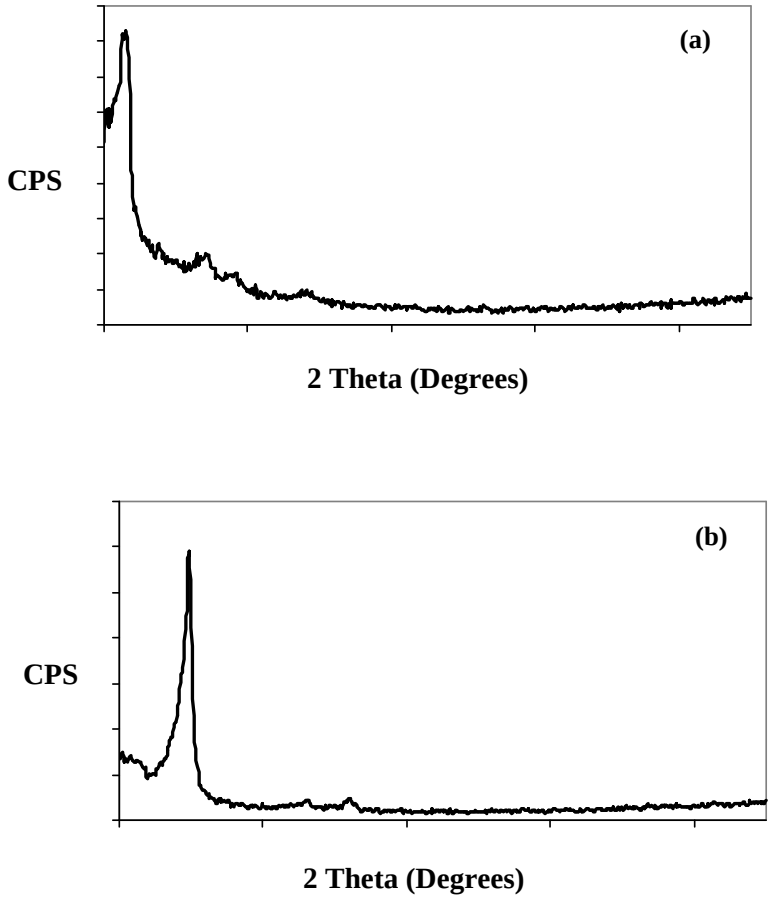

Figure S2

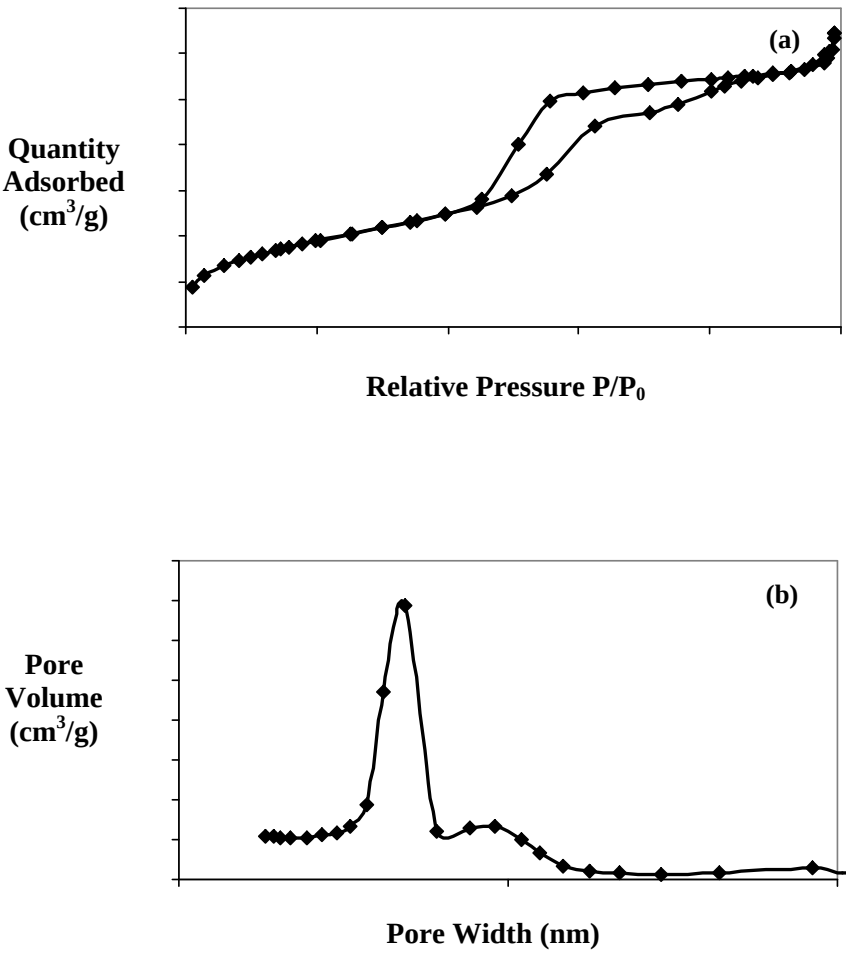
(a)
Quantity Adsorbed (cm3/g)
Relative Pressure P/P0
(b)
Pore Volume (cm3/g)
Pore Width (nm)

Figure S3

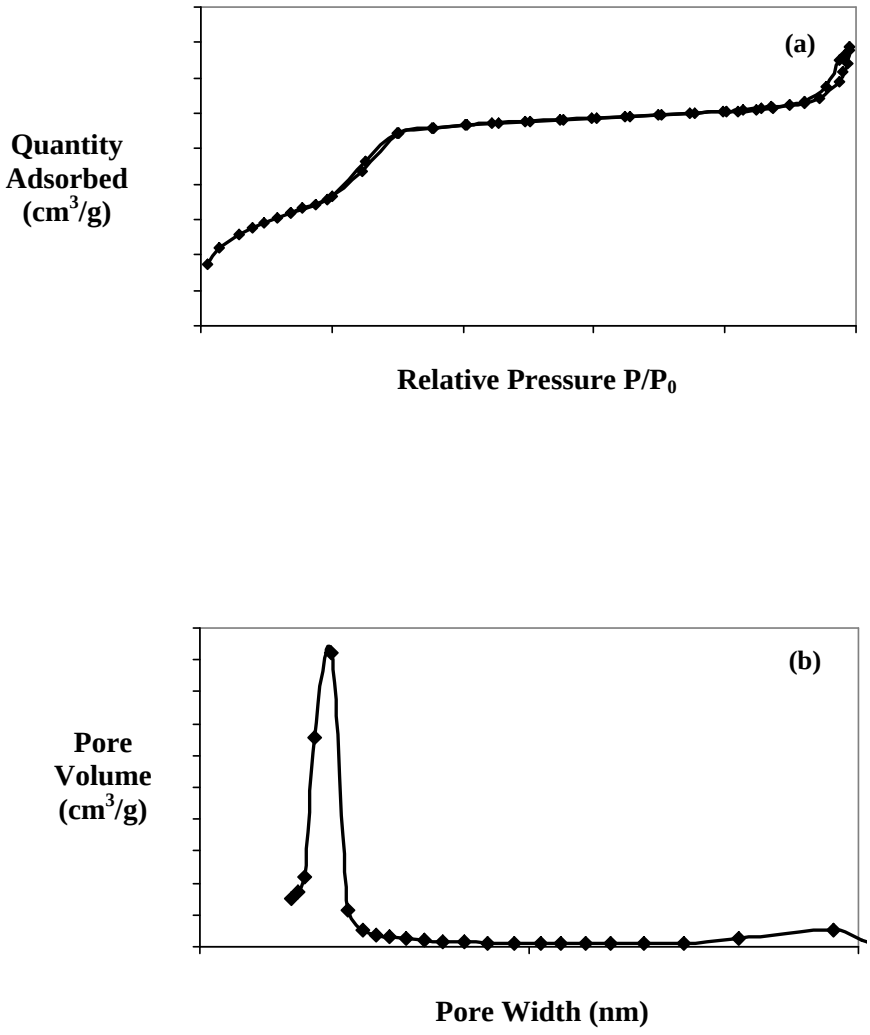
(a)
Quantity Adsorbed (cm3/g)
Relative Pressure P/P0
(b)
Pore Volume (cm3/g)
Pore Width (nm)

Figure S4

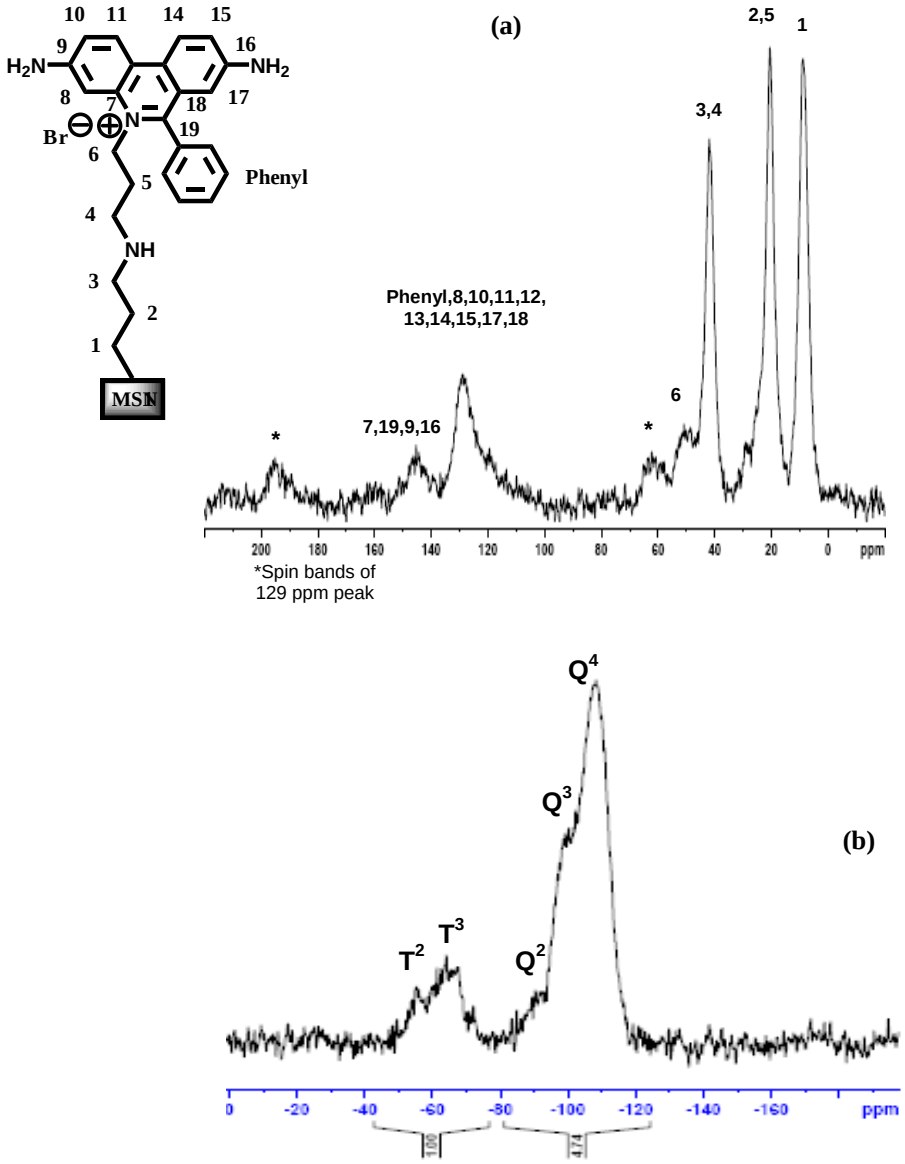
10 11 14 15
9
16
H_2N
NH_2
8
7
18
17
N
19
Br
6
5
Phenyl
4
NH
3
2
1
MSN
(a)
2,5
1
3,4
Phenyl,8,10,11,12,
13,14,15,17,18
7,19,9,16
6
*
*
200 180 160 140 120 100 80 60 40 20 0 ppm
*Spin bands of
129 ppm peak
Q^4
Q^3
(b)
T^2
T^3
Q^2
0 -20 -40 -60 -80 -100 -120 -140 -160 ppm

Figure S5

HeLa cells

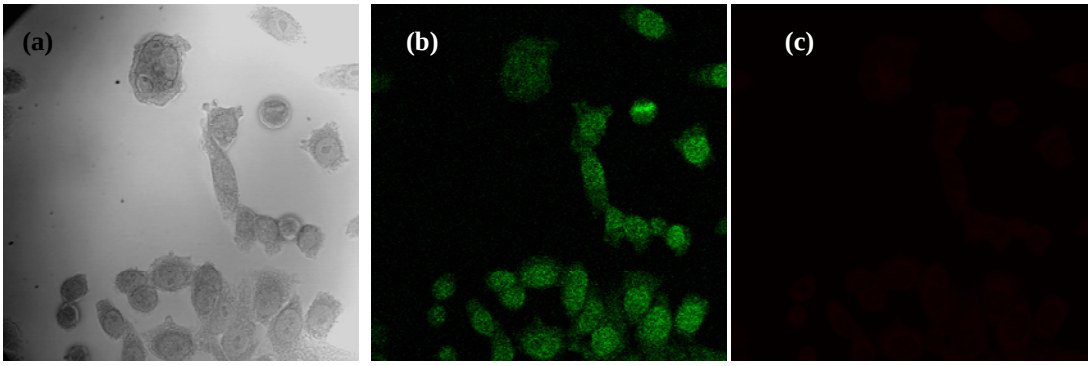

MSN

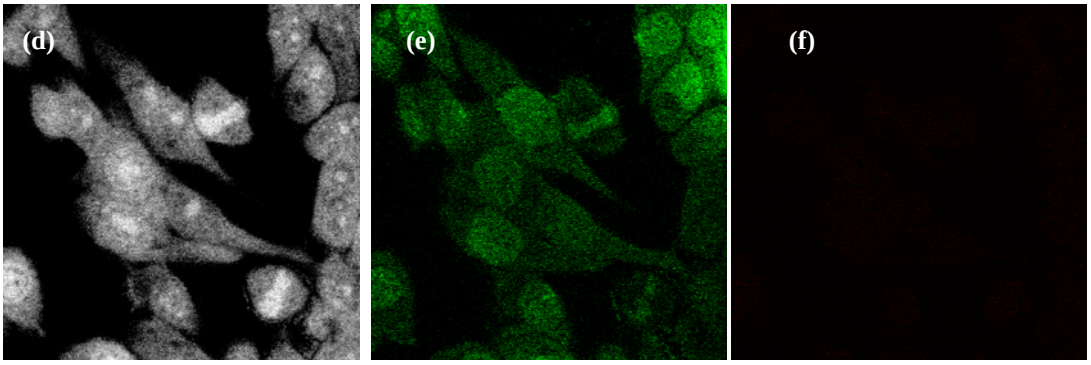

LP-MSN

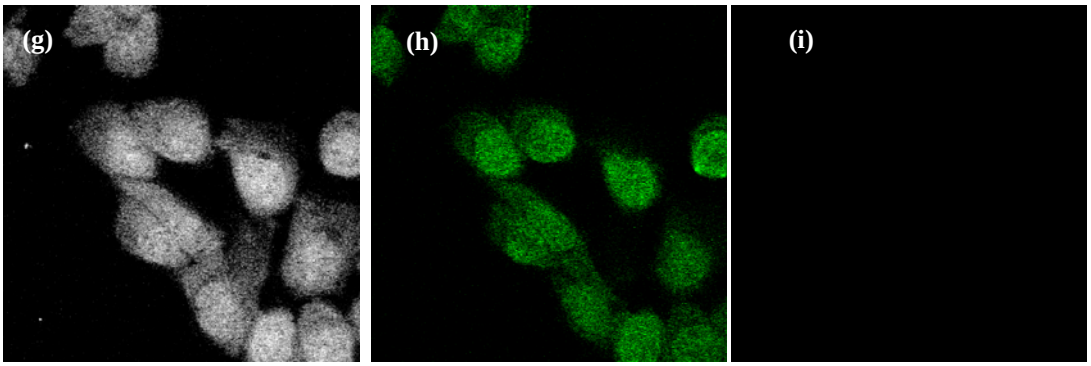

Figure S6

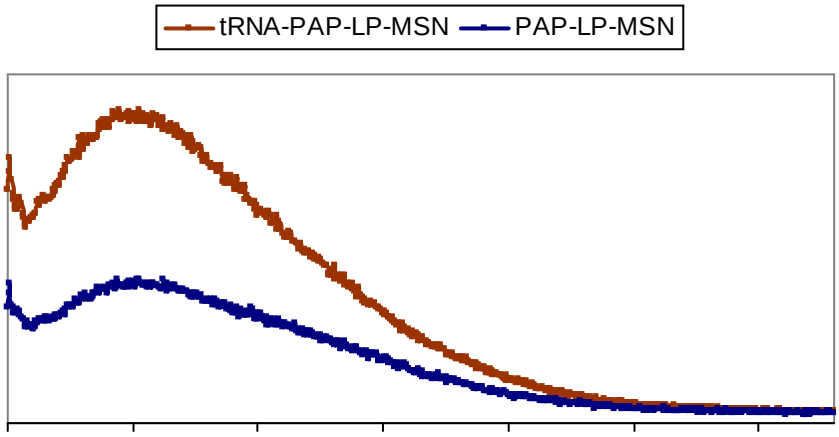

Scheme Captions

Scheme S1. Synthesis of aminopropyl-MSN (AP-MSN). Aminopropyltrimethoxysilane was first grafted to the cetyltrimethylammonium bromide (CTAB)-containing MSN in dry toluene. The CTAB surfactant template was removed under an acidic condition to afford AP-MSN.

Scheme S2. Synthesis of N-[3[(3,8-diamino-6-phenyl-5-phenanthridium)propyl]-3-aminopropyl-functionalized, MCM-41 type mesoporous silica nanoparticle materials (PAP-LP-MSN).

Scheme S3. Synthesis of aminopropyl-PAP-MSN (AP-PAP-MSN). Aminopropyltrimethoxysilane was first grafted to the cetyltrimethylammonium bromide (CTAB)-containing MSN in dry toluene. The CTAB surfactant template was removed under an acidic condition to afford AP-MSN. PAP-TMS was then grafted to the interior surface of AP-MSN in dry toluene to yield AP-PAP-MSN.

Scheme S1

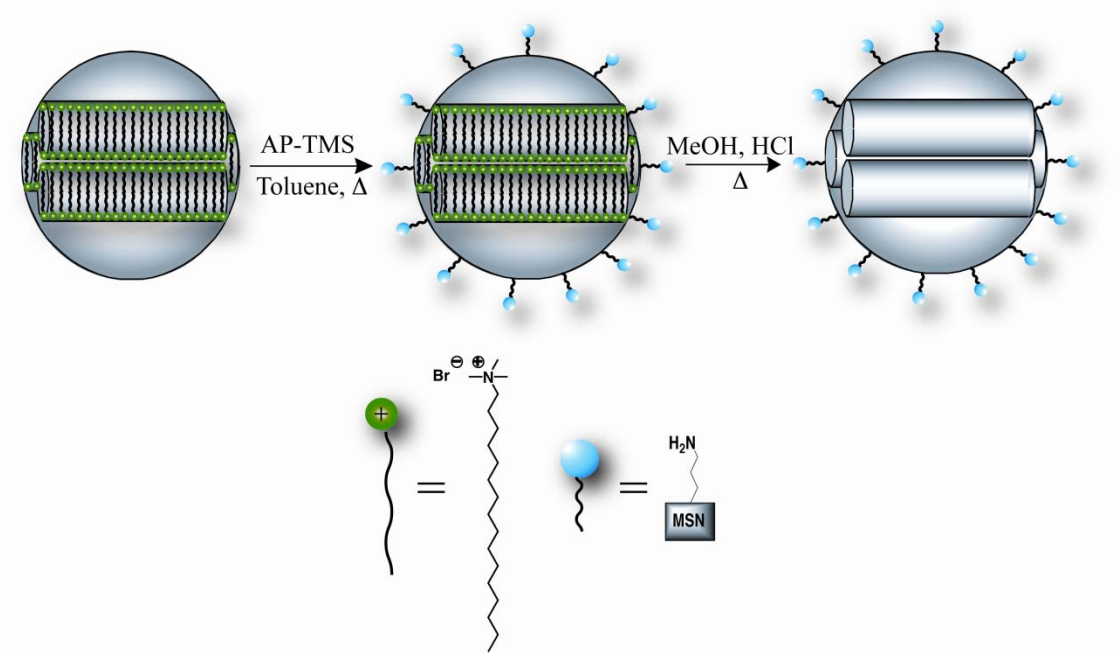

Scheme S2

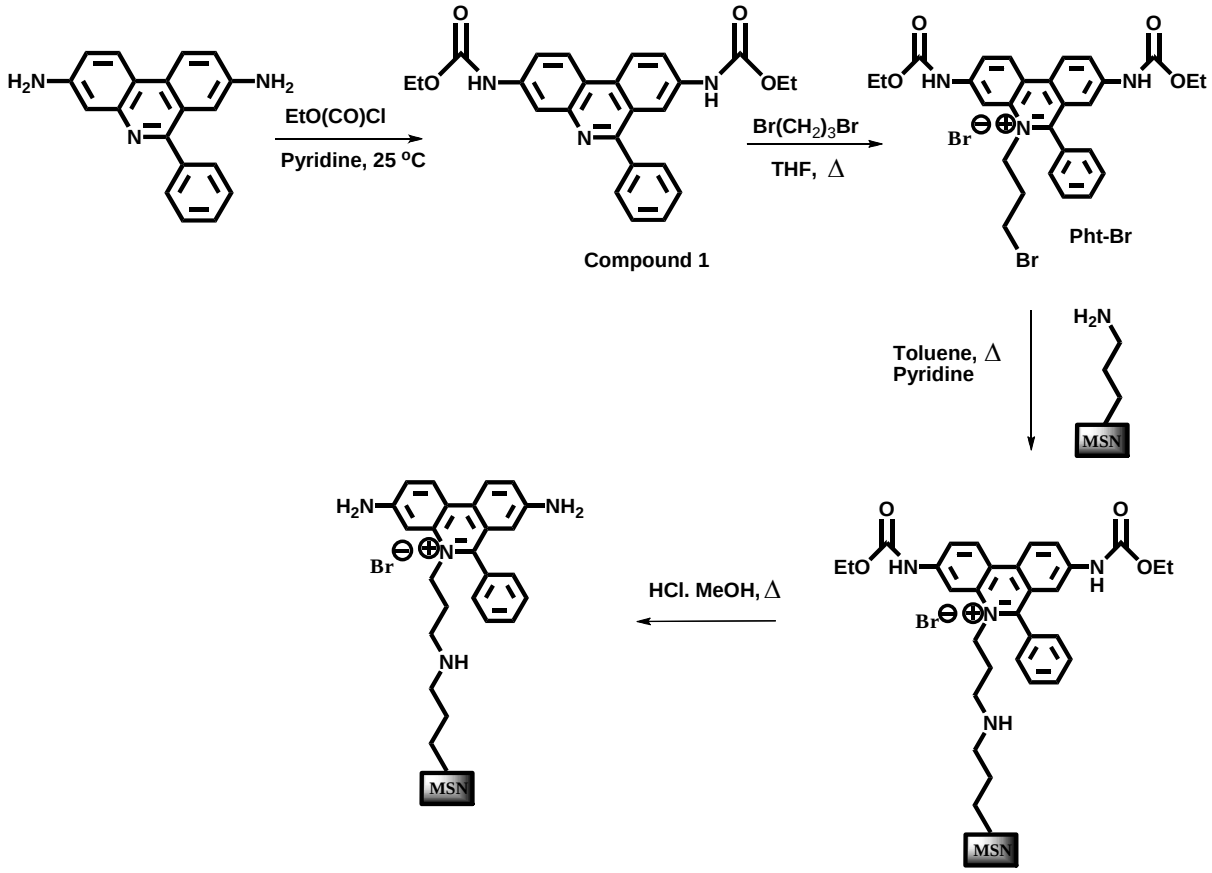
EtO(CO)Cl
Pyridine, 25 °C
Compound 1
Br(CH2)3Br
THF, Δ
Pht-Br
Toluene, Δ
Pyridine
MSN
HCl. MeOH, Δ

Scheme S3

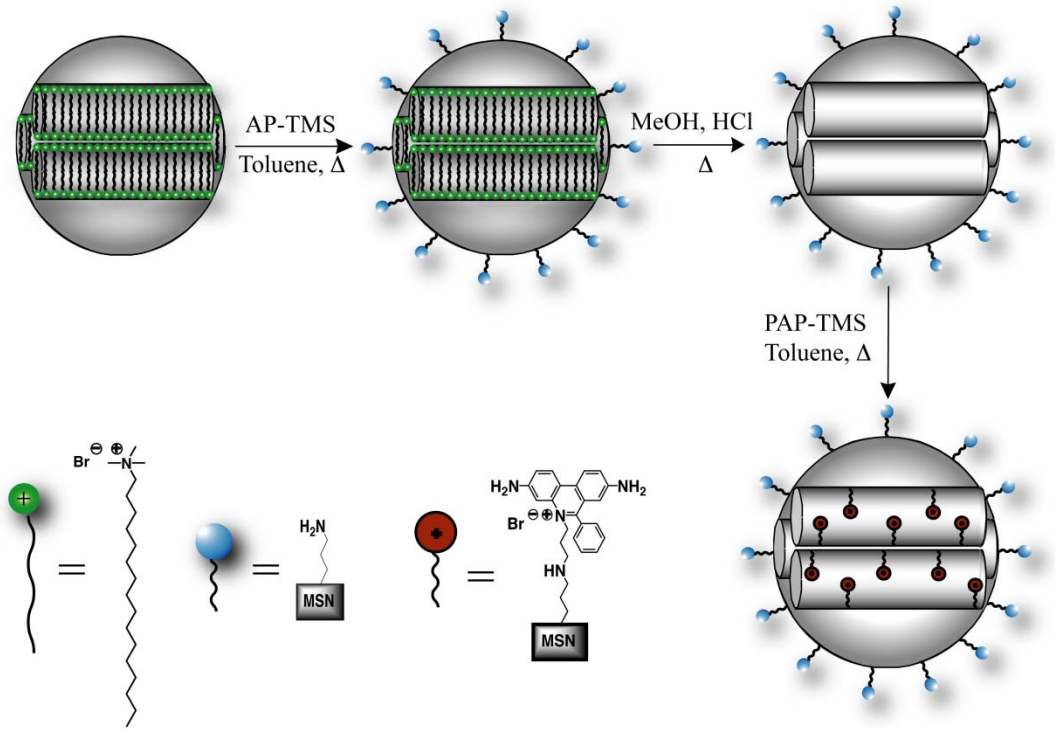
AP-TMS
Toluene, Δ
MeOH, HCl
Δ
PAP-TMS
Toluene, Δ
Br
N
H2N
MSN
H2N
NH2
Br
N
HN
MSN

CHAPTER 6. GENERAL CONCLUSIONS

The continuous advanced on the design and synthesis of therapeutic drugs for various diseases is improving our everyday life. In addition, new therapeutic strategies are currently being developed such as gene and protein therapy, which would change the current way human disease is treated. However; in some cases, such as chemotherapy for cancer where the use of toxic drugs results in acute and chronic side effects; or gene therapy where the precious cargo has to be protected from the harsh environment of the human body, the use of a vehicle that could transport and release these drugs/genes to the desired site is required. To circumvent these problems different delivery systems have been developed and others are under investigation such as polymers, liposomes, dendrimers, and inorganic nanoparticles. Prof. Dr. Victor Shang-Yi Lin and his group have contributed to this field developing mesoporous silica nanoparticles (MSNs) as a potential platform for drug delivery. Their results have demonstrated that high amount of drugs or bio-imaging molecules can be loaded, transported, and released in a controlled fashion by MSNs. The research presented in this dissertation provides novel strategies for the controlled release of guest molecules and for manipulating intracellular processes through the interaction of functionalized MSNs with bioactive molecules.

The design of site-specific stimuli-responsive drug delivery systems is of utmost importance for the continued advancement of the pharmaceutical industry. So far, different stimuli-responsive systems based on MSNs have been developed where the release of the cargo is triggered by *internal stimuli* such as change in pH, reducing environment, and enzymatic activity. However, very few delivery MSN carriers that work under biological conditions were found in the literature where the release of the guest molecule is controlled

by *external stimuli* (radiation, ultrasound, and magnetic field). The ability of manipulating the delivery of drugs using an external trigger could result in an accurate control of the time and site of release. In this study we proposed to develop a MSNs-based drug delivery vehicle where the release of the guest molecule could be trigger by irradiation under biocompatible conditions. This work took advantage of the synergy between two of the most used inorganic nanoparticles for biomedical applications, gold nanoparticles and MSNs. This irradiation-triggered system was design based on the electrostatic interaction between a gold nanoparticle bearing a positively charged photo-responsive linker and MSN. It was found that under mild irradiation conditions the release of fluorescein and the anticancer drug paclitaxel in solution and in human cells, respectively, can be accomplished. Moreover, this work demonstrated that the MSNs carrier exhibited zero premature release in absence of irradiation. For *in vivo* applications the scope of this research can be expanded developing MSNs systems that respond to irradiation with deeper penetration such as near-infrared.

The versatility of MSNs as delivery vehicle was demonstrated in this work. Besides drugs and bio-imaging agents, other biogenic molecules can be loaded to MSN and efficiently transported inside the cells. This concept was demonstrated in this study by using cysteine as cargo. This peptide is essential for the intracellular synthesis of glutathione, which has a direct impact in controlling the homeostasis of cells. The cysteine molecule was chemically attached to MSNs by a labile disulfide bond, which is broken by intracellular reducing agents. It was found that due to their high loading capacity, efficient internalization, and effective endosomal escape, MSNs can successfully release cysteine. This was further demonstrated by comparing the delivery performance of MSNs against a conventional

cysteine pro-drug, N-acetylcysteine. It was found that the efficiency of the MSN vehicle is almost 400 times better than N-acetylcysteine.

In addition to the application of MSNs as drug delivery vehicles, one of the potential areas of research for these nanomaterials is the possibility of manipulating various intracellular processes through their interaction with bioactive molecules, proteins, oligonucleotides, and/or organelles. To prove this idea, an oligonucleotide intercalating molecule was attached to the exterior particle and interior pore surface of MSNs. It was demonstrated by confocal microscopy that the MSNs that contain the intercalating molecule in the exterior surface bind to cytoplasmic oligonucleotides. Moreover, it was found that this interaction results in a sever inhibition of the cell growth. In contrast, the same intercalator group attached to the interior pore of MSNs did not exhibit any interaction with intracellular oligonucleotides. It was shown by using an extraneous plasmid DNA that is encoding for an enhanced green fluorescence protein that the intracellular interaction of the MSNs bearing the intercalator group on the external surface inhibited the expression of the protein. This work demonstrated that taking advantage of the structural and chemical features of MSNs it is possible to design nanodevices that can manipulate intracellular processes.

The work presented in this dissertation opens the door for the design of new generations of stimuli-responsive delivery MSNs systems based on *external stimuli*. In addition, new applications for the manipulation of intracellular processes can be envisioned, such as the selective interaction of MSNs with intracellular enzymes, and organelles. Further work is required to translate all these exciting findings to *in vivo* applications. For instance, the biocompatibility, biodistribution, and biodegradability *in vivo* of all these systems need to be evaluated.